Scintigraphic detection of infection and inflammation with radiolabeled Leukotriene B4 antagonists

Omslag: Samuel Kvaalen
Druk: Quickprint, Nijmegen

ISBN-10: 90-9019715-X
ISBN-13: 978-90-9019715-9

Scintigraphic detection of infection and inflammation with radiolabeled Leukotriene B4 antagonists

Een wetenschappelijke proeve op het gebied van de Medische Wetenschappen

PROEFSCHRIFT

ter verkrijging van de graad van doctor
aan de Radboud Universiteit Nijmegen
op gezag van Rector Magnificus prof. dr. C.W.P.M. Blom,
volgens besluit van het College van Decanen
in het openbaar te verdedigen op

donderdag 10 november 2005
des namiddags om 3.30 uur precies

door

Julia Elisabeth Maria van Eerd-Vismale

geboren 1 mei 1968 te Sint-Oedenrode

Promotores:	Prof. Dr. F.H.M. Corstens
	Prof. Dr. W.J.G. Oyen
Copromotor:	Dr.O.C. Boerman
Manuscriptcommissie:	Prof. Dr. J.W.M. van der Meer
	Prof. Dr. P.E. Verweij
	Prof. Dr. R.M.J. Liskamp (Universiteit Utrecht)

Choose a job you love
and you will never have to work a day in your life.

Confucius

CONTENTS

Abbreviations

^{111}In	Indium-111, radionuclide
^{18}FDG, FDG	18F-fluorodeoxyglucose
^{67}Ga	Gallium-67, radionuclide
^{99m}Tc	Technetium-99, radionuclide
BLT1, BLT2	Leukotriene B4 receptor type 1, 2
BMC(s)	Bone marrow cell(s)
BSA	Bovine serum albumine
CFU	Colony forming units
Da	Dalton
DTPA	Diethylenetriaminepentaacetic acid
FPLC	Fast performance liquid chromatography
g	gram
h	Hour
HPLC	High performance liquid chromatography
HYNIC	hydrazinonicotinamide
i.m.	intramuscular
i.v.	Intravenous(ly)
IBD	Inflammatory bowel disease
ID	Injected dose
IgG	Immunoglobulin G
IL-8	Interleukin 8
ITLC	Instant thin layer chromatography
LTB4	Leukotriene B4
M	Molar concentration (mol/liter)
MBq	Megabecquerel
mCi	Millicurie (1mCi = 37 MBq)
p.i.	Post injection
PBS	Phosphate buffered saline
PET	Positron emmission tomography
PMN	ploymorphonuclear cell
RBC	Red blood cell
RBF	receptor binding fraction
ROI	Region of interest

SD	Standard deviation
SEM (s.e.m.)	standard error of the mean
S-HYNIC	succinimidyl hydrazinonicotinamide
T/B	target to brackground ratio
TPPTS	triphenylphosphinetrisulfonate
WBC(s)	White blood cell(s)

Chapter 1

Radiolabeled chemotactic cytokines: new agents for scintigraphic imaging of infection and inflammation.

Julliëtte J.E.M. van Eerd
Otto C. Boerman
Frans H.M. Corstens
Wim J.G. Oyen

Q J Nucl Med. 2003;47:246-255

ABSTRACT

Several radiopharmaceuticals are currently used for diagnosis of inflammatory and infectious diseases in patients. Most inflammatory and infectious processes can be visualized with radiolabeled autologous leukocytes, currently considered to be the most appropriate radiopharmaceutical for this purpose. Radiolabeled leukocytes can accurately delineate most inflammatory and infectious foci. The preparation of radiolabeled leucocytes however, is time-consuming and elaborate and requires the handling of potentially contaminated blood. Therefore, there is a great interest in the development of new radiopharmaceuticals comprising the same imaging qualities but without these disadvantages. Besides radiolabeled leukocytes several other radiopharmaceuticals, such as ^{67}Ga-citrate and radiolabeled anti-granulocyte antibodies are used to image infection and inflammation. However, these latter agents accumulate in infectious and inflammatory lesions in a non-specific manner or have suboptimal diagnostic characteristics. Nowadays there is a great interest in the development of radiolabeled chemotactic and chemokinetic cytokines that accumulate and are retained in infectious and inflammatory foci by means of specific interaction with infiltrating inflammatory cells. Here we describe the specific characteristics of the chemotactic and chemokinetic compounds that are currently studied as potential radiopharmaceuticals to visualize infectious and inflammatory foci. The characteristics of a series of cytokines (IL-1, IL-2), chemokines (IL-8, PF-4, MCP-1, NAP-2), complement factors (C5a, C5adR), chemotactic peptides (fMLF) and other chemotactic factors (LTB4) are described. The potential of these compounds to serve as imaging agent are discussed.

INTRODUCTION

The role of nuclear medicine in the management of patients suspected of infectious or inflammatory disorders is eminent. Diagnosis of infectious and inflammatory disorders by means of scintigraphic imaging generally allows adequate and rapid delineation of infectious and inflammatory foci. Visualization of the localization and the extent of an inflammatory process allows guided verification procedures, therapeutic decisions and initiation of appropriate treatment in most cases. In most institutions scintigraphic imaging to detect inflammatory and infectious foci is performed with radiolabeled leukocytes[1]. However, due to several insuperable disadvantages of this agent, there is a great interest in the development of new radiopharmaceuticals for this application[2,3]. A new radiopharmaceutical should accumulate efficiently and rapidly in the infected or inflamed

tissue. Furthermore it should clear rapidly from the blood and other non-target tissues. A promising class of compounds in this field of research are chemotactic and chemokinetic mediators and their analogs[4]. The use of radiolabeled chemotactic compounds (fMLF, chemokines) is based on the high affinity interaction of these compounds with their receptors expressed on specific leukocyte sub-populations[5]. In addition, due to their low molecular weight, they can penetrate rapidly into the inflamed tissue and clear rapidly from the non-target tissue and from the circulation[6,7]. In addition, antagonists of these chemotactic mediators may provide good alternative agents, especially when biological effects of the agonistic peptides limit clinical application. Since the knowledge of the human inflammatory response has expanded and the number of identified chemokines and chemokine receptors has increased, it is now possible to investigate in detail those chemokines for their potential as radiopharmaceutical for visualization of inflammatory processes.

Chemokines and chemokine receptors

During an inflammatory response a complex variety of mediators is released in order to control this process[8]. Tissue injury and the release of mediators (e.g. histamine, TNFα) trigger the inflammatory response. The subsequent increased blood supply, increased vascular permeability and influx of leukocytes aim at efficient elimination of invading micro-organisms and repair of injured tissue[9]. Following initiation, the response is continued and finally terminated as described in Table 1. Usually the cause of the infection/inflammation is eliminated during the subsequent stages of the inflammatory response. The release of the mediators that control the process occurs following two major pathways. The first pathway (I) is the release of mediators present in the granules of macrophages and granulocytes, the second pathway (II) involves release of arachidonic acid by mast cells triggering the lipoxygenase and the cyclo-oxygenase pathway as indicated in Table 2[8,10-28]. Each mediator has its specific function and induces its biological effects by interaction with specific receptors on blood cells, endothelial cells or smooth muscle cells that align the blood vessels. The majority of mediators that is released are chemokines that target chemokine receptors that belong to the large family of G-protein-coupled receptors (GPCRs).

Membrane proteins of the GPCR superfamily, consist of seven hydrophobic transmembrane domains, always involved in signaling processes from the extracellular side of the cell towards the intracellular environment[29]. Binding of receptor specific ligands to GPCRs induces various intracellular pathways affecting the cell metabolism, gene expression and cell division. The GPCRs are classified into five families; class A through

E (Table 3). Members of the GPCR class A (receptors related to the Rhodopsin and adrenergic receptors) become activated after interaction with chemotactic compounds and cytokines[30]. In nuclear medicine radiolabeled chemotactic mediators, cytokines or their antagonists are considered promising vehicles for scintigraphic imaging of infection and inflammation[9]. It was hypothesized that the high affinity interaction of radiolabeled mediators with their receptors expressed on white blood cells (granulocytes, monocytes, macrophages) might facilitate the specific localization of the radiolabeled receptor binding ligand in the inflammatory foci[31].

Table I. Course of an inflammatory process and the adaptive immune response

	Induction of inflammatory response
1.	Inflammatory response is triggered by tissue injury or by establishment of microorganisms at the site of infection. Establishment of microorganisms involves adherence to the epithelial surface (skin or internal mucosal surfaces of the respiratory, gastro-intestinal and urogenital tract).
	Initiation of inflammatory response; increased blood supply
2.	The inflammation is initiated by release of histamine by mast cells and basophils and of serotinin by platelets, which induces increased blood supply. Activation of resident macrophages leads to release of cytokines and chemokines (TNF-α, IL-1).
	Elongation of the inflammatory process; Increased vascular permeability and emigration into the infected tissue
3.	Release of chemokines and cytokines leads to upregulation of selectin and recruitment of neutrophils and macrophages. Activation of the complement cascade (especially factor C5a) and leukotriene B4 enable these cells to cross the endothelium and enter the infected tissue. Besides IL-1 other chemokines like IL-8, NAP-2 and PF-4 are involved in chemotaxis of PMNs.
	Termination of inflammation
4.	Complement regulatory proteins and a number of anti-inflammatory cytokines (e.g. IL-10, IL-1ra, TGFβ) downregulate the inflammatory process. Once the inflammatory response leads to effective clearance of inflammatory agent and affected tissue, the tissue will return to its normal healthy situation.

Furthermore, due to the low molecular weight of these compounds these molecules are cleared rapidly from the blood. Due to tremendous progress in the field of Immunology and Molecular Biology, the knowledge of these mediators and their receptors has expanded. Characterization of genes encoding for such mediators, allowed synthesis (chemically and by recombinant DNA techniques) of several ligands. Chemotactic molecules and receptor antagonists became available as well as information on their structure and biological characteristics. Nowadays more than 45 chemokines and nearly 20 chemokine receptors have been identified, characterized and described[32]. For nuclear

medicine applications only a small fraction of these chemokines or receptor antagonists have been studied so far.

fLMF analogs

N-formyl peptides, such as N-formyl-methionyl-leucyl-phenylalanine (fMLF), were among the first identified potent chemoattractants for phagocytic leukocytes. N-formyl peptides are cleavage products of mitochondrial and bacterial proteins. These peptides activate at least two of the GPCRs found on granulocytes and monocytes via high affinity interaction (Kd = 10-30 nM)[33]. The GPCRs activated after binding of fMLF belong to the Class A GPCRs and the receptor shows partial sequence homology with the CXC receptor[34]. First studies performed with fMLF as a radiopharmaceutical for imaging of infection and inflammation were carried out in the 1980s[35,36]. These studies showed localization in the infection within one hour after injection, however, even a dose as low as 10 ng/kg induced leukopenia. Several antagonists were developed to circumvent the effect on the number of granulocytes in the circulation. Unfortunately, these antagonists showed lower uptake in the infection, most likely due to reduced affinity for the receptors[37]. Babich *et al*. compared the high affinity ^{99m}Tc-labeled N-fMLFK antagonist with a low (N-acetyl-MLFK) and a moderate affinity antagonist (N-isobutyloxycarbonyl-MLFK) in an *E. coli* infection model in rabbits[38]. The activity concentration at the site of infection of the three analogs correlated with the affinity of each compound for the receptor. Another study with ^{99m}Tc-HYNIC-fMLFK in rabbits with intramuscular infection showed that this compound visualized the infected foci at 2 h p.i. with a moderate abscess-to-normal-tissue ratio of 7.5 at 4 h p.i.. White blood cell (WBC) counts of the animals were determined and a transient drop to 65% of the initial counts was observed during the first 30 minutes after injection of the radiolabeled peptide[39]. A recent study was performed with radiolabeled f-Met-Leu-Phe-Lys (fMLFK). ^{99m}Tc-EC-f-MLFK showed high affinity binding to human granulocytes[40]. Despite this in vitro interaction, the authors concluded that after intravenous injection in normal mice the high abdominal activity (at 1 h p.i. 25% ID in the liver, 50% ID in the intestines) would limit the applicability of this compound. Unfortunately due to relative low accumulation in infected foci and biological effects on WBC counts, chemotactic fMLF analogs have limited perspective as an imaging agent.

IL-1

Interleukin-1 (IL-1) is a 17 kDa proinflammatory cytokine, mainly produced by monocytes, activated macrophages and neutrophilic granulocytes[9]. Two almost identical forms of IL-1 (IL-1-α and IL-1-β) have been identified, which both bind to the same IL-1 receptors. Two

types of IL-1 receptors have been described: IL-1R (type 1) and IL-1R (type 2). The type-1 receptor is expressed predominantly on T-cells and cells of mesenchymal origin and binds both IL-1α and IL-1β with equal affinity. The type-2 receptor is expressed on B-cells, granulocytes and macrophages and has a higher affinity for IL-1α[41]. IL-1 receptor expression increases following the stimulation of cells by IL-1. The main biological activity of IL-1 is T-cell proliferation and promotion of IL-2 synthesis[11]. The central role of IL-1 and the IL-1 receptor in the inflammatory response explains the presence of IL-1 receptor positive leukocytes at the site of an infection or an inflammation. Radiolabeled IL-1 receptor-binding agents were studied in vivo for the applicability as infection imaging agent[9]. Although radiolabeled IL-1 showed reasonable imaging characteristics in several animal models, clinical application was limited due to biological effects of this cytokine (i.e., hypotension, headache and fever) even at very low doses (10 ng/kg). In a comparative study the imaging abilities of IL-1α, IL-1β and IL-1 receptor antagonist (ra) were assessed in a rabbit model of acute infection[42]. All three agents visualized the abscess and highest uptake in this rabbit model was obtained after injection of ^{123}I-IL-1β. However, due to the strong biological effects of IL-1α and IL-1β, only IL-1ra could be studied in humans. In a clinical study in patients with reumatoid arthritis ^{123}I-IL-1ra visualized the inflamed joints with moderate target-to-background ratios (ca. 2-to-1), which were in the same range as the ratios obtained with the control agent ^{123}I-labeled human serum albumin (HSA). In addition, the major part of the agent cleared via the hepatobiliary route, impeding visualization of infectious foci in the abdomen[43]. Therefore, IL-1 receptor-binding agents were not further developed for infection imaging agent.

Table II. Release of the mediators following two major pathways.

Pathway	*Mediator*	*Source*	*Receptor*	*Target*	*Mediator effect*	*Ref*
I Granule release	Histamine	Mast cells, basophils	H1, h2, h3	CNS, smooth muscle, heart	Vasodilatation Increased vascular permeability	16
	Bradykinin	Body fluid	B1, B2	Endothelial cells, Mast cells, sensory neurons	Vasodilatation Increased vascular permeability	17 18
	Vasoactive intestinal peptide (VIP)	nerve endings, immune cells and some neoplastic cells	VPAC1R VPAC2R	Blood cells, Tissue T-cells	Vasodilatation	19 20
	Complement factor 5a (C5a)	Plasma precursor	C5a receptor	Endothelial cells, Mast cells, Phagocytes	Increased vascular permeability upregulation of adhesion molecules	10
	Platelet activating factor (PAF)	neutrophils, basophils, platelets, and endothelial cells	PAF receptor	Various cells like neuthrophils, monocytes and lung cells	Increased vascular permeability Upregulation of adhesion molecules	21 22
	Tumor necrosis factor alpha (TNF-alpha)	macrophages, monocytes, neutrophils, T-cells, NK-cells	TNFRSF1a TNFRSF1b	Epithelial cells Myeloid cells	Upregulation adhesion molecules Neutrophil mobilization	23 24
	Interleukin 1 (IL-1)	monocytes, activated macrophages or peripheral neutrophil granulocytes	CD121a (Type 1) CD121b (Type 2)	T-cells B-cells, granulocytes, macrophages	Upregulation adhesion molecules Neutrophil mobilization	11
	Interleukin 2 (IL-2)	T-cells expressing CD4	ILR2-alpha (TAC-antigen,p55) ILR2-beta (p75, CD122) IL2R-gamma	Activated T-cells	Proliferation of T-lymphocytes	8 12
	Interleukin 8 (IL-8)	monocytes, macrophages, T-lymphocytes, fibroblasts, endothelial cells, and keratinocytes	CXCR1 CXCR2	Neutrophils	Chemotaxis of PMN Activation of integrins	13 25 15
II Lipoxy-genase pathway	Leukotrienes B4 (LTB4)	neutrophil polymorphonuclear leukocytes	BLT1 BLT2	Leukocytes, thymus and Spleen	Activation of immune cells Chemotaxis Enhanced adhesion of leukocytes Enhanced vascular permeability	14
	Leukotrienes C4	macrophages and mast cells	CysLT1 CysLT2	Spleen, leukocytes lung macrophages Heart, adrenal medulla, leukocytes	Brochoconstriction Vasodilatation Increased vascular permeability	26
	Prostaglan-dines	probably all cells	EP1, EP2, EP3, EP4	Widely distributed	Platelet agregation vasodilation	27 28
	Thrombox-anes	probably all cells	TXA2	Thymus, spleen, lung, kidney, heart	Platelet agregation vasodilation	28

Table III.Chemotactic molecules target G-protein coupled receptors.

GPCR class A through E
Class A rhodopsin like GPCR
Amine receptors
- Histamine
- Serotonin
Peptide receptors
- Bradykinin
- IL-8
- Chemokines
• C-C (e.g. MCP-1: CCR2)
• C-X-C (e.g. IL-8: CXCR1, CXCR2, NAP-2: CXCR2)
- fMLP
Rhodopsin receptors
Nucleotide receptors
Platelet activating factor
Leukotriene B4
Class B secretine like
Secretine
Vasoactive intestinal peptide (VIP)
Class C metabotropic glutamate/pheromone
Class D fungal pheromone
Class E cAMP receptors (Dictostelium)

IL-2

Interleukin-2 (IL-2) is a 133 amino acid cytokine with a molecular weight of 15.4 kDa that stimulates proliferation of T-lymphocytes[12]. In addition, in the presence of other factors like IL-4, IL-2 promotes proliferation of activated B-cells as well. The biological activities of IL-2 are mediated by a membrane receptor that is expressed on activated (not on resting) T-cells. Resting granulocytes and activated B-cells express this receptor just sporadically[12,44]. Radiolabeled IL-2 receptor targeting agents could therefore be of interest mainly in chronic inflammatory processes (i.e. autoimmune disorders), characterized by minor hemodynamic changes and infiltration of T-lymphocytes[5,45]. The imaging characteristics of both radioiodinated and ^{99m}Tc-labeled IL-2 has been studied in a several animal models as well as in patients. Signore *et al*. showed that ^{123}I-Interleukin-2 accumulated in pancreatic region of diabetic non-obese diabetic (NOD) mice but not in the pancreatic region of healthy BALB/c mice[46].

These findings were confirmed by measurement of dissected organs of the mice at several time points after injection of ^{125}I-IL-2[47]. Imaging studies in patients with ^{123}I-IL-2 showed focally enhanced intestinal uptake in patients with active Crohn's Disease and Coeliac disease. Autoradiography (with ^{125}I-IL-2) of biopsy material revealed that this accumulation could be attributed to specific binding to IL2R-positive cells[48,49]. IL-2 has been labeled with ^{99m}Tc via a two-step reaction using a N_3S bifunctional chelator[50]. The

^{99m}Tc-IL-2 fully preserved affinity for the receptor and the in vivo stability of the compound was superior as compared to the ^{125}I-IL-2 stability. In a clinical study 29 patients with ileal and/or colonic Crohn's Disease underwent both ^{99m}Tc-IL-2 scintigraphy and ^{99m}Tc-HMPAO-granulocyte scintigraphy[51]. In more than 40% of the scans both the ^{99m}Tc-IL-2 and ^{99m}Tc-granulocytes scintigraphs were concordantly positive. Although both agents showed positive scans in 18 out of the 29 patients (62%), the accumulation of IL-2 and the granulocytes usually localized in different colonic segments. The difference in accumulation between the two agents indicated that depending on the stage of inflammation regions with different types infiltrated immune cells can be present. Another clinical study has been reported recently[82]. In this study, the accumulation of ^{99m}Tc-IL-2 was correlated to the degree of T-lymphocytes infiltration in patients with atypical pigmentary cutaneous lesions. Although scintigraphic images revealed low tumor to background ratios in patients with positive IL-2 scans (1.26±0.19, n=15), positive scans revealed IL-2 accumulation that correlated with the percentage of IL-2 receptor positive lymphocytes, determined by histology. Due to the findings of this study, the authors want to investigate the correlation between ^{99m}Tc-IL-2 scintigraphy and the outcomes of IL-2 immunotherapy.

IL-8

IL-8 is a member of the CXC chemokines. Classification of chemokines is based on the number and sequential relationship of the first two of four conserved cysteine residues of the aminoacid sequence. IL-8 is a non-glycosylated chemotactic cytokine (i.e. chemokine) of 8 kDa[13]. This cytokine is produced by a number of cell types such as stimulated monocytes, macrophages and endothelial cells[52]. The role of IL-8 in infection and inflammation is significant; IL-8 has chemotactic activities for all known types of migratory immune cells and inhibits the adhesion of leukocytes to activated endothelial cells. Consequently, IL-8 exhibits anti-inflammatory activity and is a cytokine found in both acute and subacute inflammatory processes[53,54]. The interleukin-8 (IL-8) receptor is a dimeric glycoprotein consisting of a 59 kDa and a 67 kDa subunit. There are at least two major IL-8 receptor types; CXCR1 en CXCR2. The receptors are mainly expressed on neutrophils and bind IL-8 with different affinity (Kd of IL-8 for CXCR1 is 0.8-4.0 nM, and for CXCR2 is 0.3-2.0 nM). Both receptors belong to the Class A GPCRs (Rhodopsin-like) peptides receptors.

Radiolabeled IL-8 has been studied extensively as infection imaging agent. The potential of radiolabeled IL-8 to image inflammation was reported for the first time by Hay *et al*.. This group showed that radioiodinated IL-8 accumulated in inflammatory lesions in a rat

model[55]. The uptake of IL-8, radioiodinated via the chloramine-T method, in carrageenan-induced sterile inflammations in rats, peaked at 1-3 hours after injection and declined thereafter. In addition, this group performed an imaging study with ^{131}I-labeled human recombinant IL-8 (rhIL-8) in patients. In this study ^{131}I-rhIL-8 succesfully delineated infections in 8 of the 8 patients with active foot infection and osteomyelitis. ^{131}I-rhIL-8 did not accumulate in degenerative joint disease or succesfully treated infections[56]. This study showed that radiolabeled rhIL-8 is a feasible infection imaging agent. Van der Laken *et al*. showed specific interaction of radioiodinated IL-8 with its receptor on human granulocytes. Imaging experiments in rabbits demonstrated that radiolabeled IL-8 visualized acute infection and inflammation already in a few hours after injection. Due to rapid blood clearance high target-to-background ratios were obtained[42]. More importantly, they demonstrated that the labeling method had a major effect on the in vivo biodistribution of radioiodinated IL-8. The scintigraphic imaging characteristics of IL-8 labeled via the Bolton-Hunter method were clearly superior to IL-8 labeled via the iodogen method[59]. The specific activity of the IL-8 preparations used in these studies in rabbits were relatively low; the imaging dose of ^{123}I-IL-8 (25 µg/kg) caused a transient drop of peripheral leukocyte counts to 45%, followed by a leukocytosis (170 % of preinjection level) during several hours. Rennen *et al*. developed a ^{99m}Tc-labeled IL-8 preparation using HYNIC as a chelator and performed in vitro as well as in vivo experiments with ^{99m}Tc-HYNIC-IL-8[57,58]. These studies demonstrated that ^{99m}Tc-IL-8 comprised excellent imaging characteristics with even higher uptake in the abscess and very high abscess-to-background ratios (>100 at 8 h p.i.) as compared to radioiodinated IL-8. The agent rapidly accumulated in infectious and inflammatory foci and low activity concentrations were found in blood already one hour after injection. Due to HYNIC conjugation and labeling with ^{99m}Tc, a 25-fold reduction of the peptide dose was achieved as compared to radioiodinated IL-8. Due to further improvements of the labeling procedure, imaging doses of ^{99m}Tc-IL-8 did not induce any changes in WBC counts in the circulation[58,59].

In a recent study, ^{99m}Tc-IL-8 was tested for its potential to visualize pulmonary infection. Radiolabeled IL-8 was evaluated in three different rabbit models of respectively fungal infection, pneumococcal and *E. coli* induced pneumonia[81]. Despite the fact, that previous results demonstrated physiologic uptake of the compound in the lungs, images showed that ^{99m}Tc-IL-8 clearly visualized pulmonary infection in all three models rapidly after injection. The currently achieved radiochemical characteristics of ^{99m}Tc-IL-8 warranted progression to clinical studies. Clinical studies with ^{99m}Tc-IL-8 started in 2004.

Platelet factor-4

Platelet factor-4 (PF-4) is a CXC chemokine synthesized in megakaryocytes and platelets that activate neutrophils and monocytes[21]. In solution PF-4 monomers may form dimers and tetramers. PF4 is structurally related to IL-8, but the native PF4 peptide does not have affinity for CXCR1 or CXCR2 receptor as is the case with IL-8. As yet no cell surface receptor for PF4 has been identified, it has been shown however that slight modifications at the N-terminus of PF-4 leads to binding to the CXCR2 receptor[60]. PF-4 also shows affinity for heparin. Moyer *et al.* tested a PF4 analogue (P483) consisting of the heparin-binding region of PF-4 and a lysine-rich sequence to facilitate rapid renal clearance. Preclinical evaluation of this PF-4 analog indicated that P483 had enhanced affinity for leukocytes when complexed with heparin. Likewise, the infection imaging properties of ^{99m}Tc-P483 could be improved after P483 complexation with heparin. They tested the radiolabeled PF4-heparin analog P483H in a rabbit model[61]. Intravenous injection of ^{99m}Tc-P483H visualized intramuscular *E. coli* abscesses in rabbits already a few hours after injection and revealed higher abscess-to-contralateral and abscess-to-blood ratios as compared to the radiolabeled WBCs. ^{99m}Tc-labeled P483H was evaluated clinically[62]. Thirty patients were injected with various doses of radiolabeled peptide (29 µg, 145 µg and 290 µg). Twenty patients also underwent ^{111}In-labeled autologous leukocyte scintigraphy for comparison. In most patients ^{99m}Tc-P438H rapidly and accurately detected the focal infection. The radiolabeled compound showed retention in kidneys, lung, thyroid liver and spleen. In this preliminary clinical evaluation P438H revealed a relatively low specificity of 81% and sensitivity of 86%. Additionally, the relatively high pulmonary uptake of P438H will limit the application of the agent to visualize infections and inflammations in the chest.

C5a

The complement anaphylatoxin C5a is a chemotactic peptide involved in several stages during the inflammatory process. This peptide induces smooth muscle contraction, increases vascular permeability and induces expression of adhesion molecules on the endothelial cells[10]. C5a also acts directly on neutrophils and monocytes by increasing their adherence to endothelial cells and their migration toward the site of infection. C5a, like other chemotactic peptides, signals via transmembrane receptors of the Class A GPCRs. A comparative study with ^{99m}Tc-HYNIC-C5a and its natural metabolite C5a-des-Arg (74) (C5adR) was recently performed in rabbits with intramuscular infection[63]. The affinity of C5a for the C5a receptor expressed on monocytes and neutrophils is approximately twenty-five times higher than that of C5adR. Consequently, C5a is biologically much more

potent than C5adR[64]. In a rabbit model both agents visualized the infection from one hour postinjection. However, this comparative study showed that the uptake of C5a in the abscess was five times higher than that of C5adR. Due to the lower affinity of C5adR for the C5a receptor there was insufficient accumulation of C5adR in tissues infiltrated with receptor-positive cells. Due to the low uptake and abscess-to-muscle ratios obtained with C5adR, the authors considered this less bioactive peptide inadequate for imaging of infectious or inflammatory foci, while C5a cannot be applied clinically due to its pronounced biological effects.

Leukotriene B4

Leukotriene B4 (LTB4) is a chemotactic dihydroxy fatty acid that is able to activate neutrophils. Binding of LTB4 to its specific receptors (BLT1 and BLT2) stimulates leukocyte functions such as trans-endothelial migration and chemotaxis[65,66] comparable with those of classic chemotactic peptides such as fMLP and IL-8[67]. Two receptors for LTB4 have been described belonging to class A of GCPRs[68,69]. The first identified receptor; BLT1 is a high affinity receptor for LTB4 and is mainly expressed on neutrophils. The second receptor, BLT2, has lower LTB4 affinity and is expressed more ubiquitously, with highest expression in spleen, leukocytes, ovary and liver[15]. Based on its receptor expression, it was hypothesized that radiolabeled BLT1 receptor binding agents could be used to visualize inflammatory processes. Several radiolabeled LTB4 antagonists have been synthesized and studied for the potential to visualize inflammatory and infectious lesions[70,71]. Early studies with a ^{99m}Tc-labeled LTB4 antagonist RP517 demonstrated that this agent accumulated rapidly and efficiently in acute intramuscular infection[72].
However, due to hepatobiliary clearance of this rather lipophilic compound (the receptor binding moiety of the agent contains three aromatic rings), clinical applicability was limited. Recently, modified LTB4 antagonists were synthesized in order to reduce physiologic uptake in abdominal organs.

MCP-1

Monocyte chemoattractant peptide-1 (MCP-1) is a cytokine that is produced mainly by monocytes and endothelial cells. MCP-1 is an activator of basophils, inducing degranulation and the release of histamines[73]. MCP-1 is a chemotactic factor for monocytes but not for neutrophils[74]. Two MCP-1 specific receptors are described that exhibit high affinity for MCP-1 (CCR1, CCR2)[75]. MCP-1 has a high affinity for the CCR2B receptor (Kd = 0.3 nM)[76]. Based on its selective receptor expression on monocytes, it was hypothesized that radiolabeled MCP-1 may be applicable to visualize subacute and

chronic inflammatory processes, because these processes are characterized by an influx of macrophages and monocytes. Blankenberg *et al.* studied whether ^{99m}Tc-labeled recombinant human MCP-1 could visualize the presence of monocyte and macrophage infiltration in subacute and chronic soft tissue inflammation in Sprague-Dawly rats[77]. This study showed that MCP-1 was able to visualize the inflammatory lesions, however, accumulation in the abscess was relatively low.

NAP-2

Recently, a study with radiolabeled neutrophil-activating-peptide-2 (NAP-2) has been described. NAP-2 is -like IL8- a CXC-subfamily chemokine consisting of 70 amino acids and selectively binds the CXCR2 receptor (Kd = 2-4 nM) and does not have affinity for the CXCR1 receptor[15,78]. In this study, both ^{125}I-NAP-2 and ^{125}I-IL-8 localized in subcutaneous carrageenan-induced abscesses in rats[79]. In this model IL-8 gave the highest activity concentration in the inflamed tissue, while at later time points the lesion-to-control hindlimb ratios of NAP-2 were higher. Additionally, a comparative study has been performed where CXCR2 receptor-affinity of three NAP-2 analogs was compared with abscess uptake of the ^{99m}Tc-labeled NAP-2 compounds[80]. The results indicated that there was a relationship between affinity of the compounds and its uptake at the site of infection.

CONCLUSIONS

Nuclear Medicine infection and inflammation imaging techniques aim at visualization of infectious and inflammatory processes. Knowledge and understanding of biological, physiological pathways and molecular interactions of the human inflammatory response encourage the development of new imaging agents. Theoretically, these new agents could accumulate rapidly and specifically at the site of inflammation due to their interaction with the receptor expressed on activated or infiltrated immune cells. From the studies on chemokines and chemotactic receptor binding agents so far, it appears that not all chemotactic agents are suitable to serve as a vehicle for infection/inflammation imaging:

1. Some of these agents induce biological effects even at very low doses, impeding clinical application (e.g. fMLP, IL-1, C5a).
2. The uptake of various agents in the target is too low. This could be either due to the low affinity for the receptor, to unfavorable pharmacokinetics or to the low receptor density on involved immune cells (e.g. fMLP, NAP-2, C5adR).
3. The physiologic uptake in the lung or bowel may hamper visualization of foci in thorax or abdomen, respectively (e.g. ^{123}I-IL-1, ^{99m}Tc-P483H).

Fortunately, various chemotactic compounds indeed have shown rapid and high accumulation in infectious foci and fast background clearance in animal models. Additionally, improved labeling procedures result in high specific activities and by this means reduce biologic effects. Because of the diverse characteristics of the various chemotactic compounds studied so far in several animal models, it is difficult to predict which compound will have the most favorable imaging characteristics. The results with ^{99m}Tc-HYNIC-IL-8 in various rabbit models reveal positive future prospects. IL-2 already showed clinical potential to visualize inflammatory disorders in various specific patient populations. Because of the large number of mediators and analogs, the search for new radiopharmaceuticals will continue in future. Clinical studies are warranted to determine the potential of these new agents in specific patient populations with infectious or inflammatory disorders.

Significant research on the characteristics of chemotactic receptor binding ligands and clinical studies still have to be performed before an applicable, safe and appropriate radiopharmaceutical will become available. The success for the development of such a radiopharmaceutical will depend on the prolific cooperation of chemists, physicists, biological scientists and nuclear medicine specialists.

OUTLINE OF THIS THESIS

Nuclear Medicine infection and inflammation imaging techniques aim to visualize infectious and inflammatory processes to determine the localization and extension of the inflammatory foci in patients. Over the last decades many compounds were studies for this application, since the current standard radiopharmaceutical for this purpose – radiolabeled leukocytes- requires laborious preparation and is accompanied with hazardous risks.

Nowadays, there is a great interest in the development of radiolabeled chemotactic and chemokinetic cytokines that accumulate and are retained in infectious and inflammatory foci by specific interaction with infiltrated inflammatory cells. Chapter 1 describes the specific characteristics of the chemotactic and chemokinetic compounds that are currently studied as potential radiopharmaceutical to visualize infectious and inflammatory foci. The characteristics of a series of cytokines (IL-1, IL-2), chemokines (IL-8, PF-4, MCP-1, NAP-2), complement factors (C5a, C5adR), chemotactic peptides (fMLF) and other chemotactic factors are described. The potentials of these compounds to serve as an imaging agent are discussed.

In chapter 2 a basic study to determine the potential of the bivalent ^{111}In-labeled leukotriene B4 (LTB4) antagonist, DPC11870, is described. The LTB4 antagonist DPC11870 was labeled with ^{111}In and analyzed for the ability to visualize intramuscular *E. coli* infection in rabbits. In addition, it was investigated whether the visualization was due to receptor-mediated interaction at the site of the infection. Once specificity of ^{111}In-DPC11870 accumulation at the site of infection was established and the agent could be used to visualize infectious lesions, the applicability of this compound was determined in more clinically relevant animal models, in chapter 3 and chapter 4. The radiolabeled LTB4 antagonist was evaluated in a rabbit model of acute colitis and in a model of pulmonary aspergillosis infection. Results of the radiolabeled LTB4 antagonist were compared with ^{99m}Tc-labeled granulocytes and ^{67}Ga-citrate, the commonly used radiopharmaceuticals to visualize abdominal infection and pulmonary infection respectively, and with ^{18}F-FDG.

In the studies mentioned above, the results indicated that accumulation of ^{111}In-DPC11870 in the abscess continued while radioactivity had cleared from the circulation almost completely. As a consequence of this remarkable observation, we investigated the pharmacodynamics of ^{111}In-DPC11870 and performed several experiments to determine the mechanism of accumulation of the radiolabeled LTB4 antagonist in the abscess (chapter 5). The pharmacodynamics was studied by serial imaging and by ex vivo counting of dissected tissues. The mechanism of abscess visualization was investigated in

rabbits where intramuscular infection was induced 16 h *after* i.v. administration of ^{111}In-DPC11870. In addition, heterologous leukocytes and bone marrow cells of a donor rabbit were labeled with ^{111}In-DPC11870 in vitro and the biodistribution of these in vitro radiolabeled cells was compared with the biodistribution of ^{111}In-DPC11870.

Since ^{99m}Tc is a radionuclide with better imaging characteristics than ^{111}In (physical half-life, gamma-energy, availability), we developed two LTB4 antagonists that were structurally related to DPC11870 and could be labeled with ^{99m}Tc. In chapter 6 we describe the chemical synthesis of the bivalent DTPA conjugated LTB4 antagonist DPC11870, the bivalent HYNIC-conjugated analog MB81 and the monovalent HYNIC-conjugated LTB4 antagonist MB88. We investigated the labeling efficiency and in vivo characteristics of ^{99m}Tc-MB81 in a rabbit model of intramuscular *E. coli* infection after radiolabeling with three different coligand systems (Tricine, TPPTS or Isonicotinic acid). In chapter 7 the imaging characteristics and kinetics of both HYNIC-conjugated LTB4 antagonists, MB81 and MB88 were evaluated and compared with the characteristics of ^{111}In-DPC11870.

REFERENCES

1. Corstens FH, van der Meer JW. Nuclear medicine's role in infection and inflammation. Lancet 1999;354: 765-770
2. Peters AM. The use of nuclear medicine in infections. Br J Radiol 1998;71: 252-261
3. Weiner RE, Thakur ML. Imaging infection/inflammations. Pathophysiologic basis and radiopharmaceuticals. Q J Nucl Med 1999;43: 2-8
4. Rennen HJ, Corstens FH, Oyen WJ, Boerman OC. New concepts in infection/inflammation imaging. Q J Nucl Med 2001;45: 167-173
5. Signore A, Chianelli M, Bei R, Oyen WJ, and Modesti A. Targeting cytokine/chemokine receptors: a challenge for molecular nuclear medicine. Eur J Nucl Med Mol Imaging. 2003;30:149-56.
6. Weiner RE, Thakur ML. Radiolabeled peptides in diagnosis and therapy. Semin Nucl Med 2001;31: 296-311
7. Boerman OC, Dams ET, Oyen WJ, Corstens FH, Storm G. Radiopharmaceuticals for scintigraphic imaging of infection and inflammation. Inflamm Res 2001;50: 55-64
8. Janeway C. Immunobiology, 5th edition. 2001.
9. van der Laken CJ, Boerman OC, Oyen WJ, van de Ven MT, van der Meer JW, Corstens FH. Scintigraphic detection of infection and inflammation: new developments with special emphasis on receptor interaction. Eur J Nucl Med 1998;25: 535-546
10. Roitt I. Essential Immunology, 9th edition. 1997.
11. Sims JE, Gayle MA, Slack JL, Alderson MR, Bird TA, Giri JG, et al. Interleukin 1 signaling occurs exclusively via the type I receptor. Proc Natl Acad Sci U S A 1993;90: 6155-6159
12. Alberts B. Molecular Biology of the cell, 4th edition. 2002

13. Murphy PM. The molecular biology of leukocyte chemoattractant receptors. Annu Rev Immunol 1994;12: 593-633
14. Toda A, Yokomizo T, Shimizu T. Leukotriene B4 receptors. Prostaglandins Other Lipid Mediat 2002;68-69: 575-585
15. Rollins BJ. Chemokines. Blood 1997;90: 909-928
16. Hill SJ, Ganellin CR, Timmerman H, Schwartz JC, Shankley NP, Young JM, et al. International Union of Pharmacology. XIII. Classification of histamine receptors. Pharmacol Rev 1997;49: 253-278
17. Prado GN, Taylor L, Zhou X, Ricupero D, Mierke DF, Polgar P. Mechanisms regulating the expression, self-maintenance, and signaling- function of the bradykinin B2 and B1 receptors. J Cell Physiol 2002;193: 275-286
18. Ahluwalia A, Perretti M. B1 receptors as a new inflammatory target. Could this B the 1? Trends Pharmacol Sci 1999;20: 100-104
19. Voice JK, Dorsam G, Chan RC, Grinninger C, Kong Y, Goetzl EJ. Immunoeffector and immunoregulatory activities of vasoactive intestinal peptide. Regul Pept 2002;109: 199-208
20. Dorsam G, Voice J, Kong Y, Goetzl EJ. Vasoactive intestinal peptide mediation of development and functions of T lymphocytes. Ann N Y Acad Sci 2000;921: 79-91
21. Ishii S, Nagase T, Shimizu T. Platelet-activating factor receptor. Prostaglandins Other Lipid Mediat 2002;68-69: 599-609
22. Ishii S, Shimizu T. Platelet-activating factor (PAF) receptor and genetically engineered PAF receptor mutant mice. Prog Lipid Res 2000;39: 41-82
23. Hohmann HP, Remy R, Brockhaus M, van Loon AP. Two different cell types have different major receptors for human tumor necrosis factor (TNF alpha). J Biol Chem 1989;264: 14927-14934
24. Pandita R, Pocsik E, Aggarwal BB. Interferon-gamma induces cell surface expression for both types of tumor necrosis factor receptors. FEBS Lett 1992;312: 87-90.
25. Bast, R. C. Cancer Medicine 5th edition, section 16. 2000.
26. Evans JF. Cysteinyl leukotriene receptors. Prostaglandins Other Lipid Mediat 2002;68-69: 587-59.
27. Yano T, Zissel G, Muller-Qernheim J, Jae SS, Satoh H, Ichikawa T. Prostaglandin E2 reinforces the activation of Ras signal pathway in lung adenocarcinoma cells via EP3. FEBS Lett 2002;518: 154-15
28. Narumiya S, Sugimoto Y, Ushikubi F. Prostanoid receptors: structures, properties, and functions. Physiol Rev 1999;79: 1193-12.
29. Lombardi MS, Kavelaars A, Heijnen CJ. Role of modulators of G-protein-coupled receptor signaling in inflammatory processes. Crit Rev Immunol. 2002;22:141-163.
30. Onuffer JJ, Horuk R. Chemokines, chemokine receptors and small-molecule antagonists: recent developments. Trends Pharmacol Sci 2002;23: 459-467
31. van der Laken CJ, Boerman OC, Oyen WJ, van de Ven MT, Edwards DS, Barrett JA, et al. Technetium-99m-labeled chemotactic peptides in acute infection and sterile inflammation. J Nucl Med 1997;38: 1310-1315
32. International Union of Immunological Societies/World Health Organization Subcommittee on Chemokine nomenclature. Chemokine/chemokine receptor nomenclature. J Leukoc Biol 2001;70: 465-466
33. Boulay F, Tardif M, Brouchon L, Vignais P. The human N-formylpeptide receptor. Characterization of two cDNA isolates and evidence for a new subfamily of G-protein-coupled receptors. Biochemistry 1990;29: 11123-11133
34. Le Y, YangY, Cui Y, Yazawa H, Gong W, Qiu C, et al. Receptors for chemotactic formyl peptides as pharmacological targets. Int Immunopharmacol 2002;2: 1-13

35. McAfee JG, Subramanian G, Gagne G. Technique of leukocyte harvesting and labeling: problems and perspectives. Semin Nucl Med 1984;14: 83-106

36. Fischman AJ, Pike MC, Kroon D, Fucello AJ, Rexinger D, ten Kate C, et al. Imaging focal sites of bacterial infection in rats with indium-111- labeled chemotactic peptide analogs. J Nucl Med 1991;32:483-491.

37. Pollak A, Goodbody AE, Ballinger JR, Duncan GS, Tran LL, Dunn-Dufault R, et al. Imaging inflammation with 99mTc-labeled chemotactic peptides: analogues with reduced neutropenia. Nucl Med Commun 1996;17: 132-139

38. Babich JW, Tompkins RG, Graham W, Barrow SA, Fischman AJ. Localization of radiolabeled chemotactic peptide at focal sites of Escherichia coli infection in rabbits: evidence for a receptor-specific mechanism. J Nucl Med 1997;38: 1316-1322

39. Edwards DS, Liu S, Ziegler MC, Harris AR, Crocker AC, Heminway SJ, et al. RP463: a stabilized technetium-99m complex of a hydrazino nicotinamide derivatized chemotactic peptide for infection imaging. Bioconjug Chem 1999;10: 884-891

40. Verbeke K, Verbeke A, Vanbilloen H, Verbruggen A.Preparation and preliminary evaluation of 99mTc-EC-For-MLFK. Nucl Med Biol 2002;29: 585-59

41. Schrader JW. Interleukin is as interleukin does. Trends Immunol 2002;23: 573-574

42. van der Laken CJ, Boerman OC, Oyen WJ, van de Ven MT, van der Meer JW, Corstens FH. Imaging of infection in rabbits with radioiodinated interleukin-1 (alpha and beta), its receptor antagonist and a chemotactic peptide: a comparative study. Eur J Nucl Med 1998;25: 347-352

43. Barrera P, van der Laken CJ, Boerman OC, Oyen WJ, van de Ven MT, van Lent PL, et al. Radiolabelled interleukin-1 receptor antagonist for detection of synovitis in patients with rheumatoid arthritis. Rheumatology (Oxford) 2000;39: 870-874

44. Smith KA. Interleukin-2: inception, impact, and implications. Science 1988;240: 1169-1176

45. Chianelli M, Mather SJ Martin-Comin J, Signore A. Radiopharmaceuticals for the study of inflammatory processes: a review. Nucl Med Commun 1997;18: 437-455

46. Signore A, Chianelli M, Toscano A, Monetini L, Ronga G, Nimmon CC, et al. A radiopharmaceutical for imaging areas of lymphocytic infiltration: 123I-interleukin-2. Labelling procedure and animal studies. Nucl Med Commun 1992;13: 713-722

47. Rolandsson O, Stigbrand T, Riklundahlstrom K, Eary J, Greenbaum C. Accumulation of 125-iodine labeled interleukin-2 in the pancreas of NOD mice. J Autoimmun 2001;17: 281-287

48. Signore A, Chianelli M, Annovazzi A, Bonanno E, Spagnoli LG, Pozzilli P et al. 123I-interleukin-2 scintigraphy for in vivo assessment of intestinal mononuclear cell infiltration in Crohn's disease. J Nucl Med 2000;41: 242-249

49. Signore A, Chianelli M, Annovazzi A, Rossi M, Maiuri L, Greco M et al. Imaging active lymphocytic infiltration in coeliac disease with iodine- 123-interleukin-2 and the response to diet. Eur J Nucl Med 2000;27: 18-24

50. Chianelli M, Signore A, Fritzberg AR, Mather SJ. The development of technetium-99m-labelled interleukin-2: a new radiopharmaceutical for the in vivo detection of mononuclear cell infiltrates in immune-mediated diseases. Nucl Med Biol 1997;24: 579-586

51. Annovazzi A., Biancone L, Caviglia R, Chianelli M, Capriotti G, Mather SJ, et al. 99mTc-interleukin-2 and 99mTc-HMPAO granulocyte scintigraphy in patients with inactive Chron's disease. Eur J Nucl Med Mol Imaging. 2003 Mar;30(3):374-82.

52. Luster AD. Chemokines-chemotactic cytokines that mediate inflammation. N Engl J Med 1998;338: 436-445

53. Baggiolini M, Dahinden CA. CC chemokines in allergic inflammation. Immunol Today 1994;15: 127-133

54. Baggiolini M, Dewald B, Moser B. Interleukin-8 and related chemotactic cytokines-CXC and CC chemokines. Adv Immunol 1994;55: 97-179

55. Hay RV, Skinner RS, Newman OC, Kunkel SL, Lyle LR, Shapiro B, et al. Scintigraphy of acute inflammatory lesions in rats with radiolabelled recombinant human interleukin-8. Nucl Med Commun 1997;18: 367-378

56. Gross MD, Shapiro B, Fig LM, Steventon R, Skinner RW, Hay RV. Imaging of human infection with 131I-labeled recombinant human interleukin-8. J Nucl Med 2001;42: 1656-1659

57. Gratz S, Rennen HJ, Boerman OC, Oyen WJ, Corstens FC. Rapid imaging of experimental colitis with 99mTc-interleukin-8 in rabbits. J Nucl Med 2001;42: 917-923

58. Rennen HJ, Boerman OC, Oyen WJ, van der Meer JW, Corstens FH. Specific and rapid scintigraphic detection of infection with 99mTc- labeled interleukin-8. J Nucl Med 2001;42: 117-123

59. van der Laken CJ, Boerman OC, Oyen WJ, van de Ven MT, van der Meer JW, Corstens FH. Radiolabeled interleukin-8: specific scintigraphic detection of infection within a few hours. J Nucl Med. 2000;41(3):463-9.

60. Clark-Lewis I, Dewald B, Geiser T, Moser B, Baggiolini M. Platelet factor 4 binds to interleukin 8 receptors and activates neutrophils when its N terminus is modified with Glu-Leu-Arg. Proc Natl Acad Sci USA 1993;90: 3574-3577

61. Moyer BR, Vallabhajosula S, Lister-James J, Bush LR, Cyr JE, Snow DA et al. Technetium-99m-white blood cell-specific imaging agent developed from platelet factor 4 to detect infection. J Nucl Med 1996;37: 673-679

62. Palestro CJ Weiland FL, Seabold JE, Valdivia S, Tomas MB, Moyer BR et al. Localizing infection with a technetium-99m-labeled peptide: initial results. Nucl Med Commun 2001;22: 695-701

63. Rennen HJ, Oyen WJ, Cain S, Monk P, Corstens FH, and Boerman OC. Tc-99m-labeled C5a and C5a-des-Arg74 for infection imaging. Nucl Med Biol 2003 (in press)

64. Marder SR, Chenoweth DE, Goldstein IM, Perez HD. Chemotactic responses of human peripheral blood monocytes to the complement-derived peptides C5a and C5a des Arg. J Immunol 1985;134: 3325-3331

65. Ford-Hutchinson AW. Leukotriene B4 in inflammation. Crit Rev Immunol 1990;10: 1-12

66. Serhan CN, Prescott SM. The scent of a phagocyte: Advances on leukotriene B(4) receptors. J Exp Med 2000;192: F5-F8

67. Yokomizo T, Izumi T, Shimizu T. Leukotriene B4: metabolism and signal transduction. Arch Biochem Biophys 2001;385: 231-241

68. Yokomizo T, Izumi T, Chang K, Takuwa Y, Shimizu T. A G-protein-coupled receptor for leukotriene B4 that mediates chemotaxis. Nature 1997;387: 620-624

69. Yokomizo T, Kato K, Terawaki K, Izumi T, Shimizu T. A second leukotriene B4 receptor, BLT2. A new therapeutic target in inflammation and immunological disorders. J Exp Med 2000;192: 421-432

70. Barrett JA, Harris TD, Heminway S. Novel technetium-99m labeled Leukotriene B4 antagonists as potential inflammation/infection imaging agents. J Nucl Med 1998;39:215P.

71. Liu S, Harris AR, Williams NE, Edwards DS. 99mTc-Labeling of a Hydrazinonicotinamide-Conjugated LTB4 Receptor Antagonist Useful for Imaging Infection and Inflammation. Bioconjug Chem 2002;13: 881-886

72. Brouwers AH, Laverman P, Boerman OC, et al. A 99Tcm-labelled leukotriene B4 receptor antagonist for scintigraphic detection of infection in rabbits. Nucl Med Commun 2000;21: 1043-1050

73. Bischoff SC, Krieger M, Brunner T, Dahinden CA. Monocyte chemotactic protein 1 is a potent activator of human basophils. J Exp Med 1992;175: 1271-1275

74. Beall CJ, Mahajan S, Kolattukudy PE. Conversion of monocyte chemoattractant protein-1 into a neutrophil attractant by substitution of two amino acids. J Biol Chem 1992;267: 3455-3459

75. Sarau HM, Rush JA, Foley JJ, Brawner ME, Schmidt DB, White JR, et al. Characterization of functional chemokine receptors (CCR1 and CCR2) on EoL-3 cells: a model system to examine the role of chemokines in cell function. J Pharmacol Exp Ther 1997;283: 411-418

76. Moore UM, Kaplow JM, Pleass RD, Castro SW, Naik K, Lynch CN, et al. Monocyte chemoattractant protein-2 is a potent agonist of CCR2B. J Leukoc Biol 1997;62: 911-915

77. Blankenberg FG, Tait JF, Blankenberg TA, Post AM, Strauss HW. Imaging macrophages and the apoptosis of granulocytes in a rodent model of subacute and chronic abscesses with radiolabeled monocyte chemotactic peptide-1 and annexin V. Eur J Nucl Med 2001;28: 1384-1393

78. Loetscher P, Seitz M, Clark-Lewis I, Baggiolini M, Moser B. Both interleukin-8 receptors independently mediate chemotaxis. Jurkat cells transfected with IL-8R1 or IL-8R2 migrate in response to IL-8, GRO alpha and NAP-2. FEBS Lett 1994;341: 187-192

79. Hay RV, Skinner RS, Newman OC, Kunkel SL, Lyle LR, Shapiro B, et al. Scintigraphy of acute inflammatory lesions in rats with radiolabelled recombinant human neutrophil-activating peptide-2. Nucl Med Commun 2002;23: 367-372

80. Rennen HJ, Frielink C, Brandt E, Zaat SA, Boerman OC, Oyen WJ, Corstens FH. Relationship between neutrophil-binding affinity and suitability for infection imaging: comparison of (99m)Tc-labeled NAP-2 (CXCL-7) and 3 C-terminally truncated isoforms. J Nucl Med. 2004 Jul;45(7):1217-23.

81. Rennen HJ, Bleeker-Rovers CP, van Eerd JE, Frielink C, Oyen WJ, Corstens FH, Boerman OC. ^{99m}Tc-Labeled Interleukin-8 for Scintigraphic Detection of Pulmonary Infections.Chest. 2004 Dec;126:1954-61.

82. Signore A, Annovazzi A, Barone R, Bonanno E, D'Alessandria C, Chianelli M, Mather SJ, Bottoni U, Panetta C, Innocenzi D, Scopinaro F, Calvieri S. ^{99m}Tc-interleukin-2 scintigraphy as a potential tool for evaluating tumor-infiltrating lymphocytes in melanoma lesions: a validation study. J Nucl Med. 2004 Oct;45(10):1647-52.

Chapter 2

A Bivalent Leukotriene B4 Antagonist for Scintigraphic Imaging of Infectious Foci.

Julliëtte J.E.M. van Eerd
Wim J.G. Oyen
Thomas D. Harris
Huub J.J.M. Rennen
D. Scott Edwards
Shuang Liu
Charles E. Ellars
Frans H.M. Corstens
Otto C. Boerman

J Nucl Med. 2003;44:1087-1091

ABSTRACT

Several radiolabeled chemotactic peptides have been tested for their suitability to visualize infection and inflammation. Leukotriene B4 (LTB4) receptor binding ligands could be useful agents to visualize neutrophilic infiltrations since the LTB4 receptor is abundantly expressed on neutrophils after an inflammatory stimulus. In this study we investigated the in vivo and in vitro characteristics of a new hydrophilic ^{111}In-labeled LTB4 antagonist.

Methods: The LTB4 antagonist DPC11870 was labeled with ^{111}In and i.v. injected in New Zealand White rabbits with *E. coli* infection in the left thigh muscle. The pharmacokinetics and biodistribution were studied by serial scintigraphic imaging (0-24 h p.i.) and by ex vivo counting of dissected tissues (6, 24 h p.i.). The receptor-mediated in vivo localization of the compound was investigated in three rabbits that received an excess of non-radioactive In-labeled agent, two minutes prior to the administration of the ^{111}In-labeled LTB4 antagonist.

Results: In rabbits with intramuscular *E. coli* infection the abscess was visualized as early as 2 h after injection. Accumulation in the abscess increased with time resulting in excellent images at 6 h p.i.. Blood clearance was rapid in the first hours after injection (t½α =30±6 min, 85%, t½β =25.7±0.8 h, 15%). Abscess-to-background ratios, as derived from the ROI analysis, increased up to 34±7 at 24 h p.i. The images of both groups showed moderate uptake in liver, spleen, kidneys and bone marrow. No activity was seen in the bladder, indicating almost complete retention in the kidneys. The uptake in the abscess could be blocked completely by injection of an excess of non-radioactive agent, indicating specific receptor-ligand interaction of the radiolabeled agent in the infected tissue. Biodistribution data showed that after saturation of the LTB4 receptor the abscess uptake was significantly reduced (0.08±0.01 %ID/g vs. 0.24±0.06 %ID/g, p =0.008).

Conclusion: The modified LTB4 antagonist, DPC11870, visualized infectious foci rapidly after injection due to specific receptor-ligand interaction. Because of the high abscess-to-background ratios that were obtained and the fact that no accumulation of radioactivity was observed in the gastro-intestinal tract, this compound has good characteristics to visualize infectious and inflammatory foci.

INTRODUCTION

For the scintigraphic imaging of infection and inflammation, the use of radiolabeled autologous leukocytes is considered the gold standard. Since the preparation of radiolabeled white blood cells is laborious and requires handling of potentially contaminated blood, there is an ongoing search for an agent that is capable to visualize infectious and inflammatory foci, and that can be prepared instantaneously[1]. Ideally, such a radiopharmaceutical preferably would be synthesized chemically instead of using material with a biologic origin. Furthermore, these compounds should be easily and rapidly radiolabeled and would not provoke immunological responses[2]. A number of compounds have been tested for this application e.g., radiolabeled antibodies, liposomes, and receptor binding peptides[3,4].

The use of radiolabeled chemotactic peptides as an infection-imaging agent is based on the enhanced expression of high affinity receptors on infiltrating granulocytes activated after an inflammatory response. Several of these peptides (chemokines, platelet factor 4, fMLP and other chemotactic compounds) have been studied for the detection of infection and/or inflammation[5].

In this study, we examined the characteristics of an ^{111}In-labeled leukotriene B4 (LTB4) antagonist for its potential to visualize infectious foci scintigraphically. LTB4 is a very potent chemoattractant that activates granulocytes and macrophages as a reaction to an inflammatory response[6,7]. At the site of the inflammation, enhanced LTB4 synthesis occurs mainly by leukocytes from arachidonic acid via the 5-lipoxygenase pathway[8]. LTB4 responses are receptor mediated, and two classes of stereospecific binding sites for LTB4 have been identified. The first type of receptor, BLT1 is a high affinity receptor (Kd for LTB4 is 1 nM) mainly expressed on human neutrophils[9]. The second receptor type, BLT2 is a low affinity receptor (Kd for LTB4 is 23 nM) that is more ubiquitously expressed[6,10]. Binding of LTB4 to BLT1 and BLT2 receptors promotes chemotaxis and chemokinesis. Therefore, LTB4 is considered to be an important mediator in both acute and chronic inflammatory diseases[9,11].

In a previous study we showed the potential of a ^{99m}Tc-labeled LTB4 antagonist, RP517, for its ability to visualize experimental infection[12-14]. The disadvantage of RP517, however, was its hepatobiliary clearance, causing high uptake in the organs of the digestive tract, relatively early after injection. This gastrointestinal uptake of RP517 limits its applicability as an infection imaging agent[12].

Since the radiolabeled LTB4 antagonist showed rapid and high accumulation in the infected tissue, we produced a hydrophilic bivalent LTB4 antagonist conjugated with a

diethylenetriaminepentaacetic acid (DTPA) moiety to allow radiolabeling with ^{111}In. In the present study, the leukocyte binding characteristics of this modified bivalent LTB4 antagonist was studied both in vitro and in vivo.

MATERIALS AND METHODS

DPC11870 synthesis

DPC11870 (Fig.1) is a bivalent LTB4 antagonist consisting of two identical LTB4 receptor-binding moieties each modified with four cysteic acid as pharmacokinetic modifiers. The LTB4-binding moieties are joined via the carboxyl groups of glutamic acid and conjugated with DTPA.

A complete description of the synthesis of DPC11870 will be described elsewhere. Briefly, the tetra-cysteic acid derivative of SG385 prepared as reported previously[15] was dimerized by reaction with the bis-TFP ester of Boc-glutamic acid. Removal of the Boc group and conjugation with DTPA anhydride gave crude DPC11870. The product was further purified by RP-HPLC. RP-HPLC analysis on a C18 column eluted with a 0.5%/min acetonitril gradient of the purified and lyophilized product gave a single peak. The purified DPC11870 was characterized further by NMR and Mass Spectrometry.

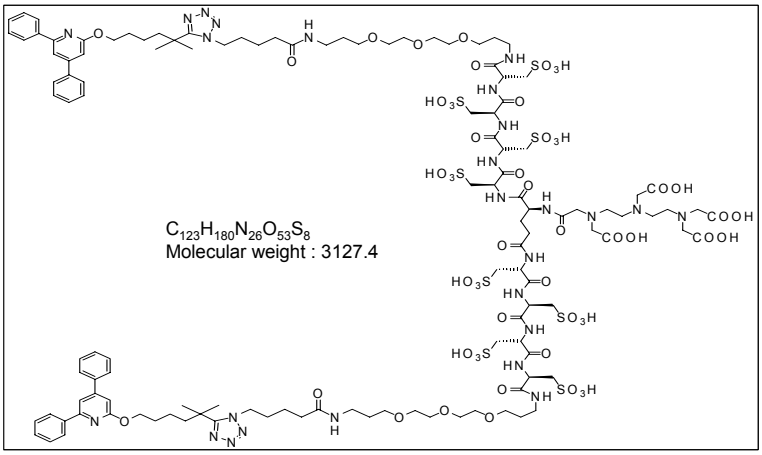

Figure 1.
Structural formula of DPC11870.

Radiolabeling of DPC11870

Labeling of DPC11870 with ^{111}In was performed in metal-free 0.25 M ammonium acetate buffer, pH 5.5 for 30 min at room temperature. Labeling experiments were performed in order to determine the maximum specific activity of the radiolabeled agent. Radiochemical

purity was checked by ITLC on silica gel strips (Gelman Sciences, Inc., Ann Arbor, MI) in 0.1 M Na-citrate buffer, pH 6.0. Strips were analyzed in a well-type gamma counter (Wizard, Pharmacia-LKB, Uppsala, Sweden). In addition, RP-HPLC was performed on a C18 column (Zorbax Rx-C18 4.6 mm x 25 cm) on a Agilent 1100 system equipped with an in-line radiodetector (Canberra Packard, Brussels, Belgium). During analysis, a gradient was used from 100 % solvent NH_4Ac, pH 7.0 to 100 % acetonitrile in 50 minutes, at a flow rate of 1 mL/min.
Labeling with non-radioactive $InCl_3$ (Aldrich, Milwaukee, WI) was performed under the same conditions as described above. A three-fold molar excess of $InCl_3$ was added to DPC11870 in ammonium acetate buffer, pH 5.5.

Receptor Binding Assay
In vitro binding studies were performed on purified human granulocytes. The granulocytes were purified as described previously[16]. To 1 x 10^8 cells increasing amounts of non-radioactive In-DPC11870 (0-10 µM) were added in the presence of 10,000 cpm ^{111}In-DPC11870 (0.4 nM) in 0.25 M Tris/HCl, pH 7.2. After incubation during 1 h at 37°C, cells were washed twice (5 min, 5000 x g), supernatant was discarded and the radioactivity in the pellet (total bound activity) was measured in a shielded well-type gamma counter (Wizard, Pharmacia-LKB, Uppsala, Sweden).
The specifically bound fraction versus the non-radioactive LTB4 antagonist concentration was plotted. The IC50 (50% inhibitory concentration) was determined as being the concentration of non-radioactive In-DPC11870 that caused 50% inhibition of the maximum binding of the ^{111}In-DPC11870.

Infection Model
Thirteen female New Zealand White rabbits weighing 2.3-2.8 kg were kept in cages (one rabbit per cage) and fed standard laboratory chow and water ad libitum. An *E. coli* infection was induced in the left thigh muscle by intramuscular injection of 4 x 10^9 colony-forming units (CFU) of *E. coli*. During this procedure the rabbits were anaesthetized by subcutaneous injection of 0.7 mL of a mixture of 0.315 mg/mL fentanyl and 10 mg/mL fluanison (Hypnorm®, Janssen Pharmaceutica, Buckinghamshire, UK). All animal experiments were approved by the local animal welfare committee in accordance with the Dutch legislation and carried out in accordance with their guidelines.

Imaging and Biodistribution

Twenty-four hours after the induction of the infection, when swelling of the infected muscle was apparent, thirteen rabbits were intravenously injected with 11 MBq ^{111}In-DPC11870 (3 µg) in the lateral ear vein. Three rabbits received 2 mg non-radioactive In-DPC11870 two minutes prior to the injection of the radiolabeled compound. The excess of non-radioactive agent was injected to induce saturation of the LTB4 receptors in vivo. This experiment was performed in order to determine receptor-specific accumulation of ^{111}In-DPC11870 in the abscess.

For scintigraphic imaging, the rabbits were immobilized in a mold and placed prone on a gamma camera (Orbiter, Siemens, Hoffman Estates, IL) using a medium-energy parallel hole collimator. Images (300,000 cts/image) were obtained up to 24 h post injection (p.i.) and stored digitally in a 256x256 matrix. All images were windowed identically, allowing a fair comparison among the various experiments. The scintigraphic results were analyzed by drawing regions of interest (ROI) over the abscess and the contralateral muscle (background). Abscess-to-contralateral muscle ratios were calculated.

The three rabbits that received an excess of non-radioactive agent and five rabbits, only injected with radiolabeled antagonist were euthanized at 6 h p.i. with a lethal dose of sodium phenobarbital to determine the biodistribution of the agent. At 24 h p.i. the other five rabbits were euthanized. A blood sample was taken by cardiac puncture. Tissues were dissected and weighed. The activity in tissues was measured in a shielded well-type gamma counter together with the injection standards and was expressed as the percentage of the injected dose per gram (%ID/g).

Pharmacokinetics

The pharmacokinetics of the ^{111}In-labeled agent were studied in detail in two rabbits that were injected with the ^{111}In-DPC11870 and two rabbits that received an excess of non-radioactive DPC11870, prior to the ^{111}In-DPC11870. Blood samples were drawn at –1, 3, 15, 30, 90, 120, 240, 360 and 1440 min p.i. The activity in the samples was determined in a gamma counter and expressed as a percentage of injected dose assuming that the total blood weight accounted for 6% of total body weight[17]. The t½α and t½β were calculated assuming a two-phase linear model for the blood clearance. In addition, blood samples were divided into two portions; one tube was used for white blood cell analysis, the second tube was centrifuged (5 min, 1500 x g) and activity in the pellet and plasma were determined. ^{111}In-DPC11870 and the plasma samples were analyzed by Fast Protein Liquid Chromatography (FPLC) on a Biosep 3000 gelfiltration column (Phenomenex), using Phosphate Buffered Saline, pH 7.2 (PBS) as eluens, 1 mL/min.

Statistical Analysis

All mean values are presented as mean ± standard deviation. Statistical analysis was performed using the two-sided Student t-test. The level of significance was set at 0.05.

RESULTS

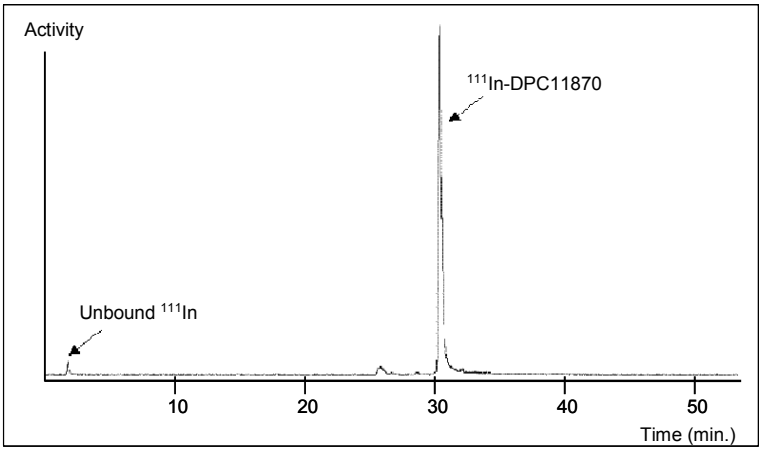

Figure 2.
HPLC radiogram of ^{111}In-DPC11870 using a C18 RP-HPLC column eluted with a 5%/min acetonitrile gradient.

Radiolabeling and Receptor Binding Studies

The RP-HPLC radioactivity elution profile showed that the unbound ^{111}In eluted with the void volume with a retention time (Rt) of 2.5 min, whereas the labeled compound eluted with a Rt of 30.1 min (51% acetonitrile) (Fig. 2).

RP-HPLC analysis showed that the maximum specific activity achieved with a labeling efficiency exceeding 95% was 3.7 MBq/µg DPC11870 (12 MBq/nmol).

The IC50 of DPC11870 was 10 nM. Nonspecific binding was determined as the binding of ^{111}In-DPC11870 to granulocytes in presence of 10 µM non-radioactive In-DPC11870. The nonspecific binding of ^{111}In-DPC11870 to the granulocytes was relatively high (40%). The competitive binding assay was also carried out using human lymphocytes and erythrocytes. ^{111}In-DPC11870 did not bind specifically to these cell types. The amount of ^{111}In-DPC11870 bound to these cells (incubated in presence and absence of non-radioactive In-DPC11870) did not exceed 5%.

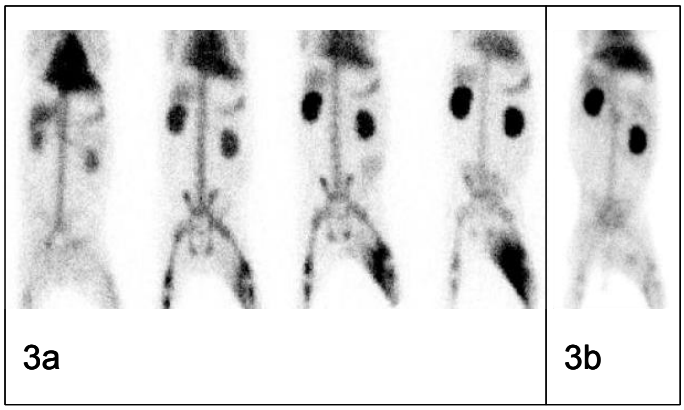

Figure 3.

3a. Scintigraphic images of a rabbit E. coli thigh muscle infections. The rabbits received 3 µg, 11 MBq ^{111}In-DPC11870 intravenously. Anterior images were acquired immediately, 2, 6 and 24 h after injection of ^{111}In-DPC11870. 3b. Scintigraphic image of a rabbit that received 2 mg non-radioactive In-DPC11870 before the injection of the ^{111}In-labeled LTB4 antagonist. This anterior image was acquired 6 h after injection of the radiolabel.

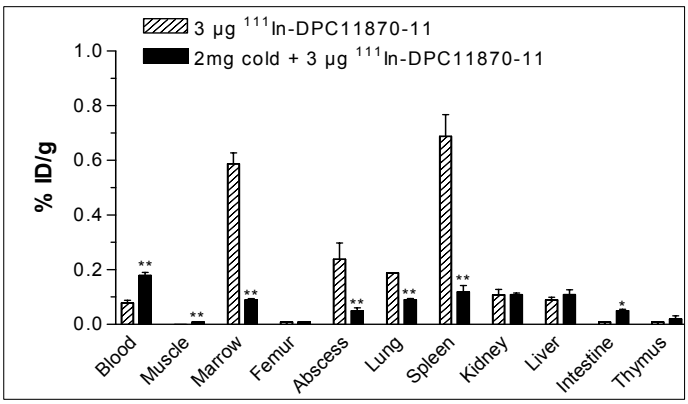

Figure 4.

*Biodistribution data obtained 6 hours postinjection of ^{111}In-DPC11870. Each bar represents the mean values ± SD. Values were analyzed using a unpaired T-test; * = P < 0.05, ** = P < 0.01. P-values refer to differences in uptake of radiolabel between rabbits also injected with 2 mg non-radioactive LTB4 antagonist, compared with rabbits only injected with the radiolabeled compound (3 µg).*

Imaging and Biodistribution

The scintigraphic images after the injection of ^{111}In-DPC11870 are shown in Fig. 3. Immediately after injection of the radiolabeled LTB4 antagonist, accumulation of radioactivity was observed in lung, liver and kidneys. Subsequently, accumulation of activity was seen in spleen and bone marrow.

As early as two hours after injection the infectious foci were visualized. Visualization of the abscess improved with time. At 24 h p.i. the abscess and kidneys were the tissues with the highest activity concentration. No activity was seen in the bladder at any time point. In

addition, there was no visualization of the digestive tract, indicating that the compound was not cleared via the hepatobiliary route (Fig. 3a). Abscess-to-contralateral muscle ratios as derived from ROI analysis of the images increased significantly between 6 h p.i. (18±4) and 24 h p.i. (34±7) (p=0.022). In the rabbits pre-injected with an excess of non-radioactive In-DPC11870 the infected thigh muscle was not visualized, indicating that abscess uptake of ^{111}In-DPC11870 was receptor-mediated (Fig. 3b).

The biodistribution data derived from ex vivo counting of dissected tissues as summarized in Fig. 4, were consistent with the scintigraphic images. Uptake of ^{111}In-DPC11870 in the abscess, at 6 h p.i. was 0.24±0.06 %ID/g and remained constant until 24 h p.i. (0.25±0.02 %ID/g). The radioactivity concentrations in the blood at 6 and 24 h p.i were 0.09±0.03 %ID/g and 0.03±0.01 %ID/g, respectively. Uptake in bone marrow and spleen was relatively high; (0.59±0.04 %ID/g and 0.69±0.08 %ID/g, respectively at 6 h p.i.), while uptake in the other tissues was relatively low.

In the rabbits pre-injected with an excess of non-radioactive In-DPC11870, the uptake of radiolabel in the abscess was significantly lower (0.03±0.02 %ID/g versus 0.24±0.06 %ID/g, p< 0.004). Uptake in the spleen and the bone marrow was also significantly lower in these animals (0.09±0.01 %ID/g versus 0.69±0.08 %ID/g, p< 0.0003, and 0.12±0.04 %ID/g versus 0.59±0.04 %ID/g, p<0.002 respectively). The blood levels in these animals were significantly higher (0.18±0.02 %ID/g versus 0.09±0.03 %ID/g, p < 0,004).

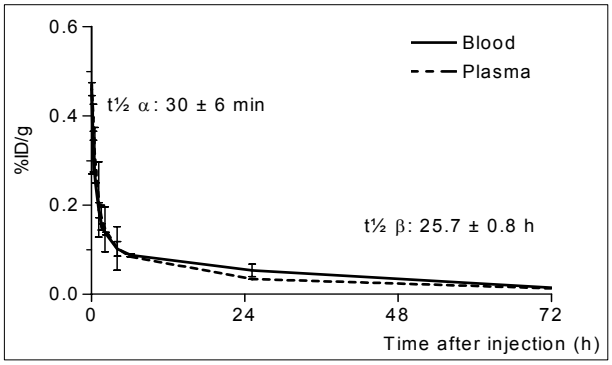

Figure 5.
Blood clearance of ^{111}In-DPC11870 in NZW rabbits. The average amount and SD of activity of two rabbits are expressed as %ID/g present in the blood and plasma. Plasma concentration was corrected using the hematocrit of the animals.

Pharmacokinetics

In Fig. 5a the radioactivity concentrations in the blood after injection of ^{111}In-DPC11870 are depicted. In the first hours after injection of the radiolabeled compound the clearance was fast (t½α 30±6 min, 85%), at later time points the compound cleared from the blood much more slowly (t½β 25.7±0.8 h, 15%). Considering the molecular weight of the agent,

the t½β is remarkably high, suggesting association to blood cells or serum proteins. Measurement of plasma samples demonstrated that more than 98% of the radioactivity was found in the plasma (Fig. 5). FPLC analysis of plasma samples on a gel filtration column showed one radioactive peak at 11 min, co-eluting with proteins with a molecular weight 50-100 kDa. Incubation of the ^{111}In-labeled compound in PBS with 0.5% bovine serum albumin (BSA) and analysis with FPLC on a gel filtration column, resulted in elution patterns with one activity peak with a retention time corresponding with BSA (11 min). Neither the rabbits injected with ^{111}In-DPC11870 nor animals injected with ^{111}In-DPC11870 and excess of non-radioactive compound showed significant changes in white blood cell counts. As shown in figure 6, the white blood cell concentration before injection of the ^{111}In-DPC11870, was 7.6±3.3x10^9/L and at all time points postinjection, the cell concentration was within the normal range (3.2-13.2x10^9/L). This indicated that this LTB4 antagonist did not induce changes in peripheral leukocyte counts.

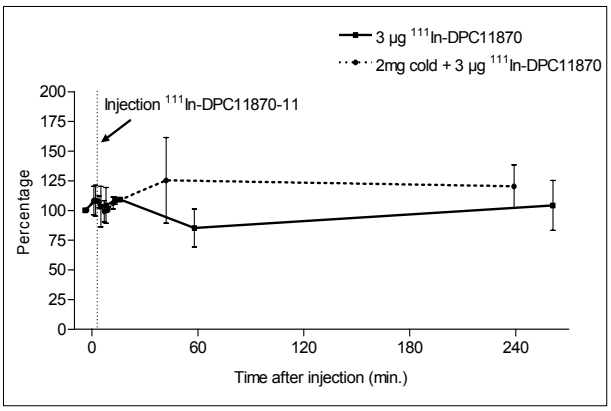

Figure 6.
White blood cell counts after injection of the ^{111}In-DPC11870. The initial amount of white blood cells is represented as 100 %. The number of cells determined after injection is calculated as percentage of this initial value.

DISCUSSION

The present studies demonstrated that DPC11870 can be labeled with ^{111}In easily and efficiently, resulting in a high specific activity and high radiochemical purity. The IC50, determined at 10 nM, indicated that ^{111}In-DPC11870 binds to its receptor with high affinity. The in vitro receptor binding results suggest that ^{111}In-DPC11870 accumulates in infected tissue by binding to LTB4 receptor-positive cells. The in vivo imaging experiments showed that the ^{111}In-labeled LTB4 antagonist was able to visualize *E. coli* infection in rabbits already a few hours after the injection. Due to rapid blood clearance in the first hours after the injection low background activity was seen which, in combination with the rapid

accumulation at the site of infection, resulted in excellent visualization of the infectious foci at 6 h p.i. The activity concentration in the infectious foci did not increase from 6 to 24 h. Improvement of contrast in the images at 24 h p.i. was due to the ongoing activity clearance from the background. The relatively high uptake of radiolabel in the bone marrow is remarkable. Apparently, the compound easily enters the bone marrow compartment, where it may bind to LTB4 receptor-positive cells.

Administration of excess of non-radioactive In-labeled compound indicated that the targeting of infectious foci was a result of specific receptor-ligand interaction. The in vivo receptor blocking experiments also indicated that the targeting of cells in the bone marrow and spleen was dependent on interaction with receptor-positive cells. These findings are in accordance with those of Yokomizo *et al.*[18] who showed that highest expression of human BLT1 mRNA was observed in leukocytes, followed by cells in the spleen and thymus.

Compared to the images obtained with the more lipophilic agent RP517, there was no accumulation in the gastro-intestinal tract[12]. Abscess uptake for ^{111}In-DPC11870 was higher at all time points as compared to that of ^{99m}Tc-RP517 (0.035±0.007 %ID/g at 4 h p.i., 0.12±0.02%ID/g at 20 h p.i.). On the other hand, blood levels of ^{99m}Tc-RP517 were lower (0.024±0.004 %ID/g at 4 h p.i, 0.004±0.0004 %ID/g at 20 h p.i.), resulting in lower background activity. In this animal model abscess-to-contralateral muscle ratios were in the same range for both agents.

Pharmacokinetic analysis showed that the compound cleared from the blood rapidly in the first hours after administration. The distribution half-life ($t_{1/2\alpha}$) was in accordance with the low molecular weight of the compound. A fraction of the radiolabeled agent (15%), however, seemed to clear more slowly from the blood ($t_{1/2\beta}$ = 25.7 h) which is unusual for a low molecular weight compound (molecular weight: 3,127 Da). This slow clearance may be due to interaction of the radiolabeled agent with serum proteins[19]. The FPLC analysis of plasma samples indeed showed that ^{111}In-DPC11870 interacted with albumin.

Radiolabeled chemotactic peptides have been intensively studied for their applicability to image infectious and inflammatory foci. Their theoretically high affinity for blood cell receptors, good penetrating ability and rapid background clearance suggest that they are ideal candidates for this application. A main disadvantage of some chemotactic and chemoattractive compounds is the induction of transient leukopenia after i.v. injection[4]. The data in this study show that In-DPC11870 does not provoke any of these changes in rabbits, even at very high doses (2 mg). Therefore, it seems unlikely that the LTB4 antagonist used in this study will provoke side effects after i.v. administration in patients.

CONCLUSION

The present study demonstrates that the radiolabeled bivalent LTB4 antagonist, DPC11870 meets the most important requirements of a radiopharmaceutical to visualize infection and inflammation. The agent visualizes infectious foci within a few hours after injection. The compound can be labeled easily and efficiently, does not provoke hematological changes in the peripheral blood and can be produced relatively easy via chemical synthesis.

Because of these findings, further in vitro and in vivo studies are warranted, preferably with an analog that can be labeled with ^{99m}Tc. Attempts to replace the DTPA moiety with a ^{99m}Tc-chelating moiety will be undertaken.

REFERENCES

1. Boerman OC, Dams ET, Oyen WJ, Corstens FH, Storm G. Radiopharmaceuticals for scintigraphic imaging of infection and inflammation. Inflamm Res. 2001;50:55-64.
2. Chianelli M, Mather SJ, Martin-Comin J, Signore A. Radiopharmaceuticals for the study of inflammatory processes: a review. Nucl Med Commun. 1997;18:437-455.
3. Corstens FH, van der Meer JW. Nuclear medicine's role in infection and inflammation. Lancet. 1999;354:765-770.
4. Weiner RE, Thakur ML. Radiolabeled peptides in diagnosis and therapy. Semin Nucl Med. 2001;31:296-311.
5. Weiner RE, Thakur ML. Imaging infection/inflammations. Pathophysiologic basis and radiopharmaceuticals. Q J Nucl Med. 1999;43:2-8.
6. Ford-Hutchinson AW. Leukotriene B4 in inflammation. Crit Rev Immunol. 1990;10:1-12.
7. Claesson HE, Odlander B, Jakobsson PJ. Leukotriene B4 in the immune system. Int J Immunopharmacol. 1992;14:441-449.
8. Engels F, Nijkamp FP. Pharmacological inhibition of leukotriene actions. Pharm World Sci. 1998;20:60-65.
9. Serhan CN, Prescott SM. The scent of a phagocyte: Advances on leukotriene B4 receptors. J Exp Med. 2000;192:F5-F8.
10. McMillan RM, Foster SJ. Leukotriene B4 and inflammatory disease. Agents Actions. 1988;24:114-119.
11. Lewis RA, Austen KF. The biologically active leukotrienes. Biosynthesis, metabolism, receptors, functions, and pharmacology. J Clin Invest. 1984;73:889-897.
12. Brouwers AH, Laverman P, Boerman OC et al. A 99mTc-labelled leukotriene B4 receptor antagonist for scintigraphic detection of infection in rabbits. Nucl Med Commun. 2000;21:1043-1050.
13. Harris TD, Glowacka SA, et al. The rapid detection of inflammation and infection using 99m-Tc-labeled LTB4 antagonists. J Labelled Compounds and Radiopharm. 1999; 42 (Suppl.): S576-S578.
14. Liu S, Harris AR, Williams NE, Edwards DS. 99mTc-Labeling of a hydrazinonicotinamide-conjugated LTB4 receptor antagonist useful for iImaging infection and inflammation. Bioconjug Chem. 2002;13:881-886.

15. Barrett JA, Cheesman EH, Harris TD, Rajopadhye M. Radiopharmaceuticals for Imaging Infection and Inflammation. PCT Int. Appl. 1998; WO 9815295: A2.
16. van der Laken CJ, Boerman OC, Oyen WJ et al. Technetium-99m-labeled chemotactic peptides in acute infection and sterile inflammation. J Nucl Med. 1997; 38:1310-1315.
17. Jain N.C. Blood volume and water balance. In : Jain ND, ed. Shalm's veterinary hematology. Philadelphia, PA: Lea and Febiger; 1986; 91:87-102.
18. Yokomizo T, Izumi T, Chang K, Takuwa Y, Shimizu T. A G-protein-coupled receptor for leukotriene B4 that mediates chemotaxis. Nature. 1997; 387:620-624.
19. Ono M, Arano Y, Mukai T, Uehara T, et al. Plasma protein binding of 99mTc-labeled hydrazino nicotinamide derivatized polypeptides and peptides. Nucl Med Biol. 2001; 28:155-64.

Chapter 3

Imaging of Experimental Colitis with a Radiolabeled Leukotriene B4 Antagonist

Julliëtte J.E.M. van Eerd
Peter Laverman
Wim J.G. Oyen
Thomas D. Harris
D. Scott Edwards
Charles E. Ellars
Frans H.M. Corstens
Otto C. Boerman

J Nucl Med. 2004;45:89-93

ABSTRACT

The use of radiolabeled leukocytes is considered the gold standard for scintigraphic imaging of inflammatory bowel disease (IBD). The disadvantages of ^{99m}Tc-HMPAO-leukocytes however, encourage the search for new imaging agents with at least similar diagnostic accuracy, but without the laborious preparation and subsequent risk of contamination. In this study, we investigated the imaging characteristics of a new imaging agent that specifically binds to the leukotriene B4 (LTB4) receptors expressed on neutrophils. Imaging characteristics of the ^{111}In-labeled LTB4 antagonist (DPC11870) were compared with those of ^{18}F-fluorodeoxyglucose (FDG) and ^{99m}Tc-HMPAO-granulocytes in a rabbit model of experimental colitis.

Methods: Acute colitis was induced in New Zealand White (NZW) rabbits by infusion of trinitrobenzene sulfonic acid (TNBS) in the descending colon. Forty-eight hours after induction of colitis all animals were injected intravenously with ^{99m}Tc-granulocytes, FDG or ^{111}In-DPC11870. The pharmacokinetics and biodistribution were studied by serial scintigraphic imaging and by ex vivo counting of dissected tissues.

Results: All three radiopharmaceuticals visualized the inflamed colon as early as 1 h postinjection. However, as compared to ^{99m}Tc-granulocytes both ^{111}In-DPC1170 and FDG were superior in visualizing the inflamed lesions. The biodistribution data showed that the uptake in the inflamed colon of ^{111}In-DPC11870 was highest (0.72±0.18 %ID/g) followed by ^{99m}Tc-granulocytes (0.40±0.11 %ID/g) and FDG (0.16±0.04 %ID/g). Due to low activity concentrations in the non-inflamed colon the radiolabeled LTB4 antagonist also revealed the highest affected-to-non-affected-colon ratio (11.6 for ^{111}In-DPC11870, 5.5 for ^{99m}Tc-granulocytes and 4.1 for FDG).

Conclusion: The radiolabeled LTB4 antagonist DPC11870 clearly delineated acute colitis lesions in NZW rabbits within one hour postinjection. Due to high uptake in the inflamed lesions and low activity concentration in the non-inflamed colon, images acquired with ^{111}In-DPC11870 were superior as compared with ^{99m}Tc-granulocytes or FDG.

INTRODUCTION

Several nuclear medicine imaging techniques are currently used as a tool for diagnosis of inflammatory and infectious diseases in patients. In general, scintigraphic imaging of inflammatory and infectious foci is performed using radiolabeled leukocytes. Especially in cases of inflammatory bowel disease (IBD) radiolabeled leukocytes are considered the best of the currently available scintigraphic imaging agents. ^{99m}Tc-HMPAO-leukocytes are

a useful radiopharmaceutical in management of patients with Crohn's disease. Uptake of radioactivity correlated with endoscopy and histology[1]. Despite the fact that ^{111}In- or ^{99m}Tc-labeled leukocytes are considered adequate imaging agents, their laborious preparation and the handling of potentially contaminated blood, has stimulated the search for an alternative radiopharmaceutical comprising the same imaging qualities. Recent reports suggest that FDG may be such an alternative[2,3]. FDG positron emission tomography (PET) is a distinguished imaging tool in clinical oncology based on its ability to image the increased glucose uptake of tumor cells. Several studies have shown that increased glucose metabolism is not restricted to malignant cells[4]. Increased FDG accumulation also occurs in inflammatory cells[5,6]. Besides FDG, chemokine receptor binding agents may be used for imaging of infection and inflammation[7,8]. The use of radiolabeled chemotactic peptides (e.g. fMLP, chemokines) is based on the high affinity interaction with their receptors specifically expressed on (activated) white blood cells. Since many of these leukocytes infiltrate at the site of inflammation, interaction with these receptors in vivo may lead to accumulation of the radiolabeled agent in the infectious or inflammatory foci. As compared with the radiopharmaceuticals currently used to image infectious and inflammatory lesions, the small molecular weight, leading to rapid penetration in the focus and fast clearance from the blood, and the absence of potential hazard associated with handling blood products are additional advantages and warrant further investigation of these agents[9]. LTB4 is one of the chemotactic molecules that potentially could be studied for this purpose. LTB4 activates granulocytes and macrophages as a reaction to an inflammatory response[10,11]. Two types of LTB4 receptors have been identified[12,13]. The first receptor type, BLT1 is a high affinity receptor mainly expressed on human neutrophils. The second receptor type, BLT2 is a low affinity receptor that is expressed more ubiquitously with high expression in spleen, leukocytes, ovary and liver[10,14]. It has been reported recently that ^{99m}Tc-labeled LTB4 antagonist RP517 binds to the neutrophil LTB4 receptor, and is also capable of imaging myocardial inflammation caused by coronary artery occlusion and reperfusion in a dog model[15]. We found that RP517 is capable of rapidly visualizing intramuscular *E. coli* abscesses in rabbits[16]. The high lipophilicity of RP517 results in predominantly hepatobiliary excretion, making imaging of infectious and inflammatory foci in the abdomen difficult. The LTB4-antagonist used in this study was DPC11870. DPC11870 is structurally related to RP517, but is made less lipophilic by the addition of pharmacokinetic modifying groups. We found that DPC11870 binds to human granulocytes with high affinity in vitro. Therefore, it was hypothesized that in vivo interaction with granulocytes at the site of inflammation, combined with reduced uptake in the GI tract, could lead to visualization of the inflamed colon. In this study we

investigated the imaging characteristics of the ^{111}In-labeled Leukotriene B4 antagonist DPC11870, 18F-fluorodeoxyglucose (FDG) and ^{99m}Tc-leukocytes in a rabbit model of acute, chemically induced colitis.

MATERIALS AND METHODS

DPC11870

DPC11870 is a bivalent LTB4 antagonist consisting of two identical LTB4 receptor-binding moieties, conjugated with DTPA in order to allow radiolabeling with ^{111}In. The labeling of 20 µg DPC11870 and 75 MBq ^{111}In was performed in metal-free 0.25 M ammonium acetate buffer, pH 5.5 during 30 minutes at room temperature[17]. Radiochemical purity was checked by ITLC on silica gel strips (Gelman Sciences, Inc., Ann Arbor, MI) in 0.1 M Na-citrate buffer pH 6.0 and by reversed phase HPLC on a C18 column (Zorbax Rx-C18, 4.6 mm x 25 cm) on an Agilent 1100 HPLC system, using a linear gradient from 100% NH_4Ac buffer, pH 7.0 to 100% acetonitrile in 50 minutes, at a flow rate of 1 mL/min. Specific activity of the ^{111}In-DPC11870 was 3.7 MBq/µg (12 MBq/nmol) and the chemical purity exceeded 95%.

Radiolabeling of Granulocytes

Since radiolabeled leukocytes obtained from infected donors showed better imaging characteristics as compared to leukocytes obtained from healthy donors[18], blood was obtained from a donor rabbit in which acute colitis was induced 48 h before as described below. The collection of 50 mL blood and the purification and labeling of granulocytes with 185 MBq ^{99m}Tc-HMPAO was performed as described previously[19]. Labeling efficiency exceeded 80%.'

^{18}FDG

^{18}FDG was commercially obtained from Tyco Healthcare (DRN 9957, Petten, The Netherlands). Activity concentration was 1.22 GBq/11.3 ml at calibration time.

Animal Model

Fifteen female NZW rabbits weighing 2.3-2.8 kg were kept in cages (one rabbit per cage) and fed standard laboratory chow and water ad libitum. Thirty minutes prior to the induction of colitis and during the imaging experiment all animals were sedated with a subcutaneous injection of 0.7 ml Hypnorm® (Fentanyl 0.315 mg/mL + Fluanisone 10 mg/mL) (Janssen Pharmaceutical, Buckinghamshire, UK). Induction of colitis was

performed as described previously, with minor modifications[20,21]. A flexible silicone tube (diameter 2.6 mm, 40 cm length) was inserted into the colon, the tip placed at 20 cm from the anal sphincter. Via the tube 1 mL 50% ethanol, followed by 1 mL ethanol containing 25 mg trinitrobenzene sulfonic acid (TNBS, Sigma Chemicals, St.Louis, MO) and 3 mL ethanol were injected into the colon. After the induction, animals had free access to the normal amount of food and water. All animal experiments were approved by the local Animal Welfare Committee in accordance with the Dutch legislation and carried out in accordance with their guidelines.

Imaging and Biodistribution

Forty-eight hours after the induction of colitis animals received an intravenous injection with 11 MBq ^{111}In-DPC11870, 18.5 MBq ^{99m}Tc-HMPAO-granulocytes or 30 MBq FDG. To compare the uptake of ^{111}In-labeled LTB4 antagonist in the abdominal region of a healthy animal, one extra healthy rabbit was also injected with 11 MBq ^{111}In-DPC11870. For scintigraphic imaging of ^{111}In-DPC11870 and ^{99m}Tc-granulocytes, the rabbits were immobilized in a mold and placed prone on a gamma camera (Orbiter, Siemens, Hoffman Estates, IL) using a low-energy (^{99m}Tc-granulocytes) or a medium-energy parallel hole collimator (^{111}In-DPC11870). Images (300,000 cts/image) were obtained at various time points after injection and stored in a 256x256 matrix. All images were windowed identically, allowing a fair comparison among the various experiments. For PET imaging, animals were imaged at one hour postinjection using a rotated half-ring dedicated PET scanner (Siemens Ecat ART/CTI, Knoxville, TN, USA), scan distance 28.35 cm for 16 minutes (38% transmission). Animals were euthanized after acquirement of the last image. A blood sample was drawn by cardiac puncture. Tissues were dissected and weighed. The amount of radioactivity in the tissues was measured in a shielded well-type gamma counter (Wizard, Canberra Packard Brussels, Belgium) together with the injection standards and was expressed as the percentage of the injected dose per gram (% ID/g). Affected-to-non-affected colon ratios were calculated for each inflamed colon segment, using uptake of the compound in an unaffected segment at the proximal end as reference value. The mean and standard deviation of the individual ratios were calculated for each radiolabeled compound. The different time points at which biodistribution was performed was considered the optimal time point for each radiolabeled compound. Imaging after injection of FDG at time points beyond 1 h p.i. is hardly feasible due to its short biological and physical half life. In case of ^{99m}Tc-HMPAO-granulocytes, leakage of ^{99m}Tc-HMPAO and subsequent excretion to the gall bladder and intestine restricts the maximum imaging and evaluation time[19,22].

Statistical Analysis

All mean values are presented as mean ± standard deviation. Statistical analysis was performed using ANOVA. The level of significance was set at 0.05.

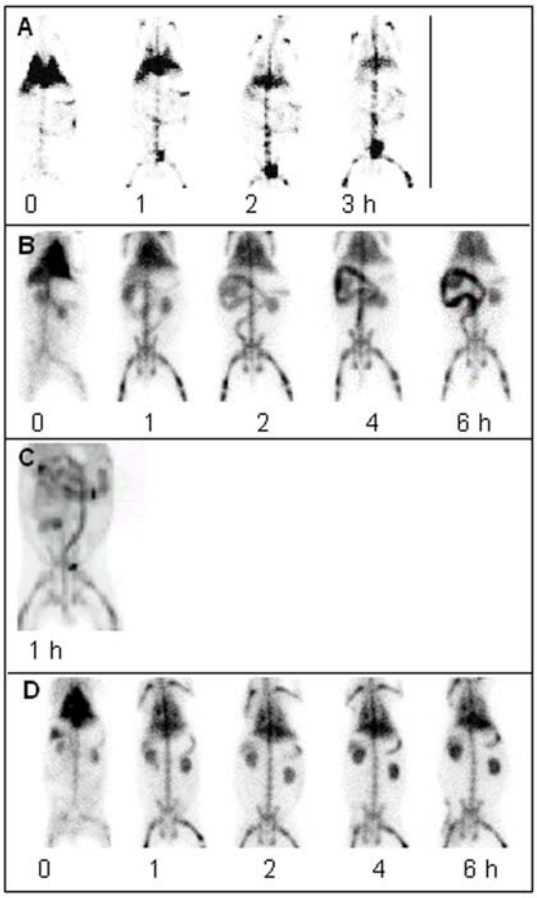

Figure 1.
Scintigraphic images of rabbits with acute colitis and a healthy rabbit acquired at several time points after iv injection of the radiopharmaceutical. Rabbits are placed prone one the gamma camera. Anterior images were acquired after injection of ^{99m}Tc-granulocytes, 18.5 MBq per rabbit, images 0, 1, 2 and 3 h p.i. (A), ^{111}In-DPC11870, 11 MBq per rabbit, images acquired 0, 1, 2, 4 and 6 h p.i (B) or FDG, 30 MBq per rabbit, 3D representation of an image acquired at 1 h p.i.(C) and ^{111}In-DPC11870, 11 MBq injected in a healthy rabbit, images acquired 0, 1, 2, 4 and 6 h p.i (D).

RESULTS

Two days after the induction of colitis all animals had diarrhea. The rabbits ate less food but their water intake and behavior were normal. The scintigraphic images acquired at several times postinjection are shown in Fig 1. Each of the three radiopharmaceuticals visualized the inflamed colon at 1 h postinjection. The uptake of radiolabeled granulocytes at the site of the inflamed colon was moderate, especially as compared to the uptake of ^{111}In-DPC11870 at the same time points. Both FDG and ^{111}In-DPC11870 clearly delineated the colitis and showed low uptake in noninflamed colon, however ^{111}In-

DPC11870 visualized the inflamed lesions even better as compared to FDG. The images acquired after injection of ^{111}In-DPC11870 in a healthy animal, showed no accumulation of radioactivity in the abdominal area at neither time points. The general in vivo behavior of the three radiotracers was very different. Immediately after injection the ^{99m}Tc-granulocytes showed high uptake in lung and liver. The activity concentration in both organs decreased with time. In all images uptake of radioactivity was seen in the bone marrow. The pharmacokinetics of ^{111}In-DPC11870 was totally different from that of the ^{99m}Tc-granulocytes. A few minutes after injection, the radiolabeled LTB4 antagonist mainly localized in the circulation (heart), liver and kidneys. At later time points the radioactivity in the circulation decreased whereas the activity accumulated in the bone marrow and inflamed colon. The PET images of rabbits acquired one hour after FDG injection showed that radioactivity concentration was high in the kidneys. Before PET scanning, the bladder was emptied by means of catheterisation.

Fig. 2 summarizes the biodistribution data of FDG at 1.5 h p.i, ^{99m}Tc-granulocytes at 3 h p.i and the ^{111}In-DPC11870 at 6 h p.i. These time points were considered optimal for the individual radiopharmaceuticals.

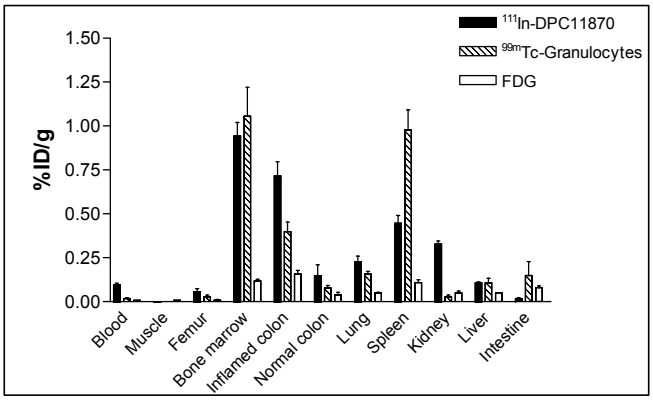

Figure 2.

Biodistribution data of rabbits (iv) injected with ^{99m}Tc-granulocytes, ^{111}In-DPC11870 and FDG. Uptake in organs and tissues is expressed as %ID/g. Each bar represents the mean values ± SD. Ex vivo biodistribution was performed at 1 h p.i. for FDG, 3 h p.i. for ^{99m}Tc-granulocytes and 6 h p.i. for ^{111}In-DPC11870.

The uptake in the inflamed colon was highest for ^{111}In-DPC11870 followed by ^{99m}Tc-granulocytes (0.72±0.18% ID/g vs 0.40±0.11% ID/g, respectively). The uptake of FDG in the inflamed colon was relatively low (0.16±0.04% ID/g). Furthermore, the total % ID in the inflamed colon was significantly higher for ^{111}In-DPC11870 as compared with the other two radioactive tracers ($P<0.004$) whereas there was no significant difference in colon uptake between ^{99m}Tc-granulocytes and FDG ($P>0.6$). Although the radioactivity concentration in the non-affected part of the colon was highest in rabbits injected with

^{111}In-DPC11870, the affected-to-non-affected colon ratio was nevertheless highest with this radiopharmaceutical (11.6 for ^{111}In-DPC11870, 5.5 for ^{99m}Tc-granulocytes and 4.1 for FDG, Fig. 3). After dissection of the tissues, the activity in the colon tissue and the content of the colon were measured separately. Each of the three radiolabeled compounds showed low activity concentrations in the content of the colon, as shown in Fig. 4. There were no significant differences in radioactivity concentrations in the content between the three agents ($p>0.6$). For the technetium-99m-labeled granulocytes the radioactivity concentration was high in spleen and bone marrow (0.98±0.23% ID/g and 1.06±0.33% ID/g, respectively). The ^{111}In-DPC11870 biodistribution data revealed a similar high uptake in bone marrow (0.95±0.17% ID/g), whereas the uptake in the spleen was considerably lower (0.45±0.10% ID/g). For this agent, a considerable amount of activity was localized in the kidneys (0.33±0.04% ID/g). Biodistribution data derived from animals injected with FDG indicated that a large fraction of the injected dose was excreted from the body already within one hour postinjection. Uptake of FDG in all organs (except inflamed colon) was very low. Activity concentration in the bone marrow and spleen were low with this agent (0.12±0.02% ID/g and 0.11±0.03% ID/g, respectively).

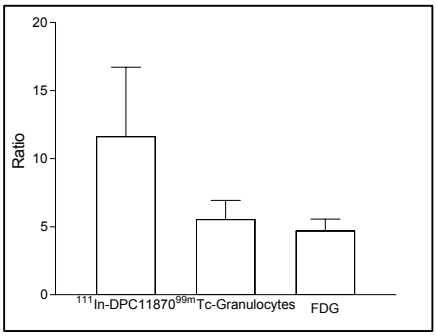

Fig. 3

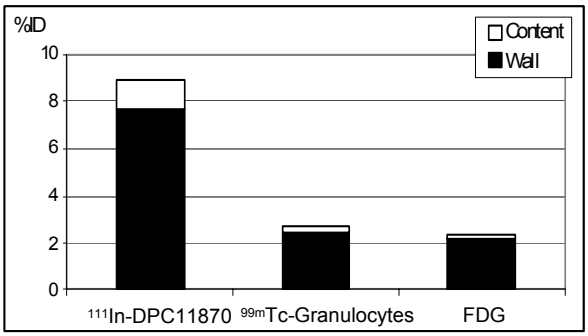

Fig. 4

Figure 3.
Mean affected-to-non-affected colon ratios derived from individual colon segments taken at dissection are presented for FDG, ^{99m}Tc-granulocytes and ^{111}In-DPC11870 at 1, 3 and 6 h p.i. respectively.

Figure 4.
Amount of activity found in the colon wall and in the content of the affected colon for the three radiopharmaceuticals ^{99m}Tc-granulocytes, ^{111}In-DPC11870 and FDG expressed as % ID.

DISCUSSION

The present study demonstrated that both ^{111}In-DPC11870 and FDG are excellent agents to visualize experimental colitis in NZW rabbits. Both agents are superior as compared to ^{99m}Tc-leukocytes, the standard imaging agent for scintigraphic evaluation of inflammatory bowel disease in patients. Images acquired after injection of ^{111}In-DPC11870, visualized the inflamed colon as early as one hour postinjection. The activity concentration of the radiolabeled DPC11870 in the colon at time 4 h p.i. was high. Visualization of the inflamed lesions in the colon was better than with FDG.

Numerous studies have focused on the role of leukotrienes and leukotriene antagonists as chemotactic compounds, to mediate infection and inflammation[10,23]. Due to the anti-inflammatory effect of LTB4 antagonists, the mechanism of interaction and the receptor specificity of these compounds have been studied extensively[24]. Yokomizu et al.[12,13] reported that two different LTB4 receptors can be identified. The high affinity receptor BLT1, is mainly expressed on activated polymorphonuclear leukocytes present at the site of infection or inflammation. Accumulation of ^{111}In-DPC11870, at the site of the inflamed colon most likely occurs due to interaction with the BLT1 receptor expressed on these infiltrated cells. In vitro binding studies showed that DPC11870 binds to purified human granulocytes with high affinity[17].

Recently, several investigators reported the applicability of FDG for imaging of infection and inflammation. Animal models demonstrated that FDG accumulates in both acute and chronic infectious lesions[2,25]. It is hypothesized that FDG accumulation in infectious and inflammatory lesions occurs as a consequence of enhanced uptake of FDG in neutrophils, macrophages, causative microorganisms and/or granulation tissue[5,26]. Uptake of FDG in these cells is enhanced because of the increased glycolysis and the intensified stimulation of the hexose monophosphate shunt in these cells[27]. In addition, activated inflammatory cells also have an increased expression of glucose transporters and, affinity of glucose transporters (for deoxyglucose) is increased by several cytokines and growth factors[28,29]. FDG-PET for visualization of infectious and inflammatory foci is nowadays a frequent subject of investigation in patient studies. Hannah et al.[27] were among the first investigators who described a patient with increased FDG bowel uptake, probably due to inflammation in the bowel wall. In a separate study in five patients diagnosed with colitis, Kresnik et al.[30] showed that FDG-PET was able to detect colitis at an early clinical stage.

The results of the present study, in rabbits with acute colitis, confirmed this increased FDG uptake in the inflamed lesions in the colon. With FDG-PET the visualization was rapid and, due to the rapid and complete clearance of activity from the remainder of the body, there

was a distinct visualization of the inflamed colon. The conventional ^{99m}Tc-granulocytes, a commonly used imaging agent in the management of patients with inflammatory bowel disease, showed increased uptake of radioactivity in the inflamed colon. However, due to the relatively high background radioactivity, the visualization of the inflamed colon was less evident than with FDG and ^{111}In-DPC11870.

Differential counting of the colon tissue and the colonic content indicated that each of the three agents almost exclusively localized in the inflamed colon wall (91%, 92% and 87% ID for ^{99m}Tc-granulocytes, FDG and ^{111}In-DPC11870) rather than in the faeces, indicating that radioactivity is cell-associated. Occasionally, some local uptake in the stool was observed. Macroscopic examination of the colonic wall and the content of the colon indicated that this was mainly observed in regions with severe tissue damage and ulcers. This presumed that occasional enhanced radioactivity in the faeces may be caused by loss of cells from the lumen.

CONCLUSION

^{99m}Tc-granulocytes, ^{111}In-labeled LTB4 antagonist DPC11870 and FDG all visualize acute colitis in NZW rabbits already at early time points after injection of each radiopharmaceutical. In this study we found that both ^{111}In-DPC11870 and FDG were superior to ^{99m}Tc-granulocytes, in visualization of the inflamed lesions. At later time points the images with ^{111}In-DPC11870 continued improving due to ongoing accumulation of radioactivity at the site of inflammation and continuous clearance from the background.

REFERENCES

1. Scholmerich J, Schmidt E, Schumichen C, Billmann P, Schmidt H, Gerok W. Scintigraphic assessment of bowel involvement and disease activity in Crohn's disease using technetium ^{99m}Tc-hexamethyl propylene amine oxine as leukocyte label. Dig Dis Sci. 1991;36:65-70.
2. Yamada S, Kubota K, Kubota R, Ido T, Tamahashi N. High accumulation of fluorine-18-fluorodeoxyglucose in turpentine- induced inflammatory tissue. J Nucl Med. 1995;36:1301-1306.
3. De Winter F, Vogelaers D, Gemmel F, Dierckx RA. Promising role of 18-F-fluoro-D-deoxyglucose positron emission tomography in clinical infectious diseases. Eur J Clin Microbiol Infect Dis. 2002;21:247-257.
4. Zhuang H, Alavi A. 18-fluorodeoxyglucose positron emission tomographic imaging in the detection and monitoring of infection and inflammation. Semin Nucl Med. 2002;32:47-59.
5. Ichiya Y, Kuwabara Y, Sasaki M, et al. FDG-PET in infectious lesions: The detection and assessment of lesion activity. Ann Nucl Med. 1996;10:185-191.
6. McCabe PM, Gonzales JA, Zaias J, et al. Social environment influences the progression of atherosclerosis in the Watanabe heritable hyperlipidemic rabbit. Circulation. 2002;105:354-359.

7. Weiner RE, Thakur ML. Radiolabeled peptides in diagnosis and therapy. Semin Nucl Med. 2001;31:296-311.
8. van der Laken CJ, Boerman OC, Oyen WJ, et al. Technetium-^{99m}-labeled chemotactic peptides in acute infection and sterile inflammation. J Nucl Med. 1997;38:1310-1315.
9. Boerman OC, Dams ET, Oyen WJ, Corstens FH, Storm G.Radiopharmaceuticals for scintigraphic imaging of infection and inflammation. Inflamm Res. 2001;50:55-64.
10. Ford-Hutchinson AW. Leukotriene B4 in inflammation. Crit Rev Immunol. 1990;10:1-12.
11. Claesson HE, Odlander B, Jakobsson PJ. Leukotriene B4 in the immune system. Int J Immunopharmacol. 1992;14:441-449.
12. Yokomizo T, Kato K, Terawaki K, Izumi T, Shimizu T. A second leukotriene B(4) receptor, BLT2. A new therapeutic target in inflammation and immunological disorders. J Exp Med. 2000;192:421-432.
13. Yokomizo T, Izumi T, Chang K, Takuwa Y, Shimizu T. A G-protein-coupled receptor for leukotriene B4 that mediates chemotaxis. Nature. 1997;387:620-624.
14. McMillan RM, Foster SJ. Leukotriene B4 and inflammatory disease. Agents Actions. 1988;24:114-119.
15. Riou LM, Ruiz M, Sullivan GW, et al. Assessment of myocardial inflammation produced by experimental coronary occlusion and reperfusion with ^{99m}Tc-RP517, a new leukotriene B4 receptor antagonist that preferentially labels neutrophils in vivo. Circulation. 2002;106:592-598.
16. Brouwers AH, Laverman P, Boerman OC, et al. A ^{99m}Tc-labelled leukotriene B4 receptor antagonist for scintigraphic detection of infection in rabbits. Nucl Med Commun. 2000;21:1043-1050.
17. van Eerd JEM, Oyen WJG, Harris TD, et. al. A bivalent Leukotriene B4 antagonist for scintigraphic imaging of infectious foci. J Nucl Med. 2003;44:1087-1091.
18. Gratz S, Rennen HJ, Boerman OC, et al. ^{99m}Tc-HMPAO-labeled autologous versus heterologous leukocytes for imaging infection. J Nucl Med. 2002;43:918-924.
19. Dams ET, Oyen WJ, Boerman OC, et al. Technetium-^{99m}-labeled liposomes to image experimental colitis in rabbits: comparison with technetium-99m-HMPAO-granulocytes and technetium-99m-HYNIC-IgG. J Nucl Med. 1998;39:2172-2178.
20. Allgayer H, Deschryver K, Stenson WF. Treatment with 16,16'-dimethyl prostaglandin E2 before and after induction of colitis with trinitrobenzenesulfonic acid in rats decreases inflammation. Gastroenterol. 1989;96:1290-300.
21. Kim HS, Berstad A. Experimental colitis in animal models. Scand J Gastroenterol. 1992;27:529-537.
22. Peters AM. The utility of [^{99m}Tc]HMPAO-leukocytes for imaging infection. Semin Nucl Med 994;24:110-127.
23. Yokomizo T, Izumi T, Shimizu T. Leukotriene B4: metabolism and signal transduction. Arch Biochem Biophys. 2001;385:231-241.
24. Wallace JL, MacNaughton WK, Morris GP, Beck PL. Inhibition of leukotriene synthesis markedly accelerates healing in a rat model of inflammatory bowel disease. Gastroenterology. 1989;96:29-36.
25. Kaim AH, Weber B, Kurrer MO, Gottschalk J, von Schulthess GK, Buck A. Autoradiographic quantification of 18F-FDG uptake in experimental soft- tissue abscesses in rats. Radiology. 2002;223:446-451.
26. Kubota R, Yamada S, Kubota K, Ishiwata K, Tamahashi N, Ido T. Intratumoral distribution of fluorine-18-fluorodeoxyglucose in vivo: high accumulation in macrophages and granulation tissues studied by microautoradiography. J Nucl Med. 1992;33:1972-1980.
27. Hannah A, Scott AM, Akhurst T, Berlangieri S, Bishop J, McKay WJ. Abnormal colonic accumulation of fluorine-18-FDG in pseudomembranous colitis. J Nucl Med. 1996;37:1683-1685.

28. Chakrabarti R, Jung CY, Lee TP, Liu H, Mookerjee BK. Changes in glucose transport and transporter isoforms during the activation of human peripheral blood lymphocytes by phytohemagglutinin. J Immunol. 1994;152:2660-2668.

29. Gamelli RL, Liu H, He LK, Hofmann CA. Augmentations of glucose uptake and glucose transporter-1 in macrophages following thermal injury and sepsis in mice. J Leukoc Biol. 1996;59:639-647.

30. Kresnik E, Gallowitsch HJ, Mikosch P, et al. 18F-FDG positron emission tomography in the early diagnosis of enterocolitis: preliminary results. Eur J Nucl Med Mol Imaging. 2002;29:1389-1392

Chapter 4

Scintigraphic detection of Pulmonary Aspergillosis in rabbits with a radiolabeled Leukotriene B4 antagonist.

Julliëtte J.E.M. van Eerd
Huub J.J.M. Rennen
Wim J.G. Oyen
Thomas D. Harris
D. Scott Edwards
Frans H.M. Corstens
Otto C. Boerman

J Nucl Med. 2004;45:1747-1753

ABSTRACT

Radiolabeled chemotactic peptides are studied for their applicability to visualize infectious and inflammatory foci. Since a radiolabeled Leukotriene B4 (LTB4) antagonist could visualize intramuscular *E. coli* abscesses in rabbits within a few hours after injection, here we tested the imaging characteristics of this agent in a more clinically relevant model of pulmonary aspergillosis.

Objectives: The pharmacokinetics and imaging characteristics of the ^{111}In-labeled LTB4 antagonist DPC11870 were studied in New Zealand White (NZW) rabbits with experimental pulmonary aspergillosis infection. Imaging characteristics of ^{111}In-DPC11870 were compared with those of ^{67}Ga-citrate, a radiopharmaceutical commonly used to detect pulmonary infections in patients.

Methods: Pulmonary aspergillosis was induced in the left lung of rabbits by intratracheal inoculation of $1x10^8$ conidia of *A.fumigatus*. Three days after the inoculation, the rabbits received ^{111}In-DPC11870 or ^{67}Ga-citrate intravenously. Images were acquired at several time points up to 24 hours postinjection (24 h p.i.).

Results: Pulmonary aspergillosis was visualized with both agents. Images acquired after injection of ^{111}In-DPC11870 showed uptake in the pulmonary lesions from 6 h p.i. Due to accumulation at the site of infection and clearance from the background the images improved with time. Region of interest analysis at 24 h p.i. revealed an infected-to-normal lung ratio of 5.0±1.5 for ^{111}In-DPC11870 as compared to 2.9±0.6 for ^{67}Ga-citrate.

Conclusion: The radiolabeled LTB4 antagonist DPC11870 clearly delineated experimentally induced pulmonary aspergillosis in rabbits. Images acquired at 24 h postinjection were superior to those obtained after injection of ^{67}Ga-citrate.

INTRODUCTION

Invasive pulmonary aspergillosis (IPA) is a common fungal infection that may affect morbidity and mortality in immunocompromised patients[1]. It is of great importance to detect aspergillosis infection at an early stage because this will improve the therapeutic outcome in patients[2]. For the diagnosis of IPA, high-resolution chest computed tomography (CT) scanning is most often performed. Besides CT, other diagnostic methods like culturing the fungus and non-culture-based methods such as serodiagnosis or polymerase-chain-reaction (PCR) may be applied[3]. Scintigraphic imaging techniques may have an additional value in the diagnosis of IPA. Scintigraphic imaging techniques are based on physiological changes in contrast to radiological techniques that are based

on morphological alterations. ^{67}Ga-citrate is a commonly used radiopharmaceutical to visualize pulmonary and mediastinal infection, especially in immunocompromised patients where low white blood cell counts (WBC) hamper the use of radiolabeled leukocytes[3]. Several other radiolabeled agents are studied for the applicability to image infection and inflammation. In particular radiolabeled chemotactic peptides are promising imaging agents because of their favorable pharmacokinetic characteristics[4,5]. In this study we investigated the ability of the Indium-111-labeled leukotriene B4 (LTB4) antagonist DPC11870 to image experimentally induced aspergillosis in NZW rabbits.

Leukotriene B4 receptors (BLT1 and BLT2) are expressed mainly on leukocytes[6]. In vitro binding of LTB4 to the BLT receptors results in intracellular signal transduction and subsequent chemotaxis[7]. LTB4 expression and receptor targeting plays an important role in the response of the immune system against infection and inflammation. Furthermore, overproduction of LTB4 contributes to inflammatory diseases and LTB4 antagonists have been developed to exploit their anti-inflammatory effect[8]. LTB4 targets leukotriene B4 receptors expressed on neutrophilic granulocytes that migrate towards and infiltrate in the inflammatory and infectious lesion[9]. This mechanism of receptor targeting may also be applicable to visualize inflammatory and infectious processes by using radiolabeled LTB4 antagonists. In this study a bivalent LTB4 antagonist was labeled with ^{111}In and its ability to visualize pulmonary aspergillosis in NZW rabbits was compared to that of ^{67}Ga-citrate.

MATERIALS AND METHODS

DPC11870

Synthesis of the compound was based on the PEG-tethered LTB4 antagonist SG385 described in a previously report[10]. Boc-cysteic acid and Boc-Glu(OTfp)-OTfp were prepared a described[11,12]. All other reagents were purchased from Aldrich Chemical Corporation or Fluka Chemical Corporation.

The tetra-cysteic acid derivative of SG385 was prepared by the sequential coupling of Boc-cysteic acid in Dimethylformamide (DMF) using Benzotriazol-tetramethyluronium-hexafluorophosphate (HBTU) coupling reagent. Boc removal was achieved by treatment with 50:50 trifluoroacetic acid (TFA): methylene-chloride(DCM). Purifications were performed after the addition of the 1st cysteic acid (partitioning between $CHCl_3$ and water) and after the addition of the 2nd and 4th cysteic acids (HPLC on C18 silica using 0.1% TFA-modified acetonitril (ACN)/water mobile phases). Products were recovered from HPLC mobile phases by lyophilization. The tetra-cysteic acid derivative 11870 was checked with HPLC and high resolution Mass Spectrometry (MS). In addition, the

dimerization was achieved by reaction of 11870 with the bis-TFP ester of Boc-glutamic acid and (Hydroxy-azabenzotriazole) HOAt in DMF. The crude reaction product was treated with TFA/DCM/Et_3SiH to remove the Boc protecting group. The product was purified with C18 HPLC in a 0.1 M ammonium acetate-modified ACN/water mobile phase. Conjugation with diethylene-triamine-penta-acetic acid (DTPA) was accomplished by reaction with DTPA anhydride in DMF. Purification gave DPC11870 in 73% yield from intermediate DPC11870. HPLC analysis of the lyophilized product gave a single peak. Additional quality control was performed with 1H NMR and performance of high resolution MS showed a value of [M+2H]: 1563.5056 for this $C_{123}H_{182}N_{26}O_{53}S_8$ structure.

Radiolabeling of DPC11870

DPC11870 labeling with $^{111}InCl_3$ was performed in metal-free 0.25 M ammonium acetate buffer, pH 5.5 for 30 minutes at room temperature. Radiochemical purity was checked by ITLC (Rf ^{111}In-DPC11870: 0-0.5, Rf unbound ^{111}In: 1.0) and by RP-HPLC on a C18 column (Zorbax Rx-C18 4.6 mm x 25 cm) as described previously[13].

^{67}Ga-citrate

^{67}Ga-citrate was commercially obtained from Tyco Healthcare (DRN 3103, Petten, The Netherlands). Activity concentration was 37 MBq/mL at calibration time.

Aspergillus Fumigatus

Aspergillus fumigatus used for the induction of the infection was isolated from an immunocompromised patient diagnosed with an aspergillosis fumigatus infection. The inoculum was prepared from a frozen isolate that was subcultured two times onto Sabouraud dextrose slants, followed by an incubation period of five days at 30°C. Conidia were harvested with phosphate buffered saline (PBS) (Gibco, Invitrogen BV, Breda, The Netherlands) containing 0.20% Tween 20 (Sigma Chemical Co. St.Louis, MO, USA). Conidia were washed three times in Hanks Balanced Salt Solution (HBSS) without Ca and Mg (BioWhittaker Europe, Verviers, Belgium) and transferred to a 50 mL conical tube and counted in a hemo-cytometer. The concentration was adjusted to give each rabbit a predetermined inoculum of $1x10^8$ conidia of *A.fumigatus* in a volume of 250 µL.

Induction of Pulmonary Aspergillosis

Fourteen female New Zealand White (NZW) rabbits weighing 2.3-2.8 kg were used during the experiments. Animals were housed individually and fed standard laboratory chow and water ad libitum. All animal experiments were approved by the local animal welfare

committee in accordance with the Dutch legislation and carried out in accordance with their guidelines.

TABLE 1 Schematic Overview of Animal Experiments

Rabbit no.	Days -4	-3	-2	-1	0	1
1–5: group A	Cytarabine Blood	Cytarabine + Induction Aspergillosis	Cytarabine	Cytarabine	Blood + ^{111}In-DPC11870 + imaging	Imaging + Biodistribution
6-10: group B	Cytarabine Blood	Induction Aspergillosis + Cytarabine	Cytarabine	Cytarabine	Blood + ^{67}Ga-citrate + imaging	Imaging + Biodistribution
11-12: group C	Cytarabine Blood	Cytarabine	Cytarabine	Cytarabine	Blood + ^{111}In-DPC11870 + imaging	Imaging + Biodistribution
13-14: group D	Blood				Blood + ^{111}In-DPC11870 + imaging	Imaging + Biodistribution

Blood samples were taken on day _4 and 0 to determine WBC count. Animals were injected with cytarabine on days _4 through 0, and aspergillosis was induced on day _3. At day 0, animals were injected with ^{111}In-DPC11870 (groups A, C, and D) or ^{67}Ga-citrate. Animals of group C were not inoculated with aspergillosis, and animals from group D were not injected with aspergillosis or cytarabine.

Twelve rabbits received cytarabine (cytosine arabinoside) injections to affect the immune system. Immunosuppression with cytarabine injections was accomplished by modification of a method to induce neutropenia in rabbits[14]. Cytarabine injections were given at 4 consecutive days in order to lower the white blood cell counts and allow the Aspergillosis infection to establish. The other two animals remained healthy and served as control animals (to compare the pharmacokinetics of ^{111}In-DPC11870 in cytarabine treated animals)(Table 1). Aspergillosis was induced essentially as described by Groll et al. with a few modifications regarding our application[14]. Cytarabine (Onco-Tain®, Faulding Pharmaceuticals nv, Brussels, Belgium) was administered intravenously (525 mg/m^2) on day –4 through –1 prior to the injection of radiolabeled compound. At day –3, after the second dose of cytarabine, *A.fumigatus* conidia were inoculated in ten animals. Two animals injected with cytarabine were not inoculated and served as a second control group. Before inoculation, animals were sedated with a subcutaneous injection of 0.7 ml Hypnorm® (Fentanyl 0.315 mg/mL + Fluanisone 10 mg/mL) (Janssen Pharmaceutical,

Buckinghamshire, UK). During inoculation the rabbits were anesthetized by inhalation anesthesia with a mixture of isoflurane, nitrous oxide and oxygen and placed on the operation table. The inoculum of $1x10^8$ conidia (250 µL was given intra-tracheally into the left lung, together with 50 µL of 5% Evans blue dye (E2129, Sigma-Aldrich, Zwijndrecht, The Netherlands) via a syringe attached to a polyethyleen 0.76x1.22 mm catheter (PE tube, Maxxim Medical, Oss, The Netherlands).

Imaging and Biodistribution

At day zero (three days after inoculation of *A.fumigatus*) nine rabbits (2 healthy, 2 injected with cytarabine only and 5 animals both injected with cytarabine and infected with *A.fumigatus*) received an injection with 11 MBq ^{111}In-DPC11870 (3 µg) via the ear vein. The other five animals pretreated with cytarabine and induced with aspergillosis received 11 MBq ^{67}Ga-citrate intravenously. Images (300,000 cts/image) were acquired immediately after injection of the radiolabeled preparations and at 2, 4, 6 and 24 h p.i. For scintigraphic imaging, the rabbits were immobilized in a mold and placed prone on the medium-energy parallel hole collimator of the gamma camera in the anterior position (Orbiter, Siemens, Hoffman Estates, IL). Images were stored digitally in a 256x256 matrix. All images were windowed identically, allowing a fair comparison of the images acquired during the various experiments. The scintigraphic results were analyzed by drawing regions of interest (ROI) over the abscess and the contralateral non-infected lung (normal). Infected-to-normal lung ratios were calculated. At 24 h p.i. all rabbits were euthanized with a lethal dose of sodium pentobarbital and organs were dissected. A blood sample was taken by cardiac puncture and tissues were weighed and measured for the amount of radioactivity to determine the biodistribution of both agents. The activity in tissues was measured in a shielded well-type gamma counter (Wizard, Pharmacia-LKB, Uppsala, Sweden) together with the injection standards. Radioactivity concentration was expressed as percentage of the injected dose per gram (%ID/g).

Hematological and Histopathological Studies

Blood samples were collected from all rabbits, both at day –4 prior to the first cytarabine injection and at day 0 (time of injection of the radiolabel), in order to determine the WBC of the animals.

During dissection of the animals samples of the infected (left) and non-infected lung were aseptically removed. One part of each lung sample was cultured for *A.fumigatus* during 24 h at 37°C on Sabouraud dextrose agar plates. A second specimen of lung tissue was fixed in phosphate-buffered formalin. After measurement of radioactivity, these tissues were

embedded in parrafin. Tissues sections were stained with hematoxylin-eosin or Grocott methenamine and histopathologically examined.

Statistical Analysis

All values are presented as mean ± standard deviation. Statistical analysis was performed using the two-sided Student t-test. The level of significance was set at 0.05.

RESULTS

Radiolabeling of DPC11870

RP-HPLC analysis and ITLC quality control indicated that the radiochemical purity (RCP) exceeded 99%. Specific activity was 3.7 MBq/µg DPC11870 (12 MBq/nmol).

Aspergillus Fumigatus

Culturing of the conidia solution confirmed that the inoculum consisted of *A.fumigatus* conidia. Animals infected with *A.fumigatus* showed clinical symptoms from two days after conidia inoculation. The respiration frequency of the rabbits was increased and the infected animals showed more shallow breathing as compared to the control animals. Intake of water and food was normal.

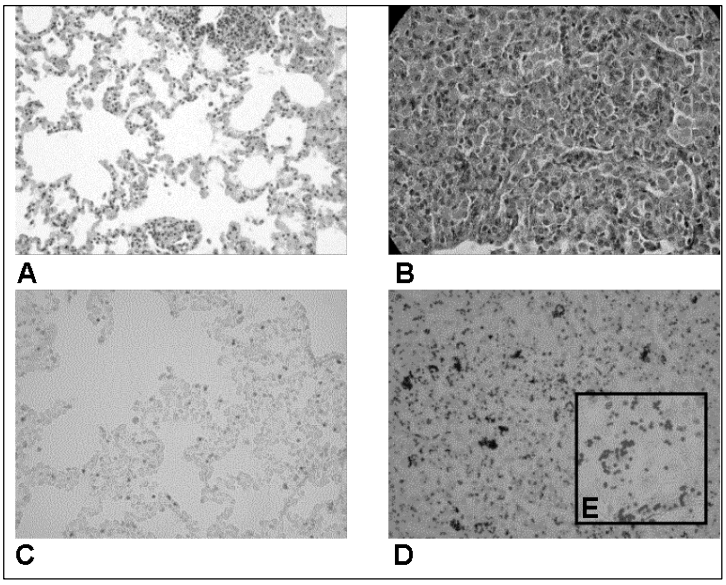

Figure 1
Histological sections of NZW rabbits of healthy lung tissue (A and C) and lung tissue with invasive pulmonary aspergillosis (B and D). Hematoxylin-eosin stain (A and B) showing massive infiltration of PMNs in the infected lung tissue (B). Grocott methenamine silver staining (C and D) indicated the presence of A.fumigatus hyphae and germinating conidia in the infected lung tissue (D). Magnification A-D: 200x. Inset in D shows magnification of 400x.

Hematological and Histopathological Studies

The mean WBC concentration of the rabbits, at the time of injection of the first cytarabine injection (day –4) was $13.5\pm5.7x10^9$/L. Four days after cytarabine administration WBC concentration of these rabbits were significantly reduced ($5.2\pm2.4x10^9$/L, p=0.0036). Normal white blood cell counts in NZW rabbits vary between 5.0 and $11.0x10^9$/L[15]. The white blood cell counts after induction of aspergillosis and injection of cytarabine indicated that the rabbits were not persistently neutropenic but the numbers were strongly reduced as compared to the first day of the experiment (day 0).

At dissection all animals inoculated with *A.fumigatus* showed macroscopic infectious lesions in the lungs. In all but one rabbit the infected lung area corresponded with the area marked with Evans blue. In one rabbit (injected with ^{111}In-DPC11870) the infection had affected both lungs. Culture of *A.fumigatus* was positive in three out of five animals injected with ^{67}Ga-citrate. In three out of the five cases, animals injected with ^{111}In-DPC11870 and inoculated with aspergillus conidia revealed positive cultures (one of these animals showed positive cultures in both lungs). One animal was only positive for staphylococcus species. Both lungs from the four control rabbits and the remainder lung tissues (control lungs not inoculated with *A.fumigatus*) were negative after culturing.

Histological examination of tissue sections of the healthy animals showed no signs of infection i.e. infiltration of macrophages or granulocytes was absent (Fig.1A). The sections of lungs infected with *A.fumigatus* conidia showed massive infiltration of mainly granulocytes (Fig.1B). Staining with methiamine revealed truncated Aspergillus hyphae and germinating conidia in all animals that were inoculated with *A.fumigatus* conidia (Fig.1D). Staining for Aspergillosis was negative for the tissue samples obtained from healthy lungs (Fig.1C).

Imaging and Biodistribution

The scintigraphic images acquired immediately, 2, 4, 6 and 24 hours after injection of ^{111}In-DPC11870 or ^{67}Ga-citrate are shown in Figure 2. Immediately after injection, rabbits injected with ^{111}In-DPC11870 showed uptake of radioactivity in heart, lung, liver and kidneys (Fig. 2A). At later time points, accumulation of activity was seen in spleen and bone marrow. Radioactivity concentration in the heart (circulation) and in the lungs decreased with time. Due to the reduction of radioactivity in the normal lung tissue and circulation, and accumulation of activity in the infectious foci, the infectious area in the lungs was visualized from 6 h p.i.. Images obtained at 24 h after the injection of the radiolabeled LTB4 antagonist showed an even more evident clearance of radioactivity from non-infected lung areas. This continuous clearance in combination with ongoing

accumulation of radioactivity in the infected lung tissue resulted in distinct visualization of the lung lesions at 24 h after injection of the radiolabel. The images showed that except for the kidneys, activity concentration in the remainder of the body was low. Images acquired at several time points after injection of ^{67}Ga-citrate showed distinct pharmacokinetics for this compound as compared to ^{111}In-labeled DPC11870 (Fig 2B). Immediately after injection ^{67}Ga-citrate distributed to the different organs and high activity concentrations were seen in the kidneys and bladder. Gallium-67 visualized pulmonary infection from 2 h postinjection. The pulmonary lesion was visible as a small focal spot in the left lung. At this moment there was also uptake of ^{67}Ga in the bone. In contrast to the ^{111}In-LTB4 antagonist, at time points later than 2 hours p.i. all images of animals injected with ^{67}Ga-citrate remained similar.

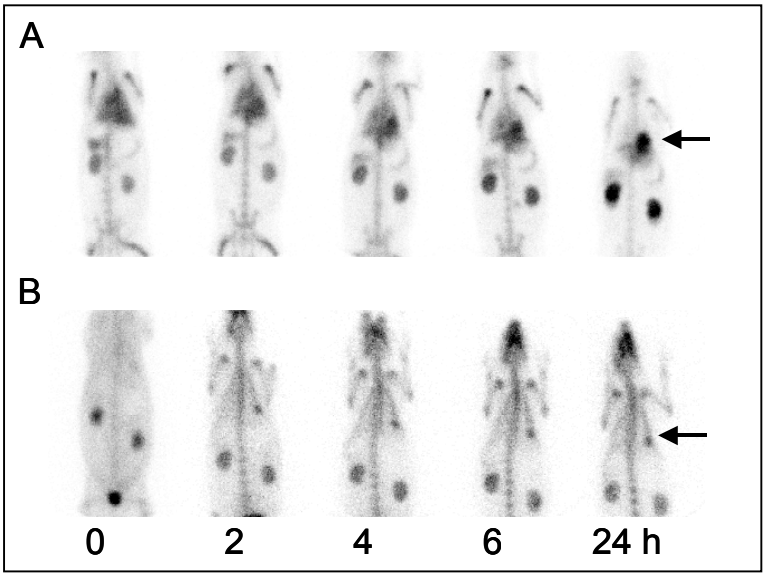

Figure 2.
Scintigraphic images of NZW rabbits with pulmonary aspergillosis. The rabbits received 11 MBq ^{111}In-DPC11870 (A) or ^{67}Ga-citrate (B) intravenously. Anterior images were acquired immediately 2, 4, 6 and 24 h postinjection of the radiolabel. Arrows indicate focus of infection.

Region of interest analysis of the normal and infected lung area showed increased infected-to-normal lung ratios in time after injection of ^{111}In-DPC11870 (Fig. 3). The infected-to-normal lung ratios show a constant increase throughout the experiment. The infected-to-normal ratios calculated for the ^{67}Ga-citrate showed an increase during the interval 0-4 h after the injection of the compound, whereas at later time points the ratio remained constant. The infected-to-normal lung ratio obtained from

the ROI analysis of the ^{67}Ga-citrate images at 24 h postinjection was 1.7-fold lower as compared to similar ratios obtained from the ^{111}In-DPC11870 images (p=0.020).

Fig. 3

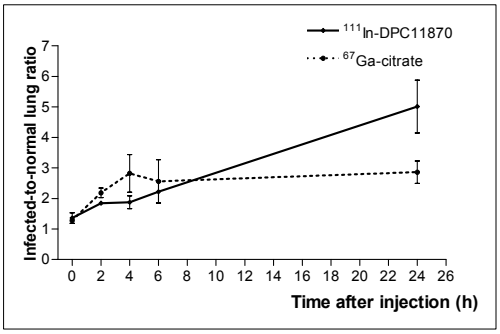

Fig. 4

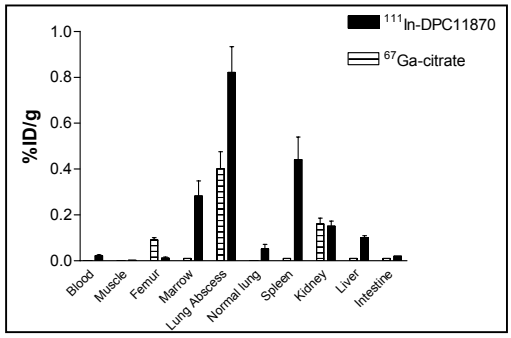

Figure 3.
Region of interest analysis from the images acquired at several time points after injection of ^{111}In-DPC11870 (n=5) or ^{67}Ga-citrate (n=5) in NZW rabbits with pulmonary aspergillosis revealed infected-to-normal lung ratios. Error bars indicate standard deviation.

Figure 4.
Biodistribution data obtained 24 hours after injection of ^{111}In-DPC11870 (n=5) and ^{67}Ga-citrate (n=5) in NZW rabbits with pulmonary aspergillosis. Error bars indicate standard deviation.

The biodistribution data (24 h p.i.) derived from the ex vivo counting of dissected tissues are presented in Figure 4. The uptake of ^{111}In-DPC11870 in the infected lung tissue at the time of biodistribution was very high. Uptake of radioactivity in the infected lung tissue was 16-fold higher as compared to the uptake in normal lung tissue (0.82% ID/g vs. 0.05% ID/g respectively, p= 0.008). Relatively high uptake of the compound was also measured in bone marrow and spleen. Biodistribution data obtained with ^{67}Ga-citrate were in concordance with the images and highest radioactivity concentration of this radiopharmaceutical was measured in the infected lung tissue. As noticed on the images, radioactivity concentration of ^{67}Ga-citrate was relatively high in the bone and in the kidneys. In contrast to the derived ROI ratios, the infected-to-normal lung ratio calculated from the biodistribution data was significantly (4.1-fold) higher at 24 h after ^{67}Ga-citrate injection than that of ^{111}In-DPC11870 (p=0.0005).

To determine whether the cytarabine injections in the animals affected the pharmacokinetics and biodistribution pattern of the radiolabeled LTB4 antagonist, non-infected control animals were included in this study. Images acquired immediately after injection of ^{111}In-DPC11870 appeared similar in all groups (data not shown). Images

acquired from a cytarabine injected and Aspergillus infected animal, a cytarabine treated noninfected animal and a healthy rabbit injected with ^{111}In-DPC11870 acquired at 24 h p.i. are shown in Figure 5.

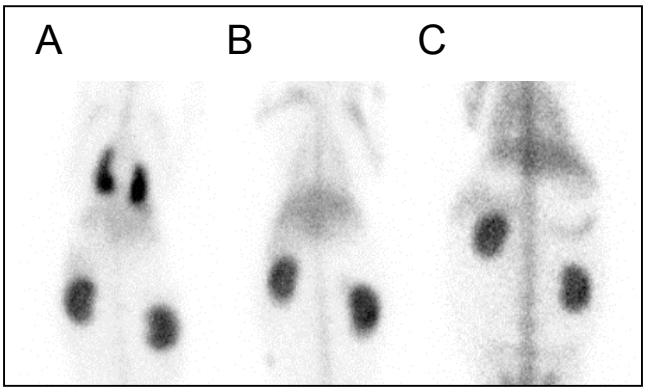

Figure 5.
Anterior images acquired 24 hours postinjection ^{111}In-DPC11870 in a NZW rabbit with pulmonary infection in both lungs (A), a non-infected animal treated with cytarabine (B) and a rabbit neither infected with Aspergillosis nor treated with cytarabine (C).

Rabbits not infected with *A.fumigatus* conidia (either untreated or treated with cytarabine) did not show any accumulation or retention of radioactivity in the lungs. Furthermore, the biodistribution of ^{111}In-DPC11870 in the main organs of these animals (exept bone marrow and spleen) were comparable with the ^{111}In-DPC11870 distribution in cytarabine treated infected rabbits. Distinct differences in radioactivity concentrations were observed in spleen and bone marrow of healthy animals and animals suffering from aspergillosis. The cytarabine treated animals showed reduced uptake of ^{111}In-DPC11870 in these organs.
The quantitative measurement of dissected organs revealed that, except for the bone marrow and spleen, there were no significant differences in radioactivity concentration in the dissected organs between the two groups of rabbits that were treated with cytarabine (healthy or infected) and the group healthy, untreated animals (Fig. 6). Radioactivity concentration measured in the bone marrow of cytarabine-injected animals (both infected and non-infected) was lower (0.28±0.15% ID/g and 0.38±0.20% ID/g, respectively) as compared to that in healthy animals (0.93±0.13% ID/g). The radioactivity concentration in the non-infected lungs of all three groups of animals was similar. Also, the ^{111}In-DPC11870 concentration in the blood of rabbits from all three groups was similar (0.02±0.01% ID/g in rabbits with aspergillosis, 0.01±0.02% ID/g in rabbits healthy but treated animals and 0.03±0.01% ID/g in healthy rabbits not treated with cytarabine).

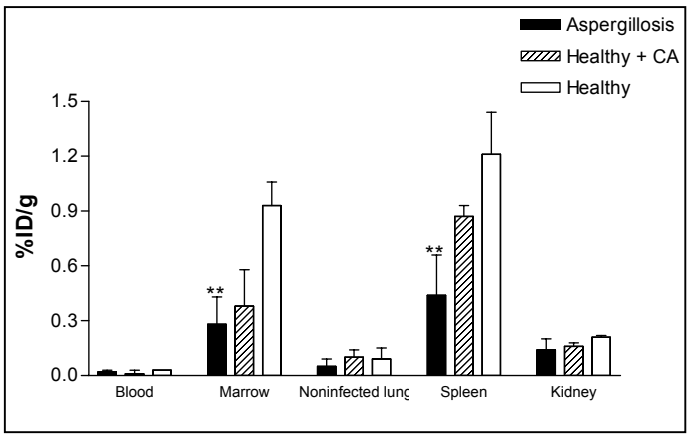

Figure 6.
*Biodistribution data obtained 24 hours postinjection of ^{111}In-DPC11870 in NZW rabbits with pulmonary infection in the lung, n=5 (A), cytarabine (CA) treated non-infected animals, n=2 (B) and healthy rabbits neither injected with cytarabine nor infected with A.fumigatus, n=2 (C) (** P < 0.05, results differ significantly with results found in healthy rabbits). Error bars indicate standard deviation*

DISCUSSION

In the present study scintigraphic imaging of pulmonary aspergillosis with a radiolabeled LTB4 antagonist was examined in a rabbit model. The imaging potential of the LTB4 antagonist was compared with that of ^{67}Ga-citrate. Serial scintigraphic images showed that ^{111}In-DPC11870 visualized the pulmonary infection from 6 h onwards. The images showed that the radiolabeled LTB4 antagonist accumulated in the infectious lesion while activity concentration in the blood and normal lung tissue decreased with time. The pharmacokinetic properties of the compound in this model were in concordance with results found in previous studies[13]. Injection of the compound in healthy animals showed that except for the amount of radioactivity in bone marrow and spleen, the localization of ^{111}In-DPC11870 was not affected by the administration of cytarabine. This implied that despite the lowered white blood cell counts in the circulation, there were sufficient activated neutrophils that migrated to the site of infection. No differences were seen in radioactivity concentration in the blood and the major organs. The lower amounts of radioactivity in the spleen and bone marrow of animals pretreated with cytarabine was probably due to the reduced number of premature white blood cells in these organs. Cytarabine is a nucleoside analog with cytotoxic activity mainly affecting replicating cells[16]. The results described above may be due to the fact that repeated injection of cytarabine will immediately reduce the numbers of proliferating (LTB4 receptor positive) promyelocytes in the bone marrow, whereas mature and activated neutrophils will be less affected and would require a longer treatment period with this antimetabolite. This is in

concordance with the fact that in these rabbits massive infiltration of leukocytes was found in the infected lung tissue (histological staining).

The primary aim of this study was to test whether the radiolabeled LTB4 antagonist ^{111}In-DPC11870 could visualize pulmonary aspergillosis in NZW rabbits. In addition we compared the imaging and biodistribution characteristics of ^{111}In-DPC11870 with those of ^{67}Ga-citrate, the radiopharmaceutical generally used to visualize pulmonary infections in patients[17]. Besides the relatively high sensitivity for acute and chronic infection and inflammation, ^{67}Ga-citrate possesses a few disadvantages such as a relatively long biological half-life and physiologic uptake in bone and excretion via the bowel (the latter mainly at later time points)[18]. Images acquired after injection of ^{67}Ga-citrate in rabbits with *A.fumigatus* infection, clearly delineated the infected lesions in the lungs at early time points. Physiologic uptake in the bone was seen on the images from 2 h p.i. and this amount of radioactivity did not decrease with time. Region of interest analysis indicated that the infected-to-normal lung ratios found with ^{111}In-DPC11870 increased with time (in contrast to the ratios found after injection of ^{67}Ga-citrate) and resulted in higher ratios for ^{111}In-DPC11870 as compared to ^{67}Ga-citrate at 24 h after the injection of the radiolabeled agents. The increasing infected-to-normal lung ratios after injection of the radiolabeled LTB4 antagonist can be explained by the continuous accumulation of radioactivity at the site of infection in combination with ongoing clearance from the blood (corresponding with background). The ^{67}Ga-citrate showed faster clearance from the circulation as compared to DPC11870 and therefore at later time points the ratios remained constant. Normally, regions of interest (ROIs) obtained from the images are evaluated for diagnosis of pulmonary infection. The physiological uptake of ^{67}Ga-citrate in the bone (background tissue) deteriorated the images and caused reduced infected-to-normal lung ratios derived from the ROI analysis. Our data indicate that despite visualization of the pulmonary lesions, physiological uptake in the bone may affect visualization of pulmonary lesions. This outcome may be more pronounced in patients especially because in general images are acquired at 18-72 hours after the injection of ^{67}Ga-citrate[19,20].

In this study we showed that ^{111}In-DPC11870 clearly visualized pulmonary Aspergillosis in rabbits. Visualization of the infection occurred due to accumulation of radioactivity. In a previous study we determined that this accumulation is specific and receptor mediated[13]. Because of the massive infiltration of granulocytes in the infectious foci and accumulation of ^{111}In-DPC11870 in the lesions, this model represents acute pulmonary infection and presumably ^{111}In-DPC11870 might visualize acute pulmonary infection in general. Since uptake of ^{111}In-DPC11870 in the bone marrow and retention of radioactivity in the kidneys could limit clinical applicability of the compound, we now aim to produce a new analogue

of the LTB4 antagonist DPC11870 that can be labeled with ^{99m}Tc. A ^{99m}Tc-labeled compound could not only reduce the absorbed dose to these organs but may also reveal improved images because of the higher resolution and reduced visualization of bone marrow (due to higher attenuation by the bone). Nevertheless, due to the distinct visualization of the pulmonary lesions after injection of ^{111}In-DPC11870, the current agent could be a valuable tool for the diagnosis of acute pulmonary infections in patients.

CONCLUSION

The present study demonstrates that the radiolabeled LTB4 antagonist DPC11870 visualized pulmonary infection in rabbits suffering from Aspergillosis. Lesions were visualized from 6 h postinjection and improved with time due to retention of radioactivity in the infected lung tissue. The results of this study indicate that ^{111}In-DPC11870 could contribute to the diagnosis of acute pulmonary infection.

REFERENCES

1. Hauggaard A, Ellis M, Ekelund L. Early chest radiography and CT in the diagnosis, management and outcome of invasive pulmonary aspergillosis. Acta Radiol. 2002;43:292-298.
2. Becker MJ, Dams ET, de Marie S, et al. Scintigraphic imaging using 99mTc-labeled PEG liposomes allows early detection of experimental invasive pulmonary aspergillosis in neutropenic rats. Nucl Med Biol. 2002;29:177-184.
3. Kontoyiannis DP, Bodey GP. Invasive aspergillosis in 2002: an update. Eur J Clin Microbiol Infect Dis. 2002;21:161-172.
4. Onuffer JJ, Horuk R. Chemokines, chemokine receptors and small-molecule antagonists: recent developments. Trends Pharmacol Sci. 2002 Oct;23(10):459-67.
5. van der Laken CJ, Boerman OC, Oyen WJ et al. Technetium-99m-labeled chemotactic peptides in acute infection and sterile inflammation. J Nucl Med. 1997; 38:1310-1315.
6. Toda A, Yokomizo T, Shimizu T. Leukotriene B4 receptors. Prostaglandins Other Lipid Mediat. 2002;68-69:575-585.
7. Ford-Hutchinson AW. Leukotriene B4 in inflammation. Crit Rev Immunol. 1990;10:1-12.
8. Engels F, Nijkamp FP. Pharmacological inhibition of leukotriene actions. Pharm World Sci. 1998;20:60-65.
9. Serhan CN, Prescott SM. The scent of a phagocyte: Advances on leukotriene B(4) receptors. J Exp Med. 2000;192:F5-F8.
10. Barrett JA, Cheesman EH, Harris TD, Rajopadhye M. Radiopharmaceuticals for Imaging Infection and Inflammation. PCT Int. Appl. WO 9815295 A2 1998.
11. Hubbuch A, Danho W, Zahn H. Synthesis of N-Protected Cysteic Acid Derivatives and Their Activated Esters. Liebigs Ann. Chem. 1979: 776-783.
12. Harris TD, Barrett JA, Carpenter AP, Rajopadhye M. Vitronectin receptor antagonist pharmaceuticals. US 6511649 B1 2003.

13. van Eerd JEM, Oyen WJG, Harris TD, et al. A bivalent leukotriene B4 antagonist for scintigraphic imaging of infectious foci. J Nucl Med. 2003;44:1087-1091.

14. Groll AH, Gonzalez CE, Giri N, et al. Liposomal nystatin against experimental pulmonary aspergillosis in persistently neutropenic rabbits: efficacy, safety and non-compartmental pharmacokinetics. J Antimicrob Chemother. 1999;43:95-103.

15. Hematology of laboratory and miscellaneous animals. In: Jain NC, ed. Schalm's Veterinary Hematology. Vol 91. Philadelphia, PA:Lea and Febiger; 1986:275-298.

16. Johnson SA. Clinical pharmacokinetics of nucleoside analogues: focus on haematological malignancies. Clin Pharmacokinet. 2000;39:5-26.

17. Seabold JE, Palestro CJ, Brown ML, et al. Procedure guideline for gallium scintigraphy in inflammation. Society of Nuclear Medicine. J Nucl Med. 1997;38:994-997.

18. Boerman OC, Dams ET, Oyen WJ, Corstens FH, Storm G. Radiopharmaceuticals for scintigraphic imaging of infection and inflammation. Inflamm Res. 2001;50:55-64.

19. Sugawara Y, Gutowski TD, Fisher SJ, Brown RS, Wahl RL. Uptake of positron emmission tomography tracers in experimental bacterial infections: a comparative study of radiolabeled FDG, thymidine, L-methionine, ^{67}Ga-citrate and 125I-HAS. European J Nucl Med. 1999;26:333-341

20. Alazraki NP. Gallium-67 imaging in infection. In: Principles and practice of nuclear medicine, 2nd edition St.Louis: Mosby-Year Book; 1995:702-713.Yamada S, Kubota K, Kubota R, Ido T, Tamahashi N. High accumulation of fluorine-18-fluorodeoxyglucose in turpentine- induced inflammatory tissue. J Nucl Med. 1995;36:1301-1306.

Chapter 5

Scintigraphic Imaging of Infectious Foci with an ^{111}In-LTB4 Antagonist is Based on In-vivo Labeling of Granulocytes.

Julliëtte J.E.M. van Eerd
Wim J.G. Oyen
Thomas D. Harris
Huub J.J.M. Rennen
D. Scott Edwards
Frans H.M. Corstens
Otto C. Boerman

J Nucl Med. 2005;46:786-793

ABSTRACT

Radiolabeled Leukotriene B4 (LTB4) antagonist DPC11870 is able to visualize infectious and inflammatory foci in distinct animal models.

Objectives: Since previous studies showed that accumulation of ^{111}In-DPC11870 in the abscess continued while the tracer had cleared from the circulation, we now investigated the pharmacodynamics of ^{111}In-DPC11870 and determined the mechanism of accumulation of the radiolabeled LTB4 antagonist in the abscess.

Methods: ^{111}In-DPC11870 was intravenously (i.v.) injected in healthy New Zealand White (NZW) rabbits and rabbits with intramuscular *E. coli* infection. The pharmacodynamics were studied by serial imaging and by ex vivo counting of dissected tissues. The mechanism of visualization of the abscess was investigated in rabbits with intramuscular infection that was induced 16 h after i.v. administration of ^{111}In-DPC11870. In addition, heterologous leukocytes and bone marrow cells of a donor rabbit were labeled with ^{111}In-DPC11870 in vitro and the biodistribution of these in vitro radiolabeled cells was compared with that of ^{111}In-DPC11870 in rabbits with an infection.

Results: The LTB4 antagonist ^{111}In-DPC11870 visualized the intramuscular abscess in rabbits already a few hours after injection. Quantitative analysis of the images confirmed accumulation of ^{111}In-DPC11870 in the abscess while the compound had cleared almost completely from the circulation. Radioactivity concentration in the bone marrow decreased more rapidly in infected animals than in healthy animals. Therefore we hypothesized that ^{111}In-DPC11870 associates with receptor positive (bone marrow) cells and accumulated in the abscess due to subsequent migration from the bone marrow to the abscess. Accumulation of radioactivity, in the abscess induced 16 h after ^{111}In-DPC11870 injection, was similar as in animals i.v. injected with the tracer 24 h after induction of the abscess (0.37±0.16 %ID/g). Moreover, differences in radioactivity concentration in the bone marrow of healthy and infected animals (0.67±0.29 %ID/g and 0.15±0.03 %ID/g at 24 h p.i., respectively) supported our hypothesis. Additional studies with peripheral blood leukocytes (WBCs) and bone marrow cells (BMCs) that were ex-vivo labeled with ^{111}In-DPC11870 showed the ability of these cells to migrate to the abscess (0.40 %ID/g and 0.52 %ID/g for the ^{111}In-DPC11870-BMCs and ^{111}In-DPC11870-WBCs respectively, 24 h p.i.).

Conclusion: The ^{111}In-labeled LTB4 antagonist DPC11870 accumulates in infectious and inflammatory foci due to binding to LTB4 receptors expressed on activated hematopoietic cells that subsequently migrate to the site of infection, which leads to visualization of the infectious lesions.

INTRODUCTION

Detection of infectious and inflammatory foci by means of scintigraphic imaging is important because it allows accurate therapeutic decisions and rapid initiation of appropriate treatment. Radiolabeled leukocytes are currently considered the gold standard to detect infectious and inflammatory lesions in patients[1]. This radiopharmaceutical enables rapid visualization of the lesion but preparation is time-consuming and is associated with a potential risk for infection[2]. At the moment there is interest in the development of new radiopharmaceuticals to detect infectious and inflammatory foci with the same accuracy as radiolabeled leukocytes but without these disadvantages. Chemotactic and chemokinetic peptides are promising agents for this application[3,4]. These compounds have the potential to accumulate at the site of infection and are cleared rapidly from non-target tissues and from the circulation. Various studies, however, indicate that the use of these agonistic compounds is often limited due to biological activity while antagonists often exhibit low receptor affinity[5]. We have developed an LTB4 antagonist, DPC11870, that can be labeled with ^{111}In and that visualizes infectious and inflammatory lesions rapidly after injection[4,6].

Leukotriene B4 is a potent chemotactic factor for granulocytes that, upon binding to its specific cell surface receptors, stimulates leukocyte functions such as chemotaxis, vascular adhesion, transendothelial migration and release of lysosomal enzymes[7,8]. Since leukotriene B4 is an important mediator and leukotriene B4 receptors are expressed by polymorphonuclear granulocytes, we investigated the imaging potential of a bivalent leukotriene B4 antagonist. We have shown that this radiolabeled antagonist could visualize infectious and inflammatory foci in various rabbit models[6,9,10]. Results also demonstrated that ^{111}In-DPC11870 cleared rapidly from the circulation. Furthermore, we demonstrated that visualization of the lesions occurred within a few hours after injection of the radiolabel. An in vivo receptor blocking experiment demonstrated that accumulation and retention at the site of infection was receptor-mediated.

The aim of this study was to elucidate the mechanism of ^{111}In-DPC11870 accumulation in the abscess. Initial experiments were performed to determine the pharmacokinetics of ^{111}In-DPC11870, whereas additional biodistribution experiments were carried out to determine the mechanism of accumulation in the abscess.

MATERIALS AND METHODS

Radiolabeling of DPC11870

DPC11870 was synthesized and characterized as described previously[6,10]. The LTB4 antagonist DPC11870 was labeled with ^{111}In with a specific activity of 3.7 MBq/µg DPC11870 (12 MBq/nmol). Quality control of the compound was performed with ITLC and HPLC as described previously[6].

Infection Model

Nineteen female NZW rabbits weighing 2.3-2.8 kg were kept in cages (one rabbit per cage) and fed standard laboratory chow and water ad libitum. An *E. coli* infection was induced in the left thigh muscle of 11 animals by intramuscular injection of 1 x 10^{11} colony-forming units (CFU) of *E. coli*. During this procedure the rabbits were anaesthetized by subcutaneous injection of 0.7 mL of a mixture of 0.315 mg/mL fentanyl and 10 mg/mL fluanison (Hypnorm®, Janssen Pharmaceutica, Buckinghamshire, UK). All animal experiments were approved by the local animal welfare committee in accordance with the Dutch legislation and carried out in accordance with their guidelines.

Whole Body Imaging and Pharmacokinetics

Twenty-four hours after the induction of the infection, when swelling of the infected muscle was apparent, five rabbits (two with intramuscular infection and three healthy) were i.v. injected with 11 MBq ^{111}In-DPC11870 (3 µg) in the lateral ear vein. For scintigraphic imaging, the rabbits were immobilized in a mold and placed prone on a dual-head Siemens Multi-Spect II gamma camera equipped with a medium-energy parallel hole collimator. The camera was connected to a Scintiview image processor and ICON computer system (Siemens). Scanning was performed (11 cm/min over 70 cm) immediately and at various time points up to 24 h p.i. and images were stored digitally in a 256x256 matrix. All images were adjusted to the same background and intensity level, to allow a fair comparison among the various experiments. The pharmacodynamics of ^{111}In-DPC11870 were studied by analyzing the images quantitatively. Regions of interest (ROI) were drawn over the total body, heart, abscess, the contralateral muscle (background), lungs, liver, spleen, kidneys and the lumbar spine (bone marrow). For each organ, except the bone marrow, the arithmetic mean value of the anterior and posterior region was used. For the bone marrow only the posterior ROI was used. ROIs were used to calculate the ^{111}In-DPC11870 concentrations in the organs at the various time points. The %ID in each organ was calculated using the total counts in the ROI of the organ and the total body

counts. Since it was not possible to draw a region over the total amount of bone marrow, here the %ID was calculated by using the amount of radioactivity measured after dissection. The correlation between the %ID found in the bone marrow and the average counts in the ROI were determined by linear regression analysis. Subsequently the %ID in the bone marrow at all imaging time points was calculated by using this correlation data (slope and Y-axis intercept).

After acquisition of the last image (24 h p.i.) the animals were sacrificed with a lethal dose of sodium phenobarbital to determine the biodistribution of the agent. A blood sample was taken by cardiac puncture. Tissues were dissected and weighed. The activity in tissues was measured in a shielded well-type gamma counter along with the injection standards and was expressed as the percentage of the injected dose per gram (%ID/g) or percentage injected dose per organ (%ID).

Studies to Determine the Mechanism of Accumulation in the Abscess

To examine the mechanism of accumulation of the tracer in the abscess in more detail, ten healthy rabbits were i.v. injected with 11 MBq ^{111}In-DPC11870 (3 µg). Sixteen hours after the injection of the radiolabel, all animals were imaged and a blood sample was taken. After this procedure, in five of these animals an intramuscular *E. coli* infection was induced in the left thigh muscle as described above. Images of the healthy and infected animals were acquired from 1 h post abscess induction up to 24 h in order to determine accumulation of radioactivity at the site of the emerging infection, while the concentration of ^{111}In-DPC11870 in the circulation was very low. For scintigraphic imaging, the rabbits were immobilized in a mold and placed prone on a gamma camera (Orbiter, Siemens, Hoffman Estates, IL) using a medium-energy parallel hole collimator. Images (300,000 cts/image) were acquired up to 24 h after induction of the abscess (i.e. 40 h postinjection (p.i.) radiolabel) and stored digitally in a 256x256 matrix. All images were windowed identically (collection of 300,000 counts, same background and intensity level), allowing a fair comparison among the various experiments. After completion of the imaging experiment animals were sacrificed and biodistribution of the radiolabel was determined as described above.

^{111}In-DPC11870 Bound to White Blood and Bone Marrow Cells

For the isolation and purification of the heterologous leukocytes[11] and the bone marrow cells, a donor rabbit with an intramuscular *E. coli* infection was used. Twenty-four hours after the induction of the abscess 50 mL of heparinized blood was collected and granulocytes were isolated as described previously[12]. The donor rabbit was sacrificed with

an overdose of phenobarbital and bone marrow cells were isolated from both femurs. The bone marrow cells were harvested and resuspended in 5 mL Phosphate Buffered Saline containing 0.5% BSA (w/v) (PBS/BSA). Cells were centrifuged for 10 minutes at 500 xg. The lipid layer and supernatant were removed. Peripheral blood leukocytes and bone marrow cells were washed twice with 50 mL incubation buffer (1 mM NaH_2PO_4, 5 mM Na_2HPO_4, 140 mM NaCl, 0.5 mM $MgCl_2$, 0.15 mM $CaCl_2$, 0.5% BSA, pH 7.4) and resuspended in 1 mL incubation buffer. Both cell suspensions were incubated with 750 µL ^{111}In-DPC11870 (30 MBq) in incubation buffer for 15 minutes at room temperature. After the incubation, cells were washed twice with 10 mL incubation buffer and resuspended in 2.5 mL PBS/BSA). The amount of cell-bound radioactivity was determined.
Three rabbits with intramuscular *E. coli* infection (induced 24 h before) were i.v. injected with either 4 MBq ^{111}In-DPC11870 (1 µg), 4 MBq of ^{111}In-DPC11870-labeled leukocytes or 4 MBq ^{111}In-DPC11870-labeled bone marrow cells. The in vitro radiolabeled white blood cells (WBCs) and bone marrow cells (BMCs) were i.v. injected to determine whether these ^{111}In-DPC11870-targeted cells would accumulate at the site of infection. Scintigraphic imaging and analysis of the images were performed as described above. The rabbits were sacrificed 24 h after the injection of the radiolabel and biodistribution was determined as described above.

Statistical Analysis
Regression analysis was performed on the data obtained from the biodistribution and the ROI data obtained from the images. The correlation between these two parameters was calculated for each organ. The regression analysis was used to calculate the %ID present in the organs at the various time points.
All mean values are presented as mean ± standard deviation. Statistical analysis was performed using the two-sided Student t-test. The level of significance was set at 0.05.

RESULTS

Radiolabeling of DPC11870
RP-HPLC analysis and ITLC quality control indicated that in all experiments the radiochemical purity of ^{111}In-DPC11870 exceeded 99%.

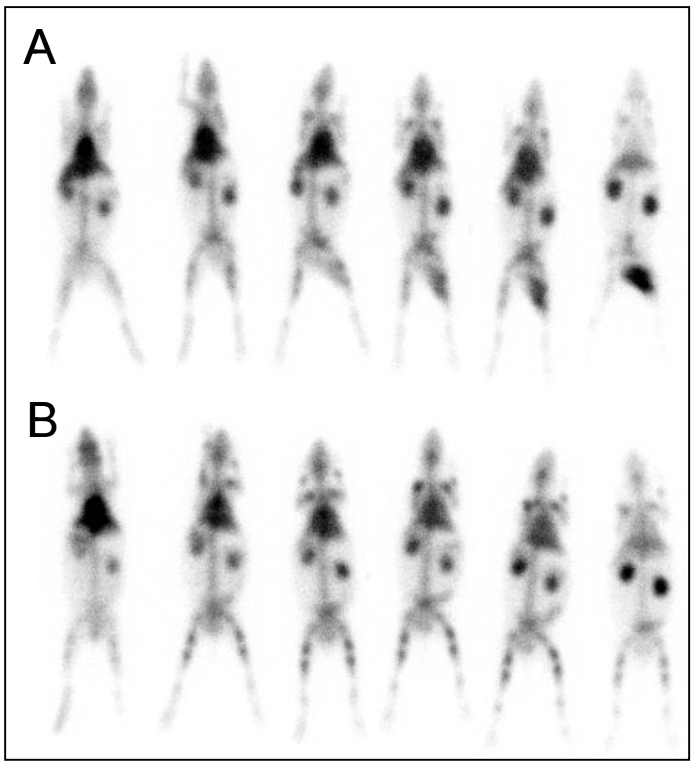

Figure 1.
Whole body images of a rabbit with E. coli thigh muscle infection (A) and a healthy rabbit (B) (anterior images are shown). The rabbits received 3 µg, 11 MBq ^{111}In-DPC11870 intravenously. Images were acquired immediately, 1, 2, 4, 8 and 24 h after injection of ^{111}In-DPC11870.

Whole Body Imaging and Pharmacokinetics

The whole body images acquired up to 24 h after injection of ^{111}In-DPC11870 demonstrated accumulation of the tracer in the abscess from a few hours after the injection (Fig. 1). The images also showed that the compound cleared rapidly from the circulation. The radiolabeled LTB4 antagonist showed some physiologic uptake in bone marrow and spleen and radioactivity was retained in the kidneys. Remarkably, the images displayed ongoing accumulation of radiolabeled compound in the abscess even when the majority of the compound had cleared from the circulation (> 4 h postinjection). Comparing the images acquired from healthy rabbits with those from rabbits with intramuscular infection, no major differences in the distribution of ^{111}In-DPC11870 were observed.

Biodistribution data are summarized in Fig. 2. The biodistribution data confirmed the relatively high uptake of the radiolabeled antagonist in the abscess, the bone marrow and the spleen. Distinct differences in radioactivity concentration were found in bone marrow and spleen of healthy and infected animals (0.67±0.29 %ID/g vs. 0.15±0.03 %ID/g in bone marrow ($p=0.011$) and 1.14±0.17 %ID/g vs. 0.27±0.05 %ID/g in spleen ($p=0.007$), for healthy and infected animals, respectively). For each organ the regression analysis

showed a good correlation between the two data sets (ROI based uptake vs. uptake in dissected tissues). Correlation coefficients were high for most tissues (r: 0.97, 0.93, 070, 0.80, 0.94, 0,71 and 0.99 for kidney, bone marrow, lung, liver, spleen, heart and muscle and abscess, respectively).

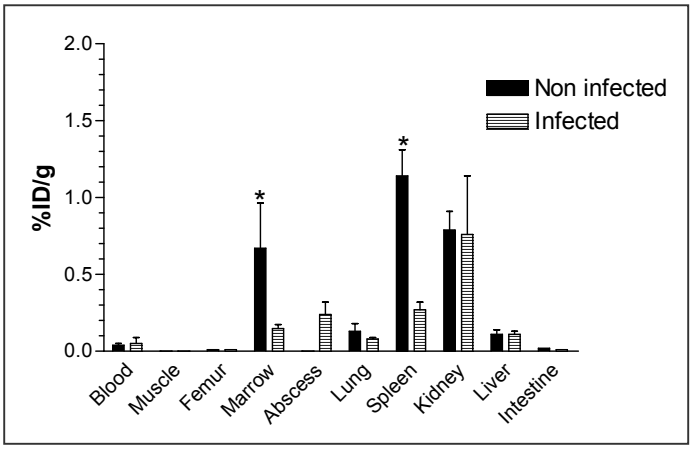

Figure 2.
*Biodistribution data obtained 24 hours postinjection of ^{111}In-DPC11870 in healthy rabbits (noninfected) and rabbits with intramuscular abscess (infected). Each bar represents the mean values ± SD. Values were analyzed using a unpaired T-test; * = P < 0.05, P-values refer to differences in uptake of radiolabel between healthy and infected animals.*

The pharmacodynamics of ^{111}In-DPC11870 for each organ is depicted in Fig. 3. The curves of a few organs, however, displayed some remarkable features. Almost immediately after injection, uptake of ^{111}In-DPC11870 was observed in lungs, liver, kidneys, spleen and bone marrow. With time, radioactivity cleared from these organs except from the kidneys. Between 8 and 24 hours postinjection, the amount of ^{111}In-DPC11870 in lung, spleen, liver remained stable, while activity concentrations continuously decreased in blood and bone marrow and increased in the *E. coli* abscess. Uptake of ^{111}In-DPC11870 in the abscess was low immediately after injection but increased continuously until 24 h postinjection. When the pharmacodynamics of ^{111}In-DPC11870 in healthy rabbits was compared to those in animals with an intramuscular infection, differences in radioactivity concentrations were observed in blood, kidney, spleen and bone marrow. Radioactivity concentration in the bone marrow was comparable in healthy and infected animals immediately after injection but radioactivity decreased more rapidly from the bone marrow of infected rabbits. Since blood levels were low from 4 h p.i. and accumulation of radioactivity in the abscess occurred throughout the whole experiment (0-24 h p.i.), the enhanced clearance of activity from bone marrow of infected animals suggested that ^{111}In-DPC11870 transferred from the bone marrow to the site of infection.

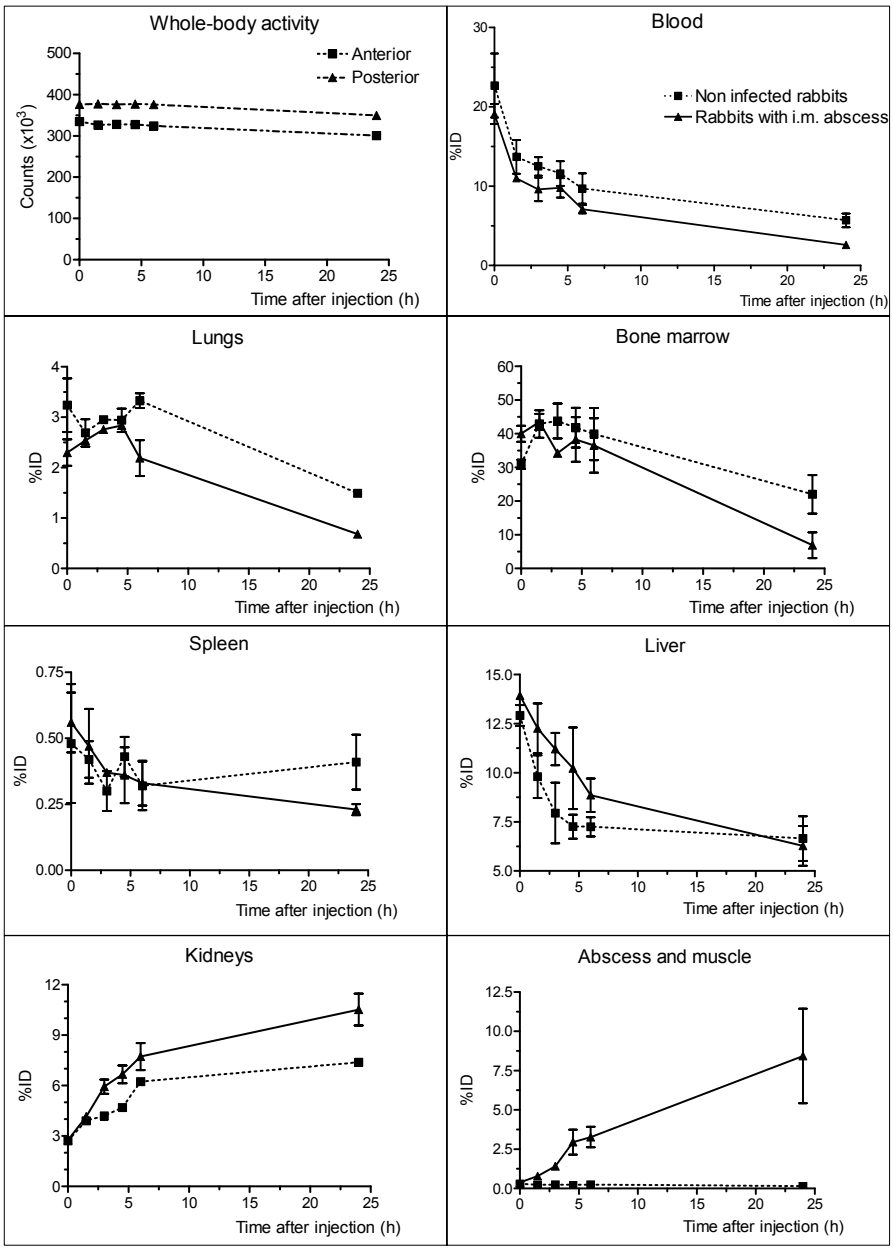

Figure 3.

The dynamics of in vivo distribution of ^{111}In-DPC11870 in non-infected (healthy) rabbits (dotted line) and rabbits with intramuscular abscess (solid line). %ID was calculated based on total body activity and is represented for total body, total blood volume, lungs, bone marrow, spleen, liver, kidneys, total muscle and the abscess. Results are reflected as mean %ID±SD.

Studies to Determine the Mechanism of Accumulation in the Abscess

From the results of the pharmacodynamic studies and analysis of the %ID calculated from the ROI data, we hypothesized that accumulation of radioactivity at the site of infection might be due to migration of radioactivity originating from the bone marrow. To validate this hypothesis, healthy animals were injected with ^{111}In-DPC11870. At 16 h p.i., when the compound had cleared from the circulation almost completely (7.2±0.9 %ID total blood pool activity), animals were imaged and subsequently in five animals an intramuscular abscess was induced. At the time of dissection, at 40 h after the injection of ^{111}In-DPC11870, 2.9±0.4 %ID and 2.2±0.4 %ID of the radioactivity remained in the circulation of respectively healthy and infected animals (p=0.012).

Images acquired just before and at several time points after induction of the abscess are shown in Fig. 4. The results of the images prior to the abscess induction (16 h p.i. ^{111}In-DPC11870) confirmed that the radioactivity concentration in the circulation (region over the heart) was low, whereas the concentration of the tracer in the bone marrow was relatively high. Subsequent images acquired after the inoculation of bacteria (Fig. 4A) showed that there was substantial accumulation of radioactivity in the abscess. In these animals there was also some degree of visualization of the bladder, indicating that a small amount of the injected dose was excreted via the urine. Comparison of these images with the images of animals that were not infected with *E. coli* (Fig. 4B) revealed that the radioactivity concentration in the bone marrow decreased more rapidly in infected animals and that ^{111}In-DPC11870 remained associated with the bone marrow in the healthy animals.

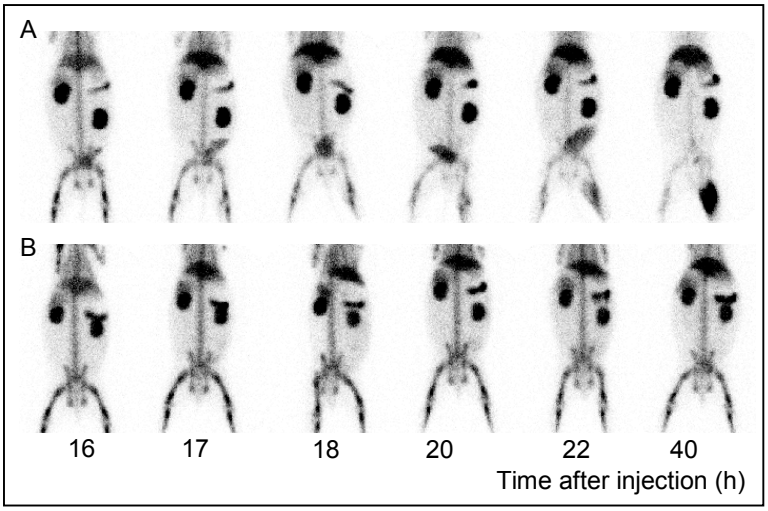

Figure 4.
Anterior images of rabbits induced with an intramuscular infection 16 h p.i of ^{111}In-DPC11870 (A) and healthy rabbits (B). Images were acquired prior to the induction of the abscess (16 h p.i. of the radiolabel) up to 40 h postinjection radiolabel (i.e. 24 h postinduction of the abscess).

The results of the biodistribution were in concordance with the images (Table 1). At the time of tissue dissection (24 h after induction of the abscess corresponding with 40 h postinjection of ^{111}In-DPC11870) the amount of radioactivity in the bone marrow of healthy animals was 33.5±4.3 %ID, whereas 9.2±2.3 %ID was found in the bone marrow of the infected animals ($p<0.0001$). The amount of radioactivity in the abscess was high (8.9±2.5 %ID) and similar to the amount of radioactivity found in the abscess of infected animals injected with ^{111}In-DPC11870 24 h after induction of the abscess. The uptake of radiolabeled ^{111}In-DPC11870 in all other organs except in the spleen was highly similar. The results of this experiment confirmed our hypothesis that accumulation of ^{111}In-DPC11870 in the abscess was due to migration of the tracer from the bone marrow. In addition, the results showed that radioactivity concentration in the bone marrow of healthy rabbits was more retained since the radioactivity concentration in the bone marrow of healthy animals was higher as compared to the concentration of the animals with the i.m. abscess.

Biodistribution ^{111}In-DPC11870 in rabbits 40 h p.i. ^{111}In-DPC11870		
	Healthy animals	E.coli infected animals 24 h after induction abscess
	%ID/g	%ID/g
Blood	0.02 ± 0.005	0.01 ± 0.003
Muscle	0.00 ± 0.001	0.00 ± 0.001
Femur	0.01 ± 0.006	0.01 ± 0.001
Marrow	0.75 ± 0.096	0.21 ± 0.050
Abscess		0.37 ± 0.161
Lung	0.08 ± 0.019	0.07 ± 0.021
Spleen	2.83 ± 0.413	1.35 ± 0.182
Kidneys	0.56 ± 0.120	0.66 ± 0.186
Liver	0.15 ± 0.033	0.15 ± 0.017
Intestine	0.01 ± 0.002	0.01 ± 0.002

Table 1.
Mean %ID/g of ^{111}In-DPC11870 with SD, in specific organs and tissues of healthy rabbits and rabbits that were induced with an intramuscular infection 16 h after injection of the radiolabel. Biodistribution was performed 40 h after injection of 11 MBq ^{111}In-DPC11870 (i.e. 24 h after induction of the abscess).

^{111}In-DPC11870 Bound to White Blood and Bone Marrow Cells

The mechanism of accumulation of radioactivity in the infectious foci was further investigated in a third experiment. In this experiment we determined if ^{111}In-DPC11870 once bound to leukocytes or bone marrow cells, was able to accumulate in the abscess.

White blood cells and bone marrow cells were isolated from a donor rabbit with an intramuscular infection. After in vitro incubation of purified cells with 30 MBq ^{111}In-DPC11870, initially 30% and 25% of the radioactivity was associated with leukocytes and bone marrow cells, respectively. After washing more than 95% of the radioactivity was cell-associated. Three animals with intramuscular *E. coli* infection were injected with either free ^{111}In-DPC11870, in vitro ^{111}In-DPC11870-labeled WBCs or in vitro ^{111}In-DPC11870-labeled BMCs. Images were acquired at several time points after injection. As shown in Fig. 5, injection of ^{111}In-DPC11870 revealed images as obtained in previous experiments. The images obtained after injection of the in vitro labeled WBCs and BMCs also demonstrated accumulation of radioactivity in the abscess. The visualization of the *E. coli* infection was similar for each of the three preparations. Furthermore, the early images showed transient entrapment of the cell-associated radioactivity in the lungs. The images demonstrated that distribution of the different radiolabels was similar.

The biodistribution data showed that radioactivity concentrations in the various organs were similar except for the kidneys (Fig. 6). Kidney uptake of ^{111}In-DPC11870 and ^{111}In-DPC11870-BMCs was 0.98 %ID/g and 1.13 %ID/g respectively, while the uptake in the kidneys after injection of ^{111}In-DPC11870-WBCs was much lower (0.54 %ID/g). Uptake of radioactivity in the kidneys represented loss or metabolized radioactivity. In all animals radioactivity concentrations in the blood was very low and the abscess uptake was comparable (between 0.34-0.52 %ID/g).

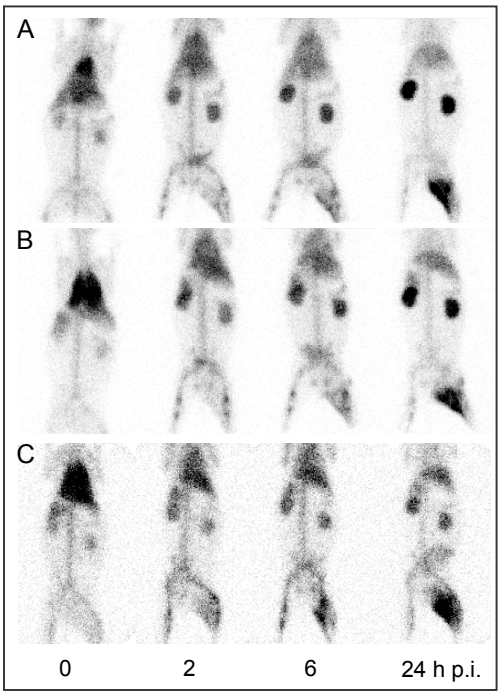

Figure 5.

Anterior images of rabbits induced with an intramuscular infection and injected with 4 MBq ^{111}In-DPC11870 (A), ^{111}In-DPC11870-BMCs (B) or ^{111}In-DPC11870-WBCs (C). Images were acquired immediately after injection of the radiolabeled compound and at 2, 6 and 24 h p.i.

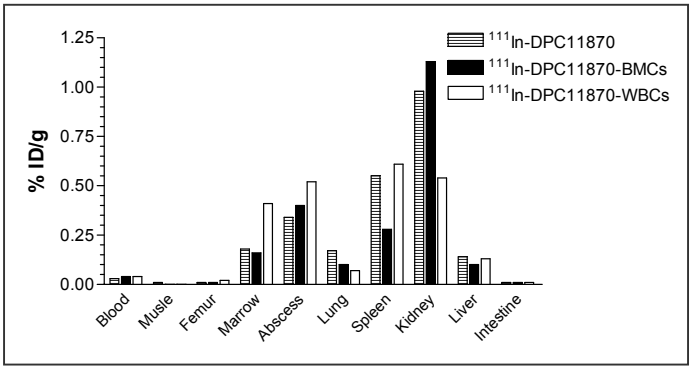

Figure 6.
Biodistribution data obtained 24 hours postinjection of ^{111}In-DPC11870, ^{111}In-DPC11870-BMCs or ^{111}In-DPC11870-WBCs. Results are presented as %ID/g found in the individual organ or tissue.

DISCUSSION

In previous studies we showed that the radiolabeled LTB4 antagonist DPC11870 efficiently visualized infection and inflammation in various rabbit models of infection and inflammation[6,9,10]. In the present study we determined the pharmacokinetics of ^{111}In-DPC11870 in detail and investigated the mechanism of accumulation in the abscess. Whole body images confirmed previous findings concerning the rapid and distinct visualization of the abscess. The results of the pharmacodynamic analysis also showed that radioactivity in the bone marrow decreased more rapidly in infected animals than in healthy animals where radioactivity remained bound in the bone marrow. Besides the bone marrow, the lungs and the liver also showed decreasing radioactivity concentrations. However, the clearance rate in these organs was similar in healthy and infected animals and could therefore not cause the accumulation of radioactivity at the site of infection. Also the differences in radioactivity concentration in the spleen, between healthy and infected animals at 24 h p.i., could not explain the uptake in the abscess since the total amount of radioactivity in this organ is by far not equivalent with the amount in the abscess. Since no other pharmacodynamic differences were found that correlated with the increasing abscess uptake, these results suggested that radioactivity from the bone marrow migrated to the abscess. We hypothesized that after injection, ^{111}In-DPC11870 targets receptor positive cells and due to subsequent migration of the tracer from the bone marrow, radioactivity accumulates in the abscess. To test this hypothesis, healthy animals were injected with ^{111}In-DPC11870. Sixteen hours later an abscess was induced. Remarkably, at 24 h after the induction of the abscess, radioactivity concentrations in the abscess of these animals were similar as compared to the abscess uptake in animals that were injected with the radiolabeled LTB4 antagonist after induction of the abscess (0.24±0.08

%ID/g and 0.37±0.16 %ID/g respectively). In this experiment there was also a significant difference between clearance of radioactivity from the bone marrow of infected animals and animals that were not infected with *E. coli* bacteria. Images showed faster clearance of radioactivity from the bone marrow after induction of the abscess, which is in line with the hypothesis of migration of in radiolabel from the bone marrow to the abscess. Apparently, the induction of the abscess induced activation of the immune system with subsequent recruitment of bone marrow cells to the site of infection. The biodistribution data further substantiated the hypothesis. Radioactivity concentration in the circulation of infected animals decreased 4.5-5.0 %ID (similar to healthy animals), whereas almost 9 %ID of the radioactivity accumulated in the abscess during the same time interval. Since the amount of radioactivity in the abscess was higher than the amount that had cleared from the circulation, and blood clearance was similar in healthy and infected animals, the radioactivity present in the abscess could not have originated from the circulation. Migration of (cell-associated) radioactivity from the bone marrow to the abscess could further explain the differences in radioactivity concentration in the bone marrow of infected animals and healthy animals at time of dissection. At the time of dissection (40 h after injection of the radiolabel) the amount of ^{111}In-DPC11870 in the bone marrow of healthy animals was approximately 24% higher as compared to the amount in infected animals (33.8±4.5%ID vs. 9.45±2.5 %ID). As a result, this experiment demonstrated that our hypothesis was valid. The question, however, remained whether the radioactivity recruited from the bone marrow to the site of infection was cell-associated. Therefore, in a third experiment we determined if in vitro ^{111}In-DPC11870 targeted WBCs and BMCs could accumulate in the abscess. The images acquired after injection of the vitro labeled cells and unbound ^{111}In-DPC11870 were comparable and demonstrated that the in vitro labeled cells also visualized the intramuscular abscess. Besides accumulation of radioactivity in the abscess all three agents showed uptake in bone marrow and spleen and a transient uptake in the lungs. These findings were in agreement with the pharmacokinetics of radiolabeled leukocytes[13,14]. Studies that focused on the kinetics of radiolabeled leukocytes showed that radiolabeled leukocytes are temporary trapped in the lungs and expose margination of activity in bone marrow and spleen. Additionally, accumulation of radioactivity in the kidneys of the rabbits was observed, which indicated clearance of released ^{111}In-DPC11870. The biodistribution data confirmed that in vitro labeled WBCs and BMCs accumulated in the abscess, comparable with ^{111}In-DPC11870. Furthermore, the biodistribution data revealed differences in radioactivity concentration in the spleen and kidneys. Uptake in the spleen indicated removal of cell-associated radioactivity and inversely correlated with radioactivity concentrations in the kidneys (released ^{111}In-

DPC11870). Since the spleen is involved in removal of scenescent granulocytes, the uptake in this organ reflects splenic granulocyte destruction and explained the difference in uptake in healthy and infected animals[15]. While in healthy animals the turnover of granulocytes is much higher this leads to higher (cell associated) radioactivity concentrations in the spleen than in infected animals where activated, in vivo radiolabeled, granulocytes were recruited to the abscess.

Although the in vitro labeled BMCs and WBCs showed some release of radioactivity, due to similar imaging characteristics, the comparable abscess uptake, the high affinity of the LTB4 antagonist for its receptor[6] and the expression of LTB4 receptors on immune cells[16], it is conceivable that accumulation of radioactivity in the abscess is mainly due to migration of cell-associated radioactivity. Moreover, in healthy animals the radiolabel also remained associated with the bone marrow cells that were present in this organ. Only at relatively early time points after the injection of the radiolabeled compound, when blood levels are high, there might be a contribution of non-cell-associated activity that enters the site of infection and binds to receptors expressed by white blood cells present in the abscess.

Taken together, our study indicates that visualization of infectious lesions with ^{111}In-DPC11870 is mainly due to accumulation of cell-associated radioactivity. The compound might therefore exhibit similar imaging characteristics as radiolabeled leukocytes. Since preparation of ^{111}In-DPC11870 is easy, rapid and without potential risks, disadvantages accompanied with preparation of radiolabeled leukocytes are absent. We therefore consider the radiolabeled LTB4 antagonist ^{111}In-DPC11870 as a potential agent to visualize infectious and inflammatory lesions in patients and it is warranted to investigate the applicability of this compound in clinical studies.

CONCLUSION

In this study the pharmacodynamics of the radiolabeled LTB4 antagonist DPC11870 were investigated in detail. The results of this study showed that the accumulation of radioactivity at the site of the infection occurs mainly due to migration of ^{111}In-DPC11870 from the bone marrow and circulation to the abscess. It is convincible that the radioactivity migrates cell-associated to the site of infection. Visualization of infectious foci with ^{111}In-DPC11870 is due to in vivo targeting of receptor positive hematopoietic cells and imaging characteristics resemble that of radiolabeled leukocytes.

REFERENCES

1. Corstens FH, van der Meer JW. Nuclear medicine's role in infection and inflammation. Lancet. 1999;354:765-770.
2. Weiner RE, Thakur ML. Imaging infection/inflammations. Pathophysiologic basis and radiopharmaceuticals. Q J Nucl Med. 1999;43:2-8.
3. Signore A, Chianelli M, Bei R, Oyen WJ, Modesti A. Targeting cytokine/chemokine receptors: a challenge for molecular nuclear medicine. Eur J Nucl Med Mol Imaging. 2003;30:149-56
4. van Eerd JE, Boerman OC, Corstens FH, Oyen WJ. Radiolabeled chemotactic cytokines: new agents for scintigraphic imaging of infection and inflammation. Q J Nucl Med. 2003;47:246-255.
5. Rennen HJ, Corstens FH, Oyen WJ, Boerman OC. New concepts in infection/inflammation imaging. Q J Nucl Med. 2001;45:167-173.
6. van Eerd JE, Oyen WJ, Harris TD, et al.. A bivalent leukotriene B(4) antagonist for scintigraphic imaging of infectious foci. J Nucl Med. 2003;44:1087-1091.
7. Toda A, Yokomizo T, Shimizu T. Leukotriene B4 receptors. Prostaglandins Other Lipid Mediat. 2002;68-69:575-585.
8. Yokomizo T, Izumi T, Chang K, Takuwa Y, Shimizu T. A G-protein-coupled receptor for leukotriene B4 that mediates chemotaxis. Nature. 1997;387:620-624.
9. van Eerd JE, Laverman P, Oyen WJ, et al.. Imaging of experimental colitis with a radiolabeled leukotriene B4 antagonist. J Nucl Med. 2004;45:89-93.
10. van Eerd JE, Rennen H, Oyen W, et al.. Scintigraphic detection of pulmonary aspergillosis in rabbits with a radiolabeled leukotriene B4 antagonist. J Nucl Med. 2004. In Press.
11. Gratz S, Rennen HJ, Boerman OC, et al.. ^{99m}Tc-HMPAO-labeled autologous versus heterologous leukocytes for imaging infection. J Nucl Med. 2002;43:918-924.
12. Dams ET, Oyen WJ, Boerman OC, et al.. Technetium-99m-labeled liposomes to image experimental colitis in rabbits: comparison with technetium-99m-HMPAO-granulocytes and technetium-99m-HYNIC-IgG. J Nucl Med. 1998;39:2172-2178.
13. Aktolun C, Ussov WY, Arka A, Glass D, Gunasekera RD, Peters AM. Technetium-99m and indium-111 double labelling of granulocytes for kinetic and clinical studies. Eur J Nucl Med. 1995;22:330-334.
14. Ussov WY, Aktolun C, Myers MJ, Jamar F, Peters AM. Granulocyte margination in bone marrow: comparison with margination in the spleen and liver. Scand J Clin Lab Invest. 1995;55:87-96.
15. Saverymuttu SH, Peters AM, Keshavarzian A, Reavy HJ, Lavender JP. The kinetics of ^{111}indium distribution following injection of ^{111}In-labelled autologous granulocytes in man. Br J Haematol. 1985;61:675-685.
16. Pettersson A, Richter J, Owman C. Flow cytometric mapping of the leukotriene B4 receptor, BLT1, in human bone marrow and peripheral blood using specific monoclonal antibodies. Int Immunopharmacol. 2003;3:1467-1475.

Chapter 6

Synthesis of Leukotriene B4 antagonists labeled with In-111 or Tc-99m to image infectious and inflammatory foci.

Matthias Broekema
Julliëtte J.E.M. van Eerd
Wim J.G. Oyen
Frans H.M. Corstens
Rob M.J. Liskamp
Otto C. Boerman
Thomas D. Harris

J Med Chem. 2005; In Press

ABSTRACT

In previous studies we demonstrated that ^{99m}Tc-labeled Leukotriene B4 (LTB4) antagonist RP517 accumulated in infectious foci in rabbits. This lipophilic tracer cleared via the hepatobiliary route hampering imaging of abdominal lesions.

Objectives: In the present study we report the synthesis and radiolabeling of three hydrophilic analogues of RP517.

Methods: DPC11870-11 (**15**) is a divalent LTB4 antagonist conjugated to DTPA for radiolabeling with In-111. Monovalent LTB4 antagonists BMS57868-88 (**13**), and divalent LTB4 antagonist BMS57868-81 (**16**), are conjugated to bifunctional chelator HYNIC for radiolabeling with ^{99m}Tc. All three of these new imaging agents use cysteic acid groups as a pharmacokinetic modifier (PKM), giving them greatly improved water solubility.

Results: The three compounds labeled efficiently with ^{111}In or ^{99m}Tc with high radiochemical purity, and high specific activities. The biodistribution properties were determined in rabbits having intramuscular *E. coli* infection. These initial studies showed that, in contrast to RP517, clearance of all three compounds was exclusively renal. Furthermore, it was shown that the in vivo behavior of the ^{99m}Tc-labeled LTB4 antagonists was affected by the chelator/radionuclide combination, by the coligands used with the HYNIC chelator, and by the monovalent or divalent nature of the receptor-binding moiety. The use of tricine and isonicotinic acid (ISO) as co-ligands with HYNIC gave the highest uptake of radioactivity in the abscess and lowest radioactivity concentration in the non-target tissues.

Conclusion: Scintigraphic images of the three new LTB4 antagonist demonstrated that all visualized infectious foci in a rabbit model of acute intramuscular abscesses. The initial results of this study warrant additional detailed pharmacokinetic studies to investigate which of the three LTB4 antagonists exhibits most optimal characteristics for imaging infection and inflammation.

INTRODUCTION

The Leukotriene B4 (LTB4) receptors are G-protein-coupled receptors (GPCR) that are involved in recruitment and activation of leukocytes during an inflammatory response[1]. At present, two LTB4 receptor types are identified; BLT1 and BLT2, which have different affinities for LTB4[2,3]. The high affinity receptor BLT1 is mainly expressed on neutrophils, while BLT2 is expressed more ubiquitously. LTB4 plays an essential regulatory role during the inflammatory response. However, its overproduction is reported to play a role in

pathological conditions such as asthma, inflammatory bowel disease and arthritis[4,5]. Consequently, a large number of LTB4 antagonists have been developed for clinical application as anti-inflammatory therapeutics[6]. The rapid detection of infectious and inflammatory foci in patients is essential for timely and adequate therapeutic intervention. One of the current methods for detection of infection and inflammation is scintigraphic imaging. The generally used radiopharmaceuticals for this purpose, ^{99m}Tc-labeled leukocytes and ^{67}Ga-citrate, have several disadvantages. The blood handling required for the preparation of radiolabeled leukocytes is accompanied by the risk of infection from blood-borne pathogens, and is a time-consuming preparation[7,8]. The nuclear and biodistribution properties of ^{67}Ga-citrate are far from ideal, resulting in poor image quality and increased radiation burden to the patient.

We previously reported the synthesis of ^{99m}Tc-labeled LTB4 antagonist RP517 (Figure 1)[9]. LTB4 antagonist RPR69698[10] was modified with a short PEG spacer to give compound **1**, and the Boc group of **1** was replaced with the bifunctional chelator hydrazinonicotinic acid (HYNIC) to give drug precursor SG380 (**2**). The hydrazine was protected as the hydrazone of sodium 2-formylbenzenesulfonate to avoid reaction with trace quantities of formaldehyde and other carbonyl compounds commonly found in the research and manufacturing environment[11]. The radiolabeling of SG380 utilized ^{99m}Tc[TcO_4]$^-$ in the presence of coligands tricine and trisodium triphenylphosphine-3,3',3''-trisulfonate (TPPTS)[12]. This radiolabeling procedure gave a rapid and clean formation of ternary ligand complex RP517. This tracer showed rapid accumulation in the infected thigh muscle in the rabbit *E. coli* model[13]. However, RP517 clears almost exclusively via the hepatobiliary route, and physiologic uptake in the intestines limits clinical applicability of this agent. Based on these observations, more hydrophilic compounds were designed, using cysteic acid (Csa) as a PKM. Initially, compound **1** was modified with four cysteic acids, converted to a bivalent ligand using glutamic acid, and conjugated to DTPA giving DPC11870-11 (**15**). [^{111}In(DPC11870-11)] (**21**) was found to rapidly visualize infectious foci in the rabbit *E. coli* infected thigh muscle model[14]. The agent cleared rapidly from non-target tissues, and excretion is almost exclusively renal.

Although the biodistribution and imaging properties of [^{111}In(DPC11870-11)] are very promising, a ^{99m}Tc-labeled tracer is generally preferred for scintigraphic imaging over an ^{111}In-labeled tracer because of the more favorable nuclear properties of ^{99m}Tc (140 keV gamma emissions, 6 h half-life) and the general availability of portable ^{99m}Tc generators. Herein we describe the synthesis and initial biological evaluation of two analogues of DPC11870-11. One compound (**16**) is structurally almost identical to DPC11870-11, with HYNIC replacing DTPA, while the other compound (**13**) is a monovalent version of **16**.

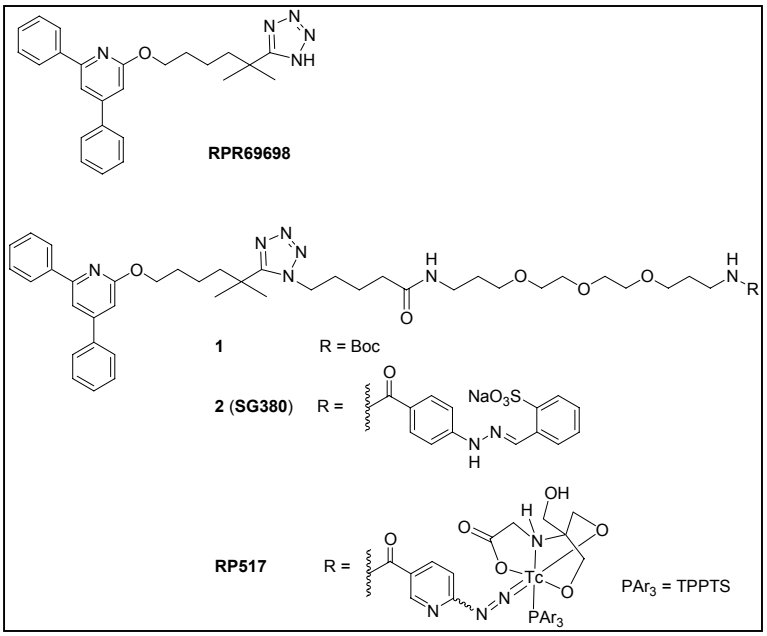

Figure 1.
*Structures of lead LTB4 antagonist **RPR69698**, PEG-modified LTB4 antagonists **1**, protected Hynic derivative **SG380** (**2**), and **RP517**, the ^{99m}Tc ternary ligand complex.*

Both of these LTB4 antagonists were radiolabeled with ^{99m}Tc and the in vivo imaging characteristics were compared with those of [^{111}In(DPC11870-11)]. Furthermore, using divalent HYNIC conjugate **16**, we have compared the biodistribution properties of three coligand systems, and shown that the coligand system can have a profound effect on the biodistribution properties of these ^{99m}Tc complexes. We also describe the complete synthesis of DPC11870-11, and provide an improved synthesis of PEGylated LTB4 antagonist **1**.

MATERIALS AND METHODS

Previously published procedures were used for the synthesis of Boc-Csa(Na)-OH[29], Boc-Glu(OTfp)-Otfp[30], 6-Hydrazinonicotinic acid[31], RPR69698[10], and N-(t-butoxycarbonyl)-4,7,10-trioxa-1,13-tridecanediamine[32]. HPLC-grade ACN was obtained from J.T. Baker. Absolute ethanol was obtained from Quantum Chemical Corp. All other reagents and solvents were purchased from Aldrich Chemical Corporation, Lancaster Synthesis, Inc., or Fluka Chemical Corporation and used as received. Merck silica gel, grade 9385, 230-400 mesh, 60 Å was used for flash chromatography. Na-$^{99m}TcO_4$ (Mo-generator) and $^{111}InCl_3$ were obtained from Tyco Mallinckrodt, Netherlands. All reactions were carried out at

ambient temperatures under a nitrogen atmosphere unless noted otherwise. Organic reaction mixtures were concentrated under reduced pressure at 40-65 °C on a rotary evaporator. Reaction monitoring and low resolution mass data were obtained with an Agilent Model 1100 LC/MSD API-electrospray system using either a Phenomenex Synergi™ Polar-RP C18 column (4 µm, 80 Å, 4.6 x 150 mm), or a Zorbax SB-CN column (5 µm, 4.6 x 150mm), operated at 50 °C with 0.1% formic acid-modified ACN/water mobile phases. Final HPLC purity determination was made with an Agilent Model 1100 HPLC system, using either a Waters Atlantis™ dC18 column (5 µm, 4.6 x 100 mm) or a Zorbax SB-CN column (5 µm, 4.6 x 150mm), and 0.1% TFA or 0.1 M NaOAc-modified ACN/water as mobile phases. UV detection was carried out at 220 and 254 nm. Preparative HPLC purifications were performed on a Varian PrepStar system using SD-1 pumps equipped with a uv/vis detector model 320, using a Waters Atlantis™ dC18 column (5 µm, 30 x 100mm) except as noted otherwise, and using the gradients and mobile phases given in the text. UV detection was carried out at 220 nm. All chromatography was carried out with HPLC grade organic solvents.

Exact mass determination was performed on a 7.0 tesla Fourier transform ion cyclotron resonance (FTICR) mass spectrometer (IonSpec Corporation, Lake Forest, CA) equipped with an electrospray ionization source. A mixture of sample and internal calibrant (polyethylene glycol or polypropylene glycol) was prepared at approximately 10 µM each in ACN:water:acetic acid (500:500:1) and infused at 1 µL/minute. A spectrum was obtained using the IonSpec OMEGA data system by averaging five transients of 512K data points per transient. Mass calibration was derived from internal calibrant ions bracketing the m/z of interest for the sample. FT-NMR spectra were obtained on a Bruker Avance 600 MHz spectrometer at 600 MHz for ^{1}H and 150 MHz for ^{13}C using the indicated solvent. Residual solvent signals were used for internal calibration. Chemical shifts are reported in parts per million (δ), and signals are expressed as s (singlet), d (doublet), t (triplet), q (quartet), p (pentet), m (multiplet), or br (broad). Elemental analyses were performed at Oneida Research Services, Inc, Whitesboro, NY; found values agree favorably with the calculated ones.

*Ethyl 5-(5-(5-(4,6-Diphenyl(2-pyridyloxy))-1,1-dimethylpentyl)-1,2,3,4-tetraazolyl)-pentanoate (**3a**)*

A solution of RPR69698 (35.0 g, 84.6 mmol) and bis(tri-n-butyltin)oxide (21.5 mL, 42.3 mmol) in absolute EtOH (1035 mL) was heated at reflux under nitrogen for 30 min. The solution was concentrated under vacuum and the resulting was dissolved in cyclohexane (3x200 mL) and again concentrated to remove traces of EtOH. The oil was dissolved in

cyclohexane (35 mL), treated with ethyl 5-bromovalerate (40.0 mL, 254 mmol), and heated at 85 ˚C in an oil bath under nitrogen for 28 h. The reaction was cooled to ambient temperatures, diluted with ether (350 mL), washed sequentially with 10% KF solution (125 mL) and saturated NaCl (400 mL), dried ($MgSO_4$), and concentrated to give yellow oil. This oil was purified by silica gel flash chromatography. The column was initially eluted with hexane/EtOAc (75/25) until the unwanted N2 isomer was off the column, and the mobile phase was switched to hexane/EtOAc (60/40) to collect the desired N1 isomer. Product fractions were concentrated and the resulting solid was recrystallized (EtOH) to give 16.58g (36%) of the title compound as a colorless solid, MP 99.5-101.5 ˚C. ^{1}H NMR ($CDCl_3$): δ 8.10-8.01 (m, 2H), 7.69-7.62 (m, 2H), 7.55-7.36 (m, 7H), 6.85 (s, 1H), 4.43 (t, J = 6.3 Hz, 2H), 4.34 (t, J = 7.5 Hz, 2H), 4.09 (q, J = 7.1 Hz, 2H), 2.32 (t, J = 7.2 Hz, 2H), 2.07-1.92 (m, 2H), 1.91-1.60 (m, 8H), 1.50 (s, 6H), 1.21 (t, J = 7.1 Hz, 3H); ^{13}C NMR ($CDCl_3$): δ 172.7, 164.1, 159.8, 155.1, 152.1, 139.1, 138.7, 129.0, 128.9, 128.6, 127.0, 126.8, 111.8, 107.1, 65.30, 60.49, 48.57, 41.32, 34.84, 33.40, 29.38, 29.30, 27.17, 21.90, 21.29, 14.18; High Resolution MS: Calcd for $C_{32}H_{40}N_5O_3$ $[M+H]^+$: 542.3131, Found: 542.3140; Anal. ($C_{32}H_{39}N_5O_3$) C,H,N.

*Ethyl 5-(4-(5-(4,6-Diphenyl(2-pyridyloxy))-1,1-dimethylpentyl)-1,2,3,5-tetraazolyl)-pentanoate (**3b**)*

Fractions from the above flash chromatography containing the unwanted N2 isomer were concentrated to give 10.2 g (22%) of the title compound as a colorless solid. ^{1}H NMR ($CDCl_3$): 8.10-8.01 (m, 2H), 7.69-7.61 (m, 2H), 7.55-7.35 (m, 7H), 6.86 (s, 1H), 4.54 (t, J = 7.1 Hz, 2H), 4.42 (t, J = 6.6 Hz, 2H), 4.09 (q, J = 7.1 Hz, 2H), 2.31 (t, J = 7.3 Hz, 2H), 2.09-1.95 (m, 2H), 1.90-1.70 (m, 4H), 1.70-1.56 (m, 2H), 1.45-1.28 (m, 8H), 1.21 (t, J = 7.1 Hz, 3H); ^{13}C NMR ($CDCl_3$): 173.50, 172.81, 164.32, 155.12, 151.97, 139.18, 138.82, 128.94, 128.84, 128.57, 127.03, 126.81, 111.66, 107.10, 65.83, 60.40, 52.32, 42.40, 34.77, 33.32, 29.59, 28.63, 27.21, 21.74, 21.31, 14.18; MS: m/e 542.4 [M+H]; High Resolution MS: Calcd for $C_{32}H_{40}N_5O_3$ $[M+H]^+$: 542.3131, Found: 542.3143; Anal. ($C_{32}H_{39}N_5O_3$) C,H,N.

*5-(5-(5-(4,6-Diphenyl(2-pyridyloxy))-1,1-dimethylpentyl)-1,2,3,4-tetraazolyl)pentanoic Acid (**4**)*

A solution of ester **3a** (16.2 g, 29.9 mmol) in inhibitor free, peroxide free THF (450 mL) was treated with 3 M LiOH (120 mL) and the resulting mixture was stirred rapidly for 19 h. The mixture was concentrated until most of the THF was removed. The resulting aqueous mixture was adjusted to pH 3 with 6 N HCl and extracted with EtOAc (1 x 450, 1 x 60 mL). The combined EtOAc extracts were washed with saturated NaCl (100 mL), dried ($MgSO_4$), and concentrated to give 15.3g (100%) of the title compound as a viscous colorless oil. ^{1}H NMR ($CDCl_3$): 8.02 (d, J = 8.4 Hz, 2H), 7.65(d, J = 8.2 Hz, 2H), 7.55-7.35 (m, 7H), 6.84 (s, 1H), 4.43-

4.31 (m, 4H), 2.36 (t, J = 7.0 Hz, 2H), 2.10-1.92 (m, 2H), 1.89-1.62 (m, 6H), 1.49 (s, 6H), 1.42-1.20 (m, 2H); High Resolution MS: Calcd for $C_{30}H_{36}N_5O_3$ $[M+H]^+$; 514.2818, Found: 514.2819.

*N-(3-(2-(2-(3-((tert-Butoxy)carbonylamino)propoxy)ethoxy)ethoxy)propyl)-5-(5-(5-(4,6-diphenyl(2-pyridyloxy))-1,1-dimethylpentyl)(1,2,3,4-tetraazolyl))pentanamide (**1**)*

A solution of **4** (5.60 g, 10.9 mmol), DIEA (4.75 mL, 27.3 mmol), and HBTU (5.68 g, 15.0 mmol) in anhydrous DMF (75 mL) was stirred for 5 min and treated with a solution of N-(t-butoxycarbonyl)-4,7,10-trioxa-1,13-tridecanediamine (4.81 g, 15.0 mmol) in anhydrous DMF (35 mL). Stirring was continued for 6 h. The DMF was removed, and the resulting viscous oil was partitioned between EtOAc (330 mL) and water (75 mL) at pH 3. The organic phase was washed consecutively with dilute (pH 3) HCl (2 x 75 mL), water (75 mL), saturated (sat.) $NaHCO_3$ (75 mL), and sat. NaCl (75 mL). The organic phase was dried ($MgSO_4$) and concentrated to give 8.80 g (99%) of 1 as an amber viscous oil. ^1H NMR ($CDCl_3$): δ 8.03 (d, J = 8.4 Hz, 2H), 7.65 (d, J = 8.4 Hz, 2H), 7.53 (d, J = 1.2 Hz, 1H), 7.49-7.37 (m, 6H), 6.83 (d, J = 1.2 Hz, 1H), 6.30 (bs, 1H), 4.95 (bs, 1H), 4.41 (t, J = 6.4 Hz, 2H), 4.34 (t, J = 7.5 Hz, 2H), 3.65-3.48 (m, 12H), 3.36-3.25 (m, 2H), 3.21-3.11 (m, 2H), 2.16 (t, J = 7.2 Hz, 2H), 2.02-1.94 (m, 2H), 1.88-1.66 (m, 10H), 1.48 (s, 6H), 1.40 (s, 9H), 1.37-1.28 (m, 2H); ^{13}C NMR ($CDCl_3$): δ 172.06, 170.25, 164.10, 159.91, 157.14, 156.10, 154.98, 152.41, 138.84, 138.58, 129.01, 128.64, 127.59, 127.07, 126.85, 111,90, 78.94, 70.45, 70.42, 70.14, 70.01, 69.93, 69.43, 65.59, 48.72, 41.28, 38.41, 37.88, 35.53, 34.84, 29.70, 29.48, 29.30, 28.90, 28.44, 27.15, 22.59, 21.33; High Resolution MS: Calcd for $C_{45}H_{66}N_7O_7$ [M+H]: 816.5024, Found: 816.5044.

*General procedure for pre-activation of Boc-Csa(Na)-OBt (**6**)*

Boc-cysteic acid mono sodium salt in anhydrous DMF (6 mL DMF for 1 mmol Boc-Csa(Na)-OH) was treated with 1 equiv of HBTU and 2 equiv of DIEA, and stirred for 25 min. The resulting solution of active ester was transferred to a solution of the reactive amine using anhydrous DMF to complete the transfer.

*LTB4-(Csa)-H (**8**)*

A solution of **1** (1.68 g, 2.1 mmol) in 50/40/5/5 DCM/TFA/TIS/H_2O (40 mL) was stirred for 30 min and concentrated yielding **5** as a yellow viscous oil. This oil was dissolved in DMF (25 mL), and made basic with DIEA (2.90 mL, 16.6 mmol). A solution of active ester Boc-Csa(Na)-OBt (6) was prepared in a separate flask from Boc-Csa(Na)-OH (1.20 g, 4.1 mmol), HBTU (1.56 g, 4.1 mmol), and DIEA (1.5 mL, 8.6 mmol) in DMF (25 mL). This solution of **6** was added to the solution of **5**, and after 2 hours of stirring, the reaction mixture was concentrated, yielding a yellow oil. This oil was redissolved in $CHCl_3$ (180 mL), washed with water (2 x 100 mL), and sat. $NaHCO_3$ (1 x 80 mL). The aqueous layer

was back-extracted with $CHCl_3$ (1 x 100 mL). The combined organic layers were dried (Na_2SO_4) and concentrated to give **7** as a pale yellow oily foam. This foam was dissolved in 50/40/5/5 DCM/TFA/TIS/H_2O (40 mL), stirred for 20 min, and concentrated to give mono-cysteic acid derivative **8** as a yellow oil. This oil was used in the subsequent reaction without further purification. MS: m/z 867.5 $[M+H]^+$.

*LTB4-(Csa)$_2$-H (**9**)*

A solution of **8** in DMF (25 mL) and DIEA (2.70 mL, 15.5 mmol) was treated with a solution of Boc-Csa(Na)-OBt (**6**) prepared from Boc-Csa(Na)-OH (1.04 g, 3.6 mmol), HBTU (1.36 g, 3.6 mmol), and DIEA (1.25 mL, 7.2 mmol) in DMF (20 mL). The solution was stirred for 1 h and concentrated to give viscous yellow oil. This oil was dissolved in 50/40/5/5 DCM/TFA/TIS/H_2O (50 mL), stirred for 20 min and concentrated. Crude product was purified by HPLC using a 3%/min gradient of 36-72% ACN containing 0.1% TFA at a flow rate of 40 mL/min. The product fraction eluting at 5.7 min was lyophilized to give dicysteic acid derivative **9** (1.03 g, 0.91 mmol, 44% from compound 1) as a colorless solid. ^{1}H NMR (CD_3OD): δ 7.97-7.94 (m, 2H), 7.94-7.91 (m, 2H), 7.88 (d, J = 1.2 Hz, 1H), 7.63-7.57 (m, 6H), 7.53 (d, J = 1.2 Hz, 1H), 4.87-4.83 (m, 1H), 4.56 (t, J = 6.3 Hz, 2H), 4.50 (t, J = 7.2 Hz, 2H), 4.30 (t, J = 6.0 Hz, 1H), 3.61-3.56 (m, 4H), 3.55-3.50 (m, 4H), 3.48-3.37 (m, 7H), 3.25-3.16 (m, 4H), 3.11-3.05 (m, 1H), 2.24 (t, J = 7.2 Hz, 2H), 1.22-1.88 (m, 6H), 1.75-1.66 (m, 6H), 1.51 (s, 6H), 1.39-1.32 (m, 2H); ^{13}C NMR (CD_3OD): δ 175.4, 171.8, 168.7, 163.4, 161.7, 160.8, 153.4, 137.5, 134.3, 132.7, 132.6, 130.8, 130.6, 129.4, 129.2, 116.1, 106.9, 72.10, 71.63, 71.32, 71.30, 70.06, 69.88, 53.02, 52.74, 51.98, 51.47, 50.21, 42.12, 38.15, 38.11, 36.41, 36.21, 30.63, 30.46, 30.36, 30.06, 27.67, 24.08, 22.3; High Resolution MS: Calcd for $C_{46}H_{68}N_9O_{13}S_2$ [M+H]: 1018.4372; Found: 1018.4386.

LTB4-(Csa)$_3$-H (10)

A solution of **9** (911 mg, 0.81 mmol), and DIEA (625 µL, 3.6 mmol) in DMF (10 mL) was treated with solution of Boc-Csa(Na)-OBt (**6**) prepared from Boc-Csa-(Na)-OH (521 mg, 1.8 mmol), HBTU (679 mg, 1.8 mmol), and DIEA (625 µL, 3.6 mmol) in DMF (10 mL). The reaction was stirred for 2 h and concentrated. The residue was dissolved in 50/40/5/5 DCM/TFA/TIS/H_2O (20 mL), stirred for 25 min, and concentrated. Crude product was purified by HPLC using a 3%/min gradient of 31.5-54% ACN containing 0.1% TFA at a flow rate of 40 mL/min. The product fraction eluting at 4.8 min was lyophilized to give tricysteic acid derivative **10** (1.01 g, 0.78 mmol, 97%) as a colorless solid. ^{1}H NMR (CD_3OD): δ 8.03-7.99 (m, 2H), 7.93-7.88 (m, 3H), 7.69-7.59 (m, 7H), 4.72 (dd, J = 3.5, 9.7 Hz, 1H), 4.65 (dd, J = 3.6, 9.6 Hz, 1H), 4.60 (t, J = 6.7 Hz, 2H), 4.54 (t, J = 7.2 Hz, 2H), 4.37 (dd, J = 3.6, 9.6 Hz, 1H), 3.63-3.58 (m, 4H), 3.58-3.53 (m, 4H), 3.53-3.39 (m, 6H), 3.36-3.30 (m, 1H), 3.30-3.19 (m, 7H), 2.36 (t, J = 7.5 Hz, 2H), 2.06-1.99 (m, 2H), 1.99-1.90 (m, 4H), 1.79-1.70 (m, 6H), 1.52 (s, 6H),

1.41-1.33 (m, 2H); ^{13}C NMR (CD_3OD): δ 176.1, 172.4, 171.7, 168.9, 162.9, 162.1, 161.7, 152.6, 136.9, 133.2, 133.0, 132.9, 130.8, 130.7, 129.8, 129.5, 116.7, 106.8, 73.30, 71.53, 71.21, 71.14, 69.91, 69.63, 53.61, 53.04, 52.30, 52.03, 51.73, 50.99, 50.16, 41.93, 38.57, 38.04, 36.18, 36.03, 30.53, 30.19, 30.09, 29.92, 27.63, 24.15, 22.23; High Resolution MS: Calcd for $C_{49}H_{73}N_{10}O_{17}S_3$ [M+H]: 1169.4312; Found: 1169.4309.

*LTB4-(Csa)$_4$-H (**11**)*

A solution of **10** (705 mg, 0.55 mmol) and DIEA (630 µL, 3.6 mmol in DMF (12 mL)) was treated with a solution of Boc-Csa(Na)-OBt (**6**) prepared from Boc-Csa-(Na)-OH (351 mg, 1.2 mmol), HBTU (457 mg, 1.2 mmol), and DIEA (420 µL, 2.4 mmol) in DMF (7 mL). The reaction was stirred for 40 min and concentrated. The residue was dissolved in 50/40/5/5 DCM/TFA/TIS/H_2O (20 mL), stirred for 25 min, and concentrated. Crude product was purified by HPLC using a 3%/min gradient of 27-54% ACN containing 0.1% TFA at a flow rate of 40 mL/min. The product fraction eluting at 5.3 min was lyophilized to give tetracysteic acid derivative **11** (674.8 mg, 0.47 mmol, 86%) as a colorless solid. ^{1}H NMR (CD_3OD & CD_3CN): δ 7.88-7.83 (m, 4H), 7.77 (d, J = 1.2 Hz, 1H), 7.61-7.53 (m, 4H), 7.34 (d, J = 1.2 Hz, 1H), 4.71 (dd, J = 3.9, 9.3 Hz, 1H), 4.57-4.51 (m, 2H), 4.46-4.39 (m, 4H), 4.37 (dd, J = 4.2, 9.0 Hz, 1H), 3.56-3.34 (m, 14H), 3.31-3.14 (m, 8H), 3.11 (t, J = 6.9 Hz, 2H), 2.17 (t, J = 7.2 Hz, 2H), 1.90 (p, J = 7.5 Hz, 2H), 1.86-1.78 (m, 4H), 1.69 (p, J = 6.6 Hz, 2H), 1.66-1.57 (m, 4H), 1.44 (s, 6H), 1.27-1.20 (m, 2H); ^{13}C NMR (CD_3OD & CD_3CN): δ 175.6, 172.4, 172.0, 171.9, 168.8, 163.3, 161.8, 159.9, 153.2, 137.2, 134.1, 132.7, 132.6, 130.8, 130.6, 129.2, 129.1, 115.8, 106.9, 71.71, 71.11, 70.91, 70.87, 69.80, 69.53, 53.06, 52.88, 52.51, 51.86, 51.67, 51.53, 51.23, 50.95, 50.13, 41.66, 37.87, 37.76, 36.32, 35.98, 30.28, 30.02, 29.84, 29.68, 27.58, 23.83, 21.99; High Resolution MS: Calcd for $C_{52}H_{78}N_{11}O_{21}S_4$ [M+2H]: 660.7162; Found: 660.7163.

*6-(2-Benzaldehydehydrazono)nicotinic acid (**12**)*

A suspension of 6-hydrazinonicotinic acid (274 mg, 1.8 mmol) in DMF (11 mL) was treated with benzaldehyde (1.1 mL, 11 mmol), and stirred for 2 days. Filtration of the reaction mixture gave **12** as a pale yellow powder. The filtrate was diluted with DCM (100 mL) to give an additional crop of **12**. The combined solids were washed with DCM and gave the title compound (284 mg, 1.2 mmol, 66%) as a light yellow powder. ^{1}H NMR (DMSO-d6 & CD_3OD): δ 8.53 (s, 1H), 8.42 (s, 1H), 8.30 (d, J = 9.0 Hz, 1H), 7.96 (s, 2H), 7.47 (dd, J = 1.8 & 5.4 Hz, 3H), 7.38 (d, J = 9.0 Hz,1H); ^{13}C NMR (DMSO-d6 & CD_3OD): δ 164.5, 141.9, 133.4, 130.7, 128.8, 127.8, 117.5; High Resolution MS: Calcd for $C_{13}H_{12}N_3O_2$ [M+H]: 242.0924; found: 242.0923.

*BMS57868-88 (**13**)*

A solution of **12** (10.2 mg, 42.3 µmol), PyBOP (19.3 mg, 37.1 µmol) and DIEA (20 µL, 115 µmol) in DMF (0.75 mL) was added to **11** (14.0 mg, 10.6 µmol) in DMF (1.0 mL), and the reaction was stirred for 40 min. Concentration gave crude **13**, which was purified by HPLC using isocratic conditions of 27% ACN containing 0.1 M NaOAc, pH 7 for 2 min at a flow rate of 25 mL/min, followed by a 1.0%/min gradient of 27-54% ACN containing 0.1 M NaOAc, pH 7 at a flow rate of 25 mL/min. The product fraction eluting at 18.1 min was diluted with 3 volumes of H_2O and reloaded on the same preparative HPLC column equilibrated with 4.5% ACN containing 0.1% TFA. The product on the column was desalted by elution with 4.5% ACN containing 0.1% TFA for 15 min at a flow rate of 25 mL/min, followed by a 5.7%/min gradient of 4.5-90% ACN containing 0.1% TFA at a flow rate 25 mL/min. Product fraction eluting a 10.4 min was lyophilized to give HYNIC conjugated monovalent tetracysteic acid derivative **13** (4.9 mg, 3.2 µmol, 30%) as a colorless powder. ^{1}H NMR (CD_3CN & D_2O): δ 8.50 (d, J = 2.1 Hz, 1H), 8.32 (dd, J = 2.1 & 9.0 Hz, 1H), 8.21 (s, 1H), 8.01-7.96 (m, 2H), 7.85-7.80 (m, 2H), 7.78-7.74 (m, 2H), 7.69 (d, J = 1.2 Hz, 1H), 7.53-7.41 (m, 9H), 7.71 (d, J = 9 Hz, 1H), 7.00 (d, J = 1.2 Hz, 1H), 4.88 (dd, J = 4.2 & 9.3 Hz, 1H), 4.65 (dd, J = 4.2 & 8.4 Hz, 1H), 4.58 (dd, J = 4.2 & 8.4 Hz, 1H), 4.52 (dd, J = 4.2 & 8.4 Hz, 1H), 4.37 (t, J = 7.2 Hz, 2H), 4.35 (t, J = 7.8 Hz, 2H), 3.53-3.44 (m, 8H), 3.44-3.35 (m, 5H), 3.35-3.25 (m, 3H), 3.25-3.15 (m, 4H), 3.13 (t, J = 6.6 Hz, 2H), 3.07 (t, J = 6.7 Hz, 2H), 2.11 (t, J = 7.6 Hz, 2H), 1.88-1.78 (m, 4H), 1.74 (p, J = 7.2 Hz, 2H), 1.65 (p, J = 6.6 Hz, 2H), 1.60 (p, J = 6.7 Hz, 2H), 1.57 (p, J = 7.6 Hz, 2H), 1.40 (s, 6H), 1.22-1.14 (m, 2H); ^{13}C NMR (CD_3CN & D_2O): δ 175.9, 172.3, 166.2, 165.1, 163.0, 162.1, 155.7, 152.4, 144.0, 139.1, 138.8, 138.4, 134.5, 132.9, 131.6, 131.5, 130.8, 130.6, 130.5, 129.6, 128.8, 128.7, 122.5, 114.1, 113.7, 107.7, 71.21, 71.17, 71.02, 70.97, 69.98, 69.74, 68.62, 53.14, 53.01, 52.75, 52.17, 52.05, 51.76, 51.70, 50.32, 41.86, 38.07, 37.87, 36.60, 36.20, 30.44, 30.17, 30.12, 29.92, 27.83, 23.99, 22.29; High Resolution MS: Calcd for $C_{65}H_{88}N_{14}O_{22}S_4$ $[M+2H]^{2+}$: 772.2535; found 772.2535.

*(LTB4-(Csa)$_4$)$_2$-Glu-H (**14**)*

A solution of **11** (264 mg, 0.18 mmol), Boc-Glu(OTfp)-OTfp (41.2 mg, 0.076 mmol), HOAt (22.7 mg, 0.17 mmol), and DIEA (130 µL, 0.75 mmol) in DMF (2 mL) was stirred for 6 hours and concentrated to give a viscous yellow oil. This oil was dissolved in DCM (6.5 mL) and treated with a solution of anisole/H_2O/TFA (0.75 mL/ 0.75 mL/ 7 mL) and stirred for 30 min. The reaction solution was concentrated to give crude title compound as a viscous yellow oil. Crude product was purified by HPLC using isocratic conditions of 36% ACN containing 0.1 M NaOAc, pH 7 for 2 min at a flow rate of 25 mL/min, followed by a 0.78%/min gradient of 36-54% ACN containing 0.1 M NaOAc, pH 7 at a flow rate of 25 mL/min. The product fraction eluting at 15 min was diluted with 3 volumes of H_2O, and

reloaded on the same preparative HPLC column equilibrated with 4.5% ACN containing 0.1% TFA. The product on the column was desalted by elution with 4.5% ACN containing 0.1% TFA for 15 min at a flow rate of 25 mL/min, followed by a 5.7%/min gradient of 4.5-90% ACN containing 0.1% TFA at a flow rate 25 mL/min. Product fraction eluting a 10 min was lyophilized to give divalent tetracysteic acid derivative **14** (134 mg, 0.047 mmol, 62%) as a colorless solid. ^{1}H NMR (CD_3CN & D_2O): δ 7.78-7.70 (m, 8H), 7.64 (d, J = 1.2 Hz, 2H), 7.59-7.47 (m, 12H), 7.26 (d, J = 1.2 Hz, 2H), 4.72 (dd, J = 3.9 & 9.3 Hz, 1H), 4.65-4.55 (m, 5H), 4.55-4.49(m, 2H), 4.38 (t, J = 7.5 Hz, 4H), 4.33 (t, J = 6.3 Hz, 4H), 3.99 (dd, J = 5.4 & 7.8 Hz, 1H), 3.53-3.43 (m, 16H), 3.42-3.35 (m, 9H), 3.32-3.14 (m, 15H), 3.12 (t, J = 7.2 Hz, 4H), 3.07 (t, J = 7.2 Hz, 4H), 2.51 (t, J = 6.9 Hz, 2H), 2.21-2.11 (m, 5H), 2.09-2.01 (m, 1H), 1.85 (p, J = 7.6 Hz, 4H), 1.81-1.71 (m, 8H), 1.65 (p, J = 6.8 Hz, 4H), 1.60 (p, J = 6.6 Hz, 4H), 1.55 (p, J = 7.4 Hz, 4H), 1.40 (s, 12H), 1.21-1.12 (m, 4H); ^{13}C NMR (CD_3CN & D_2O): δ 175.8, 175.2, 172.3, 172.1, 171.7, 170.2, 162.4, 161.7, 160.2, 152.1, 136.2, 132.9, 132.7, 132.6, 130.6, 130.5, 128.9, 128.8, 115.6, 106.2, 72.02, 70.58, 70.40, 70.35, 69.41, 69.14, 53.94, 52.43, 52.26, 52.17, 52.00, 51.73, 51.56, 51.45, 51.38, 51.23, 50.88, 49.86, 41.12, 37.53, 37.42, 35.99, 35.63, 32.18, 29.75, 29.39, 29.27, 29.10, 27.24, 26.82, 23.42, 21.52; High Resolution MS: Calcd for $C_{109}H_{159}N_{23}O_{44}S_8Na_2$ $[M+2Na]^{+2}$: 1397.9231; Found: 1397.920.

*DPC11870-11 (**15**)*

A solution of **14** (50.1 mg, 0.0182 mmol) and DIEA (64 µL, 0.364 mmol) in anhydrous DMF (2.0 mL) was treated dropwise with a solution of DTPA dianhydride (65.0 mg, 0.182 mmol) and DIEA (16 µL, 0.091 mmol) in anhydrous DMF (3.0 mL) over 10 min. The reaction was quenched after 1.5 h by the addition of water (0.1 mL), and concentrated under vacuum to give a colorless glassy solid. The crude product was purified by HPLC on a Phenomenex Jupiter™ C18 column (10µ, 21.2 x 250 mm) using a 0.9%/min gradient of 27-63% ACN containing 0.1% TFA at a flow rate of 20 mL/min. Product fraction eluting at 25.1 min was lyophilized to give **15** as a colorless solid (55.0 mg, 0.0176 mmol, 96%). ^{1}H NMR (D_2O:CD_3CN 1:9): δ 7.58 (d, J = 7.62 Hz, 8H), 7.52-7.36 (m, 14H), 7.04 (s, 2H), 4.74-4.69 (m, 1H), 4.67-4.62 (m, 4H), 4.62-4.56 (m, 4H), 4.54-4.50 (m, 2H), 4.41-4.33 (m, 5H), 4.22-4.08 (m, 12H), 3.64 (s, 2H), 3.53-3.41 (m, 20H), 3.41-3.13 (m, 25H), 3.09 (t, J = 6.75 Hz, 4H), 3.02 (t, J = 6.75 Hz, 4H), 2.42-2.27 (m, 2H), 2.16-2.08 (m, 5H), 1.94-1.86 (m, 1H), 1.84-1.73 (m, 8H), 1.72-1.47 (m, 16H), 1.39 (s, 12H), 1.12-1.04 (m, 4H); High Resolution MS: Calcd for $C_{123}H_{182}N_{26}O_{53}S_8$ $[M+2H]^{2+}$: 1563.5056; Found: 1563.505.

*BMS57868-81 (**16**)*

A solution of **12** (17.5 mg, 73 µmol), PyBOP (37.8 mg, 72.7 µmol), and DIEA (20 µL, 115 µmol) in DMF (1.0 mL) was stirred for 15 min and added to a solution of **14** (50.0 mg, 17.4

μmol) and DIEA (30 μL, 172 μmol) in DMF (1.0 mL). Stirring was continued for 20 h and the reaction mixture was concentrated. Crude product was purified by HPLC using isocratic conditions of 40.5% ACN containing 0.1 M NaOAc, pH 7 for 2 min at a flow rate of 25 mL/min, followed by a 0.39%/min gradient of 40.5-49.5% ACN containing 0.1 M NaOAc, pH 7 at a flow rate of 25 mL/min. The product fraction eluting at 11 min was diluted with 3 volumes of H_2O and reloaded on the same preparative HPLC column equilibrated with 4.5% ACN containing 0.1% TFA. The product on the column was desalted by elution with 4.5% ACN containing 0.1% TFA for 15 min at a flow rate of 25 mL/min, followed by a 5.7%/min gradient of 4.5-90% ACN containing 0.1% TFA at a flow rate 25 mL/min. Product fraction eluting a 10.6 min was lyophilized to give HYNIC-conjugated divalent tetracysteic acid derivative **16** (40.2 mg, 13.5 μmol, 78%) as a colorless solid. ^{1}H NMR (D_2O:CD_3CN 1:1): δ 8.58-8.55 (m, 1H), 8.12-8.07 (m, 1H), 8.05-8.00 (m, 4H), 7.98 (s, 1H), 7.73-7.65 (m, 6H), 7.62 (d, J = 1.2 Hz, 2H), 7.50-7.38 (m, 12H), 7.35 (t, J = 7.2 Hz, 2H), 7.32-7.24 (m, 2H), 6.83 (d, J = 1.2 Hz, 2H), 4.75-4.68 (m, 3H), 4.66 (dd, J = 4.6 & 8.3 Hz, 1H), 4.61 (dd, J = 4.6 & 8.1 Hz, 2H), 4.55-4.50 (m, 2H), 4.45 (dd, J = 4.8 & 8.3 Hz, 1H), 4.33 (t, J = 6.9 Hz, 8H), 3.53-3.42 (m, 16H), 3.42-3.10 (m, 28H), 3.07 (t, J = 6.9 Hz, 4H), 2.42 (t, J = 7.6 Hz, 2H), 2.22-2.16 (m, 1H), 2.13-2.07 (m, 4H), 2.07-2.00 (m, 1H), 1.86-1.75 (m, 8H), 1.70 (t, J = 7.2 Hz, 4H), 1.66 (t, J = 6.6 Hz, 4H), 1.60 (t, J = 6.6 Hz, 4H), 1.54 (t, J = 7.6 Hz, 4H), 1.38 (s, 12H), 1.21-1.12 (m, 4H); ^{13}C NMR (D_2O:CD_3CN 1:1): δ 181.22, 175.76, 175.33, 174.19, 172.47, 172.18, 172.00, 171.88, 171.78, 168.97, 165.27, 161.58, 159.24, 156.23, 153.30, 143.78, 139.73, 138.96, 135.84, 130.40, 130.30, 130.19, 129.80, 128.06, 127.78, 121.42, 118.75, 116.81, 112.70, 107.69, 107.46, 70.64, 70.73, 70.47, 70.41, 69.45, 69.25, 66.61, 54.99, 52.40, 52.39, 52.22, 52.05, 52.00, 51.90, 51.68, 51.62, 49.76, 41.39, 37.57, 37.34, 36.08, 35.66, 32.96, 29.93, 29.81, 29.62, 29.41, 27.30, 24.45, 23.45, 21.84; High Resolution MS: Calcd for $C_{122}H_{170}N_{26}O_{45}S_8$ $[M+2H]^{+2}$: 1487.4784; Found: 1487.482.

Receptor Binding Assay

In vitro binding studies were performed on purified human granulocytes, purified as described previously[33]. Briefly, increasing amounts of DPC11870-11, SG380, BMS57868-81, or BMS57868-88 (0-20 μM) were added to 1 x 10^8 cells in the presence of 10,000 cpm [^{111}In(DPC11870-11)] (0.5 nM) in 0.25 M Tris/HCl, pH 7.2. The cell suspensions were incubated for 1 h at 37 °C, the cells were washed twice (5 min, 5000 x g), supernatant was discarded, and the radioactivity in the pellet (total bound activity) was measured in a shielded well-type gamma counter (Wizard, Pharmacia-LKB, Uppsala, Sweden). The specifically bound fraction versus the LTB4 antagonist concentration was plotted. The IC_{50} (50% inhibitory concentration) was determined as being the

concentration of the LTB4 antagonist that caused 50% inhibition of the maximum binding of [^{111}In(DPC11870-11)].

*General Procedure for ^{99m}Tc-Radiolabeling of BMS57868-81 (**16**)*

A solution of BMS57868-81 (**16**) (10 µg), $SnSO_4$ (25 µL of a 1 mg/mL solution in 0.1 N HCl), coligand(s), and 110 MBq Na-$^{99m}TcO_4$ in 350 µL PBS, pH 7.0 was heated for 30 min at 100 °C. Radiochemical purity was checked by instant thin layer chromatography (ITLC) on silica gel strips (Gelman Sciences, Inc., Ann Arbor, MI) in 0.1 M Na-citrate buffer, pH 6.0. Strips were analyzed in a well-type gamma counter (Wizard, Pharmacia-LKB, Uppsala, Sweden). In addition, RP-HPLC was performed on a C18 column (Zorbax Rx-C18 4.6 mm x 25 cm) on an Agilent 1100 HPLC system equipped with an in-line radio detector (Canberra Packard, Brussels, Belgium), using 5%/min gradient of 0-100% ACN containing 10 mM Ammonium acetate pH 7.2 at a flow rate of 1.0 mL/min. The radiolabeling efficiency was >95% in all cases.

*[^{99m}Tc(BMS57868-81)(tricine)(TPPTS)] (**17**)*

From **16**, tricine (65 µg), and TPPTS (5 mg).

*[^{99m}Tc(BMS57868-81)(tricine)$_2$] (**18**)*

From **16**, and tricine (15 mg).

*[^{99m}Tc(BMS57868-81)(tricine)(ISO)] (**19**)*

From **16**, tricine (15 mg), and isonicotinic acid (2 mg).

*[^{99m}Tc(BMS57868-88)(tricine)(ISO)] (**20**)*

A solution of BMS57868-88 (25 µg), tricine (15 mg), isonicotinic acid (2 mg), $SnSO_4$ (25 µL of a 1 mg/mL solution in 0.1 N HCl) and 555 MBq Na-$^{99m}TcO_4$ in 350 µL PBS (pH 7.0) was heated for 30 minutes at 100 °C.

*[^{111}In(DPC11870-11)] (**21**)*

DPC11870-11 (**15**) (10 µg) was labeled with 37 MBq ^{111}In in metal-free 0.25 M ammonium acetate buffer, pH 5.5 as described previously.[14]

Infection model

All animal experiments were approved by the local animal welfare committee in accordance with Dutch legislation and carried out in accordance with their guidelines. Nine

female New Zealand White (NZW) rabbits weighing 2.3-2.8 kg were kept in cages (one rabbit per cage) and fed standard laboratory chow and water ad libitum. Rabbits were anaesthetized by subcutaneous injection of 0.7 mL of a mixture of 0.315 mg/mL fentanyl and 10 mg/mL fluanison (Hypnorm®, Janssen Pharmaceutica, Buckinghamshire, UK). Twenty minutes after administration of anesthesia an *E. coli* infection was induced in the left thigh muscle by intramuscular injection of 4 x 10^9 colony-forming units of *E. coli* bacteria. Twenty-four hours after induction of the abscess, when swelling of the infected muscle was apparent, three rabbits were intravenously injected with 37 MBq [^{99m}Tc(BMS57868-81)L_1L_2] (3.0 µg), where L_1L_2 equals one of the coligand systems tricine/TPPTS, tricine$_2$, or tricine/isonicotinic acid.
In a following experiment fifteen animals were divided in three groups of five rabbits. To compare the imaging characteristics of the divalent compounds and the monovalent compound five animals each were injected with 37 MBq [^{99m}Tc(BMS57868-81)(tricine)(ISO)] (**19**), 37 MBq [^{99m}Tc(BMS57868-88)(tricine)(ISO)] (**20**), and 11 MBq [^{111}In(DPC11870-11)] (**21**) in the lateral ear vein.

Imaging studies
For scintigraphic imaging, the rabbits were immobilized in a mold and placed prone on a gamma camera (Orbiter, Siemens, Hoffman Estates, IL) using a low-energy parallel hole collimator in case of the ^{99m}Tc-labeled compounds, whereas a medium-energy collimator was used during acquisition of rabbits injected with ^{111}In-DPC11870-11. Images (300,000 cts/image) were obtained at several time points after injection starting immediately after injection until 8 h postinjection (p.i.). Images were stored digitally in a 256 x 256 matrix. All images were windowed identically, allowing a fair comparison among the various experiments. At 8 h p.i. all rabbits were euthanized. A blood sample was taken by cardiac puncture. Tissues were dissected and weighed. The activity in tissues was measured in a shielded well-type gamma counter together with the injection standards and was expressed as the percentage of the injected dose per gram (%ID/g).

Statistical Analysis
All mean values are presented as mean ± standard deviation. Statistical analysis was performed using one-way ANOVA. Results were corrected for multiple comparisons with the Bonferroni Multiple Comparisons Test. The level of significance was set at 0.05.

RESULTS

Synthesis

PEG-modified LTB4 antagonist **1** was synthesized as outlined in Scheme 1. The tetrazole ring of RPR69698 was alkylated with ethyl 5-bromovalerate in ACN. Selectivity for alkylation at the N1 position was increased by blocking the N2 position with the tri-n-butyltin group[15].

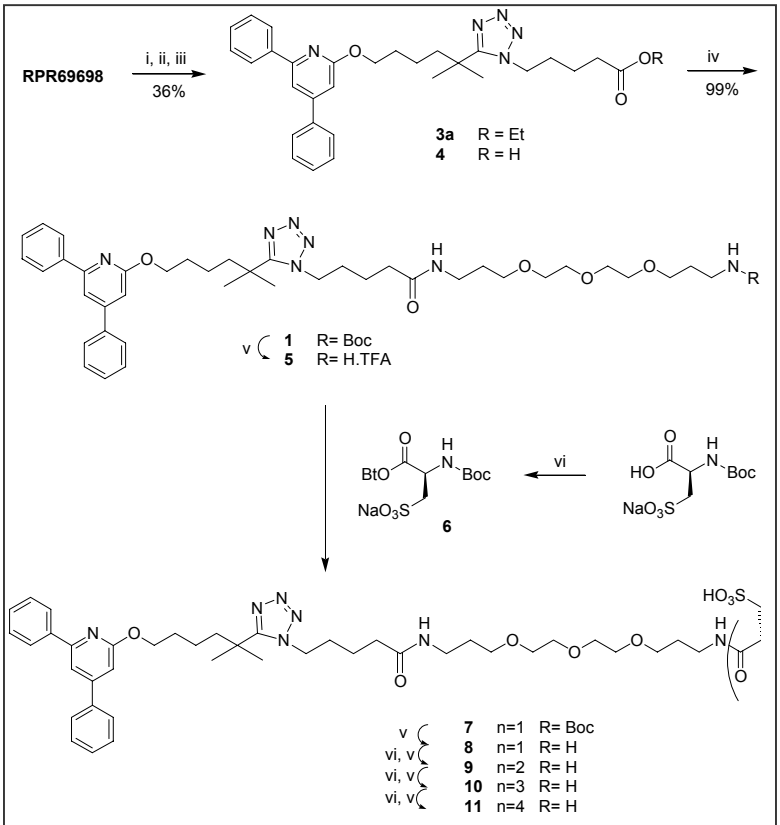

[a]Reagents: i) bis(tri-n-butyltin)oxide, EtOH; ii) ethyl 5-bromovalerate, cyclohexane, 36%; iii) aq LiOH, THF, 100%; iv) N-(t-butoxycarbonyl)-4,7,10-trioxa-1,13-tridecanediamine, HBTU, DIEA, 99%; v) TFA, DCM, TIS, water; vi) Boc-Csa(Na)-OH, HBTU, DIEA, DMF.

Scheme 1

*Synthesis of Tetra-Cysteic Acid-Modified LTB4 Antagonist **11**[a]*

Flash chromatography gave a 36% yield of the desired N1-alkylation product **3a**, along with 22% of the unwanted N2 isomer **3b**. The ester group of **3a** was hydrolyzed with LiOH in aqueous THF to give a quantitative yield of compound **4**. Conjugation of **4** with N-(t-butoxycarbonyl)-4,7,10-trioxa-1,13-tridecanediamine using HBTU coupling reagent afforded a 99% yield of **1**.

The tetracysteic acid derivative of **1** was synthesized by the sequential coupling of four Boc-cysteic acid-mono sodium salt residues (Boc-Csa(Na)-OH) as shown in Scheme 1. The Boc-protecting group of **1** was removed using a mixture of trifluoroacetic acid (TFA), dichloromethane (DCM), water, and triisopropylsilane (TIS). The amine TFA salt (**5**) resulting after concentration of the reaction solution was used without purification.

Boc-Csa(Na)-OH was pre-activated using HBTU, and DIEA in DMF solution, and the resulting N-hydroxybenzotriazole ester (**6**) was added to a solution of **5** in DMF. The resulting Boc-protected cysteic acid derivative (**7**) was purified my means of extraction into $CHCl_3$, and washing with H_2O and sat. $NaHCO_3$. The sat. $NaHCO_3$ wash removed the 1-hydroxybenzotriazole (HOBt) from the organic layer, and the crude product was used without further purification. The Boc group of compound **7** was removed as described above giving **8**. The products of the second, third and fourth deprotection/cysteic acid coupling cycles (**9**, **10**, and **11**, respectively) were too hydrophilic for purification by partitioning between aqueous and organic phases, and therefore were purified by preparative reverse phase HPLC on a C18 column. Products were recovered from the aqueous eluants by lyophilization, and were obtained as flocculent colorless solids.

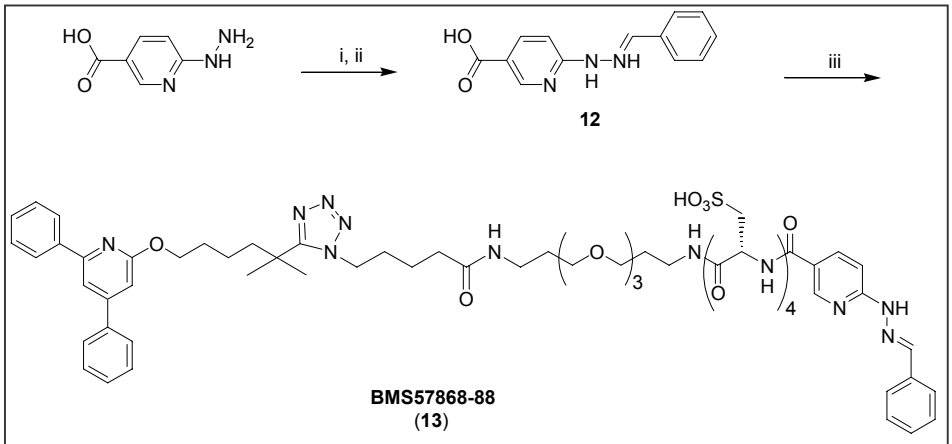

[a]Reagents: i) benzaldehyde, DMF; ii) DCM wash, 66%; iii) **11**, PyBOP, DIEA, DMF, 30%

Scheme 2.

Synthesis of Monovalent Hynic Conjugate BMS57868-88 (13)a

6-Hydrazinonicotinic acid was converted to 6-(2-benzaldehydehydrazono)nicotinic acid (**12**) using an excess of benzaldehyde as shown in Scheme 2[11,16]. Unreacted benzaldehyde was removed by trituration with DCM to give pure **12** in 66% yield. The conjugation reaction between **11** and **12** was mediated with benzotriazol-1-yl-oxytripyrrolidinophosphonium hexafluorophosphate (PyBOP) and DIEA in DMF solution to give a 30% purified yield of BMS57868-88 (**13**).

Preparation of the bivalent LTB4 antagonist was achieved by the conjugation of tetracysteic acid derivative **11** to both of the carboxylic groups of Boc-glutamic acid, using Boc-Glu(OTfp)-OTfp as the activated form (Scheme 3). The addition of HOAt significantly increased the reaction rate, and the reaction was complete in 6 h at ambient temperature. The Boc group was removed using a cocktail of TFA/DCM/water/anisole, and the resulting amine was purified by HPLC to give a 62% yield of divalent LTB4 antagonist **14** as a flocculent, colorless solid. Compound **14** was used for the preparation of divalent DTPA conjugate DPC11870-11 (**15**) and divalent HYNIC conjugate BMS57868 (**16**). Reaction of **14** with DTPA dianhydride in DMF gave a 96% yield of **15** after HPLC purification. HYNIC conjugate **16** was isolated in 78% yield by a PyBOP-mediated coupling of **14** and **12** in DMF.

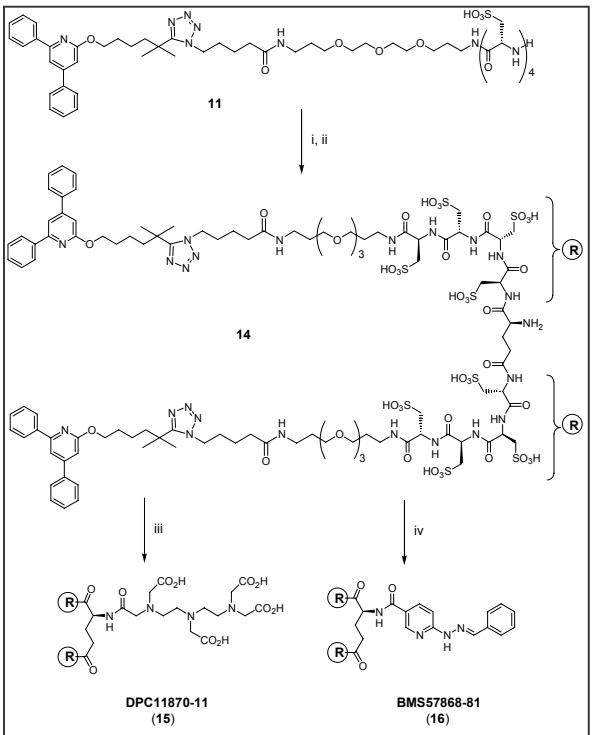

Scheme 3.

Synthesis of Hynic and DTPA Chelator Conjugates of Bivalent LTB4 Antagonist[a]

[a]Reagents: i) Boc-Glu(OTfp)-OTfp, HOAt, DIEA, DMF; ii) TFA, DCM; iii) DTPA dianhydride, DIEA, DMF; iv) 6-(2-benzaldehydehydrazono)nicotinic acid (**12**), PyBOP DIEA, DMF.

Receptor Binding Assay.

The IC_{50} values for all of the chelator conjugates described here were obtained in a competition assay with [^{111}In(DPC11870-11)]. As shown in Table 1, the receptor affinities of monovalent conjugates SG380 and BMS57868-88, and divalent DTPA conjugate DPC11870-11 were nearly identical to that of parent LTB4 antagonist RPR69698. Divalent HYNIC conjugate BMS57868-81 showed a greater than 10-fold loss of receptor affinity.

Table 1. *IC_{50} Values (nM) of Chelator Conjugates*

	Competing Agent	
Compound	[^{3}H]LTB$_4$	[^{111}In(**DPC11870-11**)]
RPR69698	20[a]	
SG380	45 (n = 4)[b]	44 (n = 2)
14	8 (n = 2)[b]	
DPC11870-11	54 (n = 2)[b]	30 (n = 2)
BMS57868-88		16 (n = 2)
BMS57868-81		230 (n = 2)

[a] Reference 10. [b] NovaScreen, Hanover, MD

Radiolabeling.

HPLC analyses, performed after ^{99m}Tc-labeling of divalent HYNIC-conjugated compound BMS57868-81 (**16**), indicated that with all three coligand systems the compound labeled at a specific activity of 37 MBq/µg (110 MBq/nmol) with a labeling efficiency >95%. Monovalent HYNIC-conjugated LTB4 antagonist BMS57868-88 (**13**) labeled at a specific activity of 110 MBq/nmol with a labeling efficiency >95%. Divalent DTPA-conjugated LTB4 antagonist DPC11870-11 (**15**) was labeled with ^{111}In at a specific activity of 12 MBq/nmol with a labeling efficiency >95%.

Animal studies

Divalent LTB4 antagonist BMS57868-81 was radiolabeled with ^{99m}Tc using three different coligand systems, tricine/TPPTS, tricine$_2$, and tricine/ISO, to give complexes of the general formula [^{99m}Tc(BMS57868-81)L_1L_2]. The structures of these three ligand systems are shown in Figure 2.

Figure 2.
Comparison of the structures of [^{99m}Tc(HYNIC)(L_1)(L_2)] complexes and [^{111}In(DCP11870-11)].

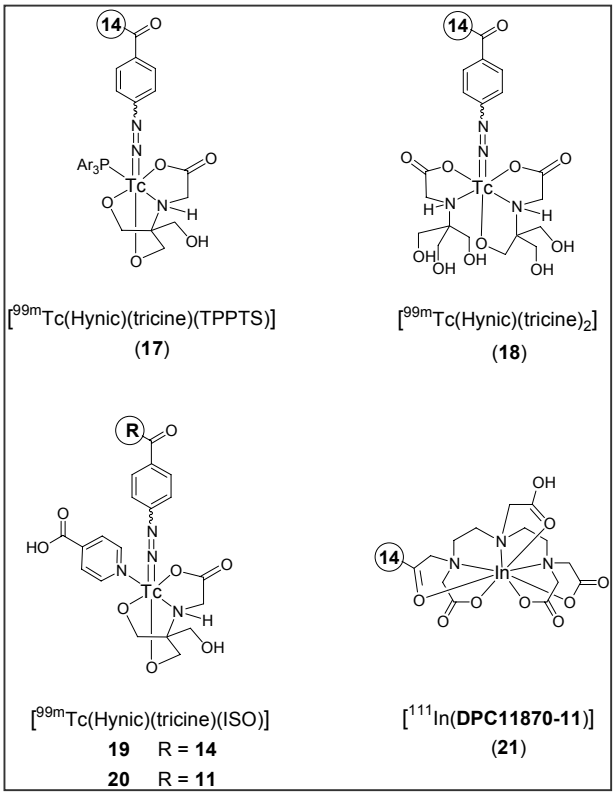

Pharmacokinetics of these three tracers were studied in three groups of rabbits with *E. coli* infection, with images acquired 5 min, 4 h and 8 h post injection (p.i.). As shown in Figure 3, immediately after injection the distribution of [^{99m}Tc(BMS57868-81)L_1L_2] was similar for all three coligand systems. Uptake of the tracer was observed in the heart, lungs, liver, and kidneys and in the bone marrow. At 4 h and especially at 8 h after injection of the compounds, the radioactivity had accumulated in the abscess resulting in clear delineation of the infectious lesions. The images acquired at 8 h p.i. clearly indicated that the coligand used during the labeling procedure affected the in vivo distribution of the LTB4 antagonist. Visualization of the abscess was better when TPPTS or ISO was used as coligand in combination with tricine, than when tricine was used alone.

Ex vivo biodistribution determination of radioactivity concentration in the dissected tissues confirmed the observations in the imaging experiment (Figure 4). Radioactivity concentrations in the abscess were highest when [^{99m}Tc(BMS57868-81)] was labeled with the tricine/TPPTS and tricine/ISO coligand systems. Uptake in non-target organs was also affected by the coligand system. The radioactivity concentration in the spleen and kidneys

was significantly higher using tricine/TPPTS coligands, as compared to the uptake in these organs using tricine/ISO or tricine alone ($p<0.01$). Altogether, the abscess visualization was best after injection of [^{99m}Tc(BMS57868-81)(tricine)(ISO)] (**19**), because this preparation combined high uptake in the abscess with low radioactivity concentration in non-target tissues, particularly in the kidneys.

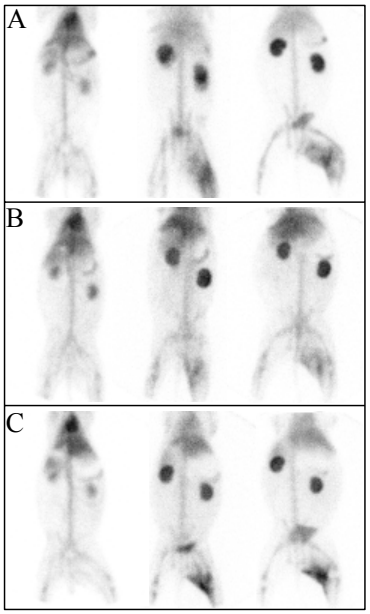

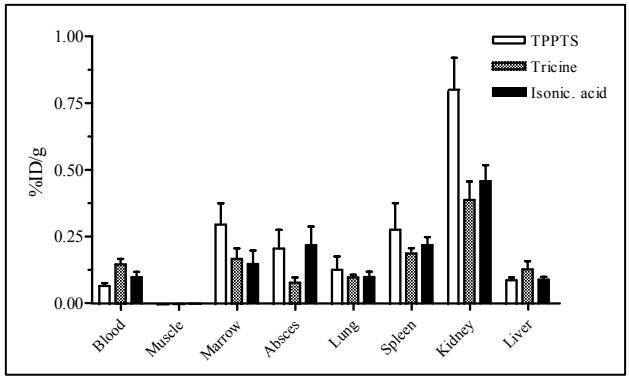

Figure 4. *Biodistribution data obtained 8 h p.i. using divalent imaging agent [^{99m}Tc(BMS57868-81)] radiolabeled using tricine/TPPTS, tricine$_2$, and tricine/ISO coligand systems. Each bar represents the mean values ± SD.*

Figure 3. *Anterior images of rabbits induced with an intramuscular infection. Images were acquired immediately, 4 and 8 h p.i of 37 MBq divalent imaging agent [^{99m}Tc(BMS57868-81)], radiolabeled using tricine/TPPTS (A), tricine$_2$ (B) and tricine/ISO (C) coligand systems.*

In the next imaging experiment, rabbits with intramuscular infection were injected with either the divalent or monovalent ^{99m}Tc-labeled LTB4 antagonist [^{99m}Tc(BMS57868-81)(tricine)(ISO)] (**19**) or [^{99m}Tc(BMS57868-88)(tricine)(ISO)] (**20**), respectively) or with the ^{111}In-labeled divalent LTB4 antagonist [^{111}In(DPC11870-11)] (**21**). The images acquired at 8 h p.i. showed that all three tracers visualized the intramuscular abscess (Figure 5). When the three agents were compared, it appeared that the distribution of both divalent analogs was very similar. All three analogs clearly delineated the intramuscular abscess. Non-target uptake of radioactivity for the three agents was similar in bone marrow, liver, and spleen. However, the kidney uptake of monovalent agent [^{99m}Tc(BMS57868-88)(tricine)(ISO)] (**20**) appeared to be significantly lower.

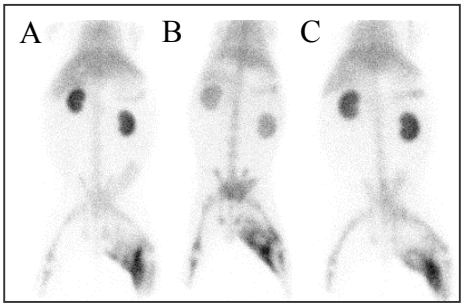

Figure 5.
Comparison of divalent imaging agent [^{99m}Tc(BMS57868-81)(tricine)(ISO)] (A), monovalent imaging agent [^{99m}Tc(BMS57868-88)(tricine)(ISO)] (B) and divalent imaging agent [^{111}In(DPC11870-11)] (C). All are anterior images of rabbits induced with an intramuscular infection. Images were acquired 8 h p.i of 37 MBq for (A) and (B) and 11 MBq for (C).

DISCUSSION

Leukotriene B4 (LTB4) is a potent pro-inflammatory lipid mediator derived from arachidonic acid via the 5-lipoxygenase pathway. It is produced by neutrophils, monocytes, macrophages, keratinocytes, lymphocytes, and mast cells. The physiological responses to LTB4 include potent neutrophil chemotactic activity, adhesion of PMNs to the vascular endothelium, stimulation of the release of lysosomal enzymes and superoxide radicals by PMNs, and an increase in vascular permeability. Increased levels of LTB4 have been detected in patients with asthma, acute respiratory distress syndrome, chronic obstructive pulmonary disease, contact dermatitis, cystic fibrosis, inflammatory bowel disease, gout, myocardial ischemia, psoriasis, and rheumatoid arthritis. Thus, it is widely believed that LTB4 is an important mediator of acute and chronic inflammatory events. This has made the LTB4 receptor the target of intense research by major pharmaceutical companies for therapeutic applications, and in recent years, a number of highly potent and selective LTB4 antagonists have been reported. These compounds have been shown to be safe and efficacious in both animal models and in humans[6,17,18]. This wealth of information on LTB4 antagonists made the LTB4 receptor the most attractive of the various approaches available for the development of a neutrophil-binding radiolabeled infection/inflammation imaging agent.

In the present study the syntheses of three structurally related LTB4 antagonists are described. These antagonists were designed for scintigraphic visualization of infectious and inflammatory foci. In the field of nuclear medicine, there is an ongoing search for the ideal radiopharmaceutical to visualize infectious and inflammatory foci. For this purpose many radiolabeled peptides, cytokines and antagonists have been studied[8]. In our original work in this area we synthesized LTB4 antagonist SG380 (structure **2**, Figure 1), for the visualization of infectious and inflammatory lesions. This compound was based on

RPR69698, a lipophilic BLT1 receptor-binding ligand[10]. SG380 is a conjugate of bifunctional chelator hydrazinonicotinic acid (HYNIC) to allow efficient radiolabeling with ^{99m}Tc. The ternary ligand complex of **2**, utilizing TPPTS and tricine as coligands (RP517 in Figure 1), accumulated rapidly in infected tissues containing infiltrated BLT1-positive neutrophils[12,13]. However, due to the lipophilicity of the receptor-binding moiety of RP517, the tracer cleared via the hepatobiliary route, and the rapid physiologic uptake of the tracer in the liver and the intestines interfered with visualization of inflammatory lesions in the abdomen[13].

Various strategies have been used to enhance the hydrophilicity of radiopharmaceutical drugs, in order to increase their water solubility and/or renal clearance. These include the introduction of polar function groups (carboxyl, amine, etc.)[19] and PEG chains[20], and the use of different radionuclide chelators[21]. Our experience with SG380 indicated that we were unlikely to achieve a significant change in solubility or biodistribution properties by the introduction of simple PEG tethers. Here we present the synthesis and characterization of three hydrophilic tracers (DPC11870-11 (**15**), BMS57868-81 (**16**), and BMS57868-88 (**13**) in Schemes 2 and 3) based on the same receptor binding moiety used in the synthesis of SG380. The lipophilicity of SG380 was reduced by the introduction of multiple cysteic acids as a PKM. Cysteic acid was chosen for this role because of the high polarity of the sulfonic acid group, and because it is an unnatural amino acid and is therefore less likely to undergo metabolism. We have also examined the effect of two different radionuclide chelators (DTPA for coordination to ^{111}In, and HYNIC for coordination to ^{99m}Tc) because it is known from other studies that the chelator can influence the biodistribution of the tracer[21]. Finally, we have examined the effect of different coligands with HYNIC because previous reports have shown that the nature of the coligand can have a marked effect on biodistribution[22,23].

In our original synthesis of SG380 the tetrazole ring of RPR69698 was alkylated with ethyl 5-bromovalerate in refluxing ACN in the presence of DIEA as base[24]. Alkylation of 5-substituted tetrazoles under these conditions always produces the N2 isomers in greater proportion than the N1 isomers. In our original synthesis the N1/N2 ratio was a very unfavorable 0.14. We subsequently learned that the product ratio could be shifted in favor of the N1 isomer by blocking the N2 position with the tri-n-butyltin group[15]. Preparation of the 2-(tri-n-butylstannyl)tetrazole was accomplished by treatment of RPR69698 with bis(tri-n-butyltin)oxide in refluxing EtOH (Scheme 1). The EtOH solvent was replaced with cyclohexane, ethyl 5-bromovalerate was added, and the solution was heated to reflux. The reaction solution was then diluted with ether and washed with aqueous KF to remove tin by-products. Final purification by flash chromatography gave a 36% yield of the N1

isomer (**3a**), and a N1/N2 ratio of 1.64. We discovered that formation of the N1 isomer is favored by the use of nonpolar solvents, and that even trace quantities of EtOH remaining from the formation of the 2-(tri-n-butylstannyl)tetrazole have a negative effect on the yield of the N1 isomer. With this improvement over our original synthesis we were able to carry out the tetrazole alkylation on a relatively large scale, producing 16.58 g of purified **3a**. The remaining steps in the synthesis of compound **1** followed our original procedures, as described in the experimental section. The four cysteic acid PKMs were added stepwise in a series of deprotection/coupling cycles, as shown in Scheme 1. Boc-Csa(Na)-OH was preactivated using HBTU and the resulting N-hydroxybenzotriazole ester (**6**) was added to a DMF solution of the amine. After the addition of one cysteic acid residue (i.e., **7**, R = Boc), the product was still sufficiently lipophilic that polar by-products could be removed by water washes. But subsequent cysteic acid coupling cycles gave products that were too hydrophilic for an aqueous workup procedure. These compounds were deprotected and the products (i.e., **9**, **10**, **11**) of these reactions were purified by reverse phase HPLC and isolated from the eluants by lyophilization. The overall yield for these four coupling cycles was 37%.

The biomolecules employed as the basis for development of radiopharmaceuticals are frequently very potent, and elicit a biological response even at low doses. Radiolabeling in the clinical setting must therefore be carried out using very small quantities of the biomolecule, and a substantial effort has been made to find radionuclide chelators that can be easily radiolabeled in aqueous solution at very low concentrations of the biomolecule, and with high specific activity. One of the best chelators for ^{99m}Tc is 6-hydrazinonicotinic acid (HYNIC), which is efficiently labeled in aqueous solutions having a ligand concentration as low as 10^{-5} molar[12]. Protection of the hydrazine group of HYNIC during conjugation to the targeting molecule is essential in order to prevent unwanted conjugation reactions. Protection is also desirable during manufacturing of the lyophilized kit used for preparation of the radiopharmaceutical, because the hydrazine moiety reacts readily with aldehydes and ketones found in the manufacturing environment. Such materials are extracted from various rubber and plastic materials and are also used in common disinfectants. Formaldehyde is particularly ubiquitous. In our initial work in this area we discovered that hydrazones of aromatic aldehydes were particularly useful as hydrazine protecting groups on HYNIC[11]. These hydrazones are stable during synthesis and HPLC purification, and protect the hydrazine moiety from reaction with common carbonyl impurities. The hydrazone is spontaneously cleaved during the radiolabeling process allowing formation of the diazenido-technetium bond. We found that the hydrazone of 2-formylbenzaldehyde was especially useful because the sulfonic acid group

greatly improved water solubility of the HYNIC conjugate (see Figure 1). With multiple cysteic acid PKMs present on the LTB4 antagonists described here, a further increase in water solubility was unnecessary, and we used the simpler hydrazone of benzaldehyde for protection of the hydrazine moiety (**12** in Scheme 2). Conjugation of **12** to tetracysteic acid derivative **11** was accomplished using PyBOP to give a 30% purified yield of BMS57868-88 (**13**).

Many interactions in biological systems are polyvalent in nature (e.g., DNA helix, carbohydrate interactions, virus-cell wall interactions). However, it is only recently that polyvalency has begun to be explored in drug development[25]. In previous studies we have shown that divalency of a cyclic RGD peptide targeting the vitronectin receptor on tumors caused enhanced receptor affinity and enhanced retention in the target tissue in vivo[26]. We have explored the effect of divalency in these radiolabeled LTB4 antagonists by preparing the pseudo-dimer of **11**. Tetracysteic acid derivative **11** was efficiently converted to a divalent ligand by reaction with Boc-Glu(OTfp)-OTfp and HOAt in DMF (Scheme 3). The HOAt greatly accelerated the reaction rate, reducing the reaction $t_{½}$ from 12 h to 1 h. Removal of the Boc protecting group gave a 62% yield of **14** after HPLC purification. Conjugation of **14** to DTPA was accomplished by using a 10-fold excess of DTPA dianhydride, and gave a 96% purified yield of DPC11870-11 (**15**). Conjugation of **14** to **12** gave a 78% purified yield of divalent HYNIC conjugate BMS57868-81 (**16**).

The IC_{50} values of the chelator conjugates reported in this study are shown in Table 1. Lipophilic HYNIC conjugate SG380 has a receptor affinity of 48 nM, which is only slightly weaker than the 20 nM value of parent LTB4 antagonist RPR69698. Divalent water-soluble amine **14** shows a slight increase in receptor affinity to 8 nM, while the corresponding DTPA conjugate (DPC11870-11) shows a slight loss of affinity to 54 nM. These data confirm our original hypothesis that the LTB4 receptor is very tolerant of substitutions on the tetrazole ring. Monovalent water-soluble HYNIC conjugate BMS57868-88 has affinity of 16 nM, but surprisingly the divalent version (BMS57868-81) shows a large loss of receptor affinity with an IC_{50} value of 230 nM. Comparison with the affinities of the other divalent LTB4 antagonist (DPC11870-11) suggests this is not due solely to the divalent nature of the molecule, and comparison with the other two HYNIC conjugates (SG380 and BMS57868-88) suggests this is not due solely to the HYNIC chelator. This value does not appear to be an outlier as the duplicate numbers are nearly identical. At this time we have no explanation for the relatively low receptor affinity of BMS57868-81.

Divalent DTPA conjugate DPC11870-11 (**15**) was radiolabeled with ^{111}In as described in a previous publication to give [^{111}In(DCP11870-11)] (**21**) as shown in Figure 2[14]. The ^{99m}Tc

complexes of divalent HYNIC conjugate BMS57868-81 (**16**) were prepared from Na-$^{99m}TcO_4$, $SnSO_4$, and one of three coligand systems by heating at 100 °C for 30 min in phosphate buffered saline, pH 7.0. The three coligand systems (tricine/TPPTS, $tricine_2$, and tricine/ISO) gave complexes **17**, **18**, and **19** as shown in Figure 2. Radiolabeling was rapid and efficient using each of the three coligand systems. The radiochemical purity of all complexes was verified by the analytical methods described in the experimental section. While the binary complex formed from tricine alone (**18**) has been used extensively in pre-clinical research, it suffers from the drawback that it exists in solution in several isomeric forms, many of which are interconverting at room temperature[27]. It would be very difficult to develop such a system for clinical use. In contrast, ternary complexes formed from TPPTS and tricine (e.g., **17**) form only two non-interconverting diastereomeric radiolabeled products when the biomolecule is itself chiral[12].

Scintigraphic images after injection of divalent ^{99m}Tc complexes **17**, **18**, and **19** are shown in Figure 3. Whole body distribution of the three agents was similar immediately after injection, with significant activity in the lungs and heart (blood pool), and in the kidneys. By four hours p.i. uptake in the abscesses was clearly visible with all three agents, and there was high activity in the kidneys. Images acquired eight hours p.i. clearly showed that uptake in the abscesses was greater with the tricine/TPPTS and tricine/ISO complexes (**17** and **19**). It was also apparent that kidney uptake was higher with tricine/TPPTS complex **17**. Thus, the images obtained with ternary complex **19** were qualitatively superior to the images obtained with the other divalent ^{99m}Tc complexes. The biodistribution data for complexes **17**, **18**, and **19** at eight hours p.i. (Figure 4) confirmed these visual impressions. Uptake of **17** and **19** in the abscesses was twice that of **18**, and the kidney uptake of **17** was nearly twice that of **18** and **19**. In addition, the levels of **17** were slightly higher in the spleen and marrow, and **18** showed slightly slower clearance from the blood. Thus, for this divalent LTB4 antagonist platform, the tricine/ISO coligand system (**19**) combined the highest uptake in the abscess with the lowest uptake in non-target tissues.

In a final experiment we compared divalent tricine/ISO ternary complex **19** with monovalent tricine/ISO ternary complex **20**, and with divalent ^{111}In-DTPA complex **21**. Scintigraphic images eight hours p.i. are shown in Figure 5. The radioactivity concentration in the abscesses is similar for all three agents, but the kidney concentration appears significantly lower for monovalent complex **20**. This combination of high uptake in the target tissue and low uptake in non-target tissues makes monovalent [^{99m}Tc(BMS57868-88)(tricine)(ISO)] (**20**) the qualitatively superior imaging agent. It is interesting that there is little difference in the images resulting from divalent ^{99m}Tc-HYNIC

complex **19** and divalent ^{111}In-DTPA complex. Structurally, the two chelator-radionuclide complexes are very different. It is also interesting that the potential divalent interaction with LTB4 receptors on the cell membrane of the neutrophils did not enhance the accumulation of the either **19** or **21** in the abscess. However, divalent agent [^{99m}Tc(BMS57868-81)(tricine)(ISO)] (**19**) did showed enhanced retention in the kidneys as compared to monovalent compound [^{99m}Tc(BMS57868-88)(tricine)(ISO)] (**20**). In this instance, divalency did not result in enhanced uptake in the target, but apparently the divalent compound was more efficiently reabsorbed in the renal tubules as has been observed with other HYNIC-conjugated tracers[28]. As a result, abscess-to-background ratios of the monovalent compound were higher, resulting in scintigraphic images with improved contrast.

CONCLUSION

This study describes the syntheses of three new radiolabeled LTB4 antagonists for imaging infection and inflammation. All three of these tracers visualized intramuscular infection in rabbits within a few hours after injection, and the incorporation of multiple cysteic acid PKMs allowed these tracers to be cleared exclusively via the kidneys. The structural parameters investigated with these tracers included the use of either ^{99m}Tc-HYNIC or ^{111}In-DTPA complexes, monovalent vs. divalent LTB4 antagonists, and the coligands used in the ^{99m}Tc-HYNIC complexes. The coligand system had a marked effect on biodistribution in the rabbit model, with the ternary complex using tricine and ISO as coligands (i.e., **19**) providing the best scintigraphic images and the best biodistribution data of the divalent HYNIC derivatives. Monovalent ternary ^{99m}Tc-HYNIC complex **20** gave better scintigraphic images than either divalent ^{99m}Tc-HYNIC complex **19**, or divalent ^{111}In-DTPA complex **21**. Tracer **20** appears to be the most promising of these new tracers, combining the highest uptake in abscesses with lowest uptake in non-target tissues. More detailed studies of the pharmacokinetic and imaging properties of this promising infection/inflammation imaging agent are ongoing and will be published elsewhere.

REFERENCES

1. Tager, A. M.; Luster, A. D. BLT1 and BLT2: the leukotriene B4 receptors. Prostaglandins Leukot. Essent. Fatty Acids 2003, 69, 123-134.
2. Yokomizo, T.; Izumi, T.; Chang, K.; Takuwa, Y.; and Shimizu, T. A G-protein-coupled receptor for leukotriene B4 that mediates chemotaxis. Nature 1997, 387, 620-624.

3. Yokomizo, T.; Kato, K.; Terawaki, K.; Izumi, T.; and Shimizu, T. A second leukotriene B4 receptor, BLT2. A new therapeutic target in inflammation and immunological disorders. J. Exp. Med. 2000, 192, 421-432.
4. Toda, A.; Yokomizo, T.; Shimizu, T. Leukotriene B4 receptors. Prostaglandins Other Lipid Mediat. 2002, 68-69, 575-585.
5. McMillan, R. M.; Foster, S. J. Leukotriene B4 and inflammatory disease. Agents Actions. 1988, 24, 114-119.
6. Brooks, C. D.; Summers, J. B. Modulators of Leukotriene Biosynthesis and Receptor Activation. J. Med. Chem. 1996, 39, 2629-2654.
7. van Eerd, J. E.; Boerman, O. C.; Corstens, F. H.; Oyen, W. J. Radiolabeled chemotactic cytokines: new agents for scintigraphic imaging of infection and inflammation. Q. J. Nucl. Med. 2003, 47, 246-255.
8. Bleeker-Rovers, C. P.; Boerman, O. C.; Rennen, H. J.; Corstens, F. H.; Oyen, W. J. Radiolabeled compounds in diagnosis of infectious and inflammatory disease. Curr. Pharm. Des. 2004, 10, 2935-2950
9. Harris, T. D.; Glowacka, D.; Kalogeropoulos, S. A.; Edwards, D. S.; Liu, S.; Barrett, J.A.; Heminway, S. Synthesis and evaluation of Tc-99m labeled LTB4 antagonist as potential infection/inflammation imaging agents. Abstracts of papers for the American society of chemistry. 1998, 216: U211-U211 035.
10. Labaudiniere, R.; Dereu, N.; Cavy, F.; Guillet, M.; Marquis, O.; Terlain, B. ω-[(4,6-Diphenyl-2-pyridyl)oxy]alkanoic Acid Derivatives: A New Family of Potent and Orally Active LTB4 Antagonists. J. Med. Chem. 1992, 35, 4315-4324.
11. Harris, T. D.; Sworin, M.; Williams, N.; Rajopadhye, M.; Damphousse, P. R.; Glowacka, D.; Poirier, M. J.; Yu, D. Synthesis of Stable Hydrazones of a Hydrazinonicotinyl-Modified Peptide for the Preparation of 99mTc-Labeled Radiopharmaceuticals. Bioconj. Chem. 1999, 10, 808-814.
12. Edwards, D. S.; Liu, S.; Barrett, J. A.; Harris, A. R.; Looby, R. J.; Ziegler, M. C.; Heminway, S. J.; Carroll, T. R. New and Versatile Ternary Ligand System for Technetium Radiopharmaceuticals: Water Soluble Phosphines and Tricine as Coligands in Labeling a Hydrazinonicotinamide-Modified Cyclic Glycoprotein IIb/IIIa Receptor Antagonist with 99mTc. Bioconj. Chem. 1997, 8, 146-154.
13. Brouwers, A. H.; Laverman, P.; Boerman, O. C.; Oyen, W. J.; Barrett, J. A.; Harris, T. D.; Edwards, D. S.; Corstens, F. H. A 99mTc-labelled leukotriene B4 receptor antagonist for scintigraphic detection of infection in rabbits. Nucl. Med. Commun. 2000, 21, 1043-1050.
14. van Eerd, J. E.; Oyen, W. J.; Harris, T. D.; Rennen, H. J.; Edwards, D. S.; Liu, S.; Ellars, C. E.; Corstens, F. H.; Boerman, O. C. A bivalent leukotriene B(4) antagonist for scintigraphic imaging of infectious foci. J. Nucl. Med. 2003, 44, 1087-1091
15. Isida, T.; Akiyama, T.; Nabika, K.; Sisido, K.; Kozima, S. The Formation of Tin-Nitrogen Bonds. V. The Selective 1-Substitution Reaction of Tetrazoles by the Reaction of 5-substituted 2-(Tri-n-butylstannyl)tetrazoles with Methyl Iodide, Methyl p-Toluenesulfonate, Dimethyl Sulfate, and Ethyl Bromoacetate. Bull. Chem. Soc. Japan, 1973, 46, 2176-2180.
16. Edwards, D .S.; Liu, S.; Ziegler, M. C.; Harris, A. R.; Crocker, A. C.; Heminway, S. J.; Barrett, J. A.; Bridger, G. J.; Abrams, M. J.; Higgins, J. D. 3rd. RP463: a stabilized technetium-99m complex of a hydrazino nicotinamide derivatized chemotactic peptide for infection imaging. Bioconjug Chem. 1999, 884-91.
17. Djuric, S. W.; Fretland, D. J.; Penning, T. D. The Leukotriene B4 receptor antagonists: A most discriminating class of antiinflammatory agent? Drugs of the future.1992, 17, 819-830.
18. Cohen, N.; Yagaloff, K. A. Recent progress in the development of Leukotriene B4 antagonists. Current Drugs. 1994, 13-22.

19. Lin, K. S.; Luu, A.; Baidoo, K. E.; Hashemzadeh-Gargari, H.; Chen, M. K.; Brenneman, K.; Pili, R.; Pomper, M.; Carducci, M. A.; Wagner, H. N. Jr. A New High Affinity Technetium-99m-Bombesin Analogue with Low Abdominal Accumulation. Bioconjug Chem. 2005, 16, 43-50.

20. Chen, X.; Park, R.; Shahinian, A. H.; Bading, J. R.; Conti, P. S. Pharmacokinetics and tumor retention of 125I-labeled RGD peptide are improved by PEGylation. Nucl Med Biol. 2004, 3, 11-9.

21. Decristoforo, C.; Mather, S. J. The influence of chelator on the pharmacokinetics of 99mTc-labelled peptides. Q J Nucl Med. 2002, 46,195-205. Review

22. Rennen, H. J.; van Eerd, J. E.; Oyen, W. J.; Corstens, F. H.; Edwards, D. S.; Boerman, O. C. Effects of coligand variation on the in vivo characteristics of Tc-99m-labeled interleukin-8 in detection of infection. Bioconjug. Chem. 2002, 13, 370-377.

23. Su, Z.; He, J.; Rusckowski, M.; Hnatowich, D. J.; In Vitro Cell Studies of Technetium-99m Labeled RGD-HYNIC Peptide, A Comparison of Tricine and EDDA as Co-Ligands. Nuc. Med. Biol. 2003, 30, 141-149.

24. Barrett, J. A.; Cheesman, E. H.; Harris, T. D.; Rajopadhye, M. Radiopharmaceuticals for Imaging Infection and Inflammation. U.S. 6,416,733, 2002.

25. Mammen, M.; Choi, S.; Whitesides, G. M. Polyvalent Interactions in Biological Systems: Implications for Design and Use of Multivalent Ligands and Inhibitors. Angew. Chem. Int. Ed. 1998, 37, 2754-2794.

26. Janssen, M.; Oyen, W. J.; Massuger, L. F.; Frielink, C.; Dijkgraaf, I.; Edwards, D. S.; Radjopadhye, M.; Corstens, F. H.; Boerman, O. C. Comparison of a monomeric and dimeric radiolabeled RGD-peptide for tumor targeting. Cancer Biother Radiopharm. 2002, 17, 641-646.

27. Liu, S.; Edwards, D. S.; Looby, R. J.; Harris, A. R.; Poirier, M. J.; Barrett, J. A.; Heminway, S. J.; Carroll. T. R. Labeling a Hydrazino Nicotinamide-Modified Cyclic Iib/IIIa Receptor Antagonist with 99mTc Using Aminocarboxylates as Coligands. Bioconj. Chem. 1996, 7, 63-71.

28. Decristoforo, C.; Melendez-Alafort, L.; Sosabowski, J. K.; Mather, S. J. 99mTc-HYNIC-[Tyr3]-octreotide for imaging somatostatin-receptor-positive tumors: preclinical evaluation and comparison with 111In-octreotide. J Nucl Med. 2000, 41,1114-9.

29. Hubbuch, A.; Danho, W.; Zahn, H. Synthesis of N-Protected Cysteic Acid Derivatives and Their Activated Esters. Liebigs Ann. Chem. 1979, 776-783.

30. Harris, T. D.; Barrett, J. A.; Carpenter, A. P.; Rajopadhye, M. Vitronectin receptor antagonist pharmaceuticals. US 6511649 B1 2003.

31. Schwartz, D. A.; Abrams, M. J.; Giademenico, C. M.; Zubieta, J. A. Certain Pyridyl Hydrazines and Hydrazides Useful for Protein Labeling. U.S. Patent 5,206,370, 1993.

32. Wilbur, D. S.; Hamlin, D. K.; Buhler, K. R.; Pathare, P. M.; Vessella, R. L.; Stayton, P. S.; To, R. Streptavidin in Antibody Pretargeting. 2. Evaluation of Methods for Decreasing Localization of Streptavidin to Kidney while Retaining Its Tumor Binding Capacity. Bioconj. Chem. 1998, 9, 322 – 330.

33. van der Laken, C.J.; Boerman , Oyen, W.J.; van de Ven, M. T.; Edwards, D. S.; Barrett, J. A.; van der Meer, J. W.; Corstens, F. H. Technetium-99m-labeled chemotactic peptides in acute infection and sterile inflammation. J Nucl Med. 1997, 38, 1310-1315.

Chapter 7

Imaging of infection with an improved ^{99m}Tc-labeled LTB4 antagonist.

Julliëtte J.E.M. van Eerd
Matthias Broekema
P.Laverman
Thomas D. Harris
D. Scott Edwards
Wim J.G. Oyen
Frans H.M. Corstens
Otto C. Boerman

J Nucl Med. 2005; In Press

ABSTRACT

Previous studies demonstrated that the bivalent ^{111}In-labeled Leukotriene B4 (LTB4) antagonist, DPC11870 visualized infectious and inflammatory lesions in various rabbit models. The radioactive tracer accumulated quickly at the site of infection and cleared rapidly from the circulation, resulting in high-quality images.

Objectives: In this study, two new HYNIC-conjugated compounds, which are structurally related to DPC11870, were studied, in order to further improve image quality.

Methods: A bivalent HYNIC-conjugated LTB4 antagonist (MB81), and a monovalent one (MB88) were labeled with ^{99m}Tc. The radiolabeled compounds were intravenously (i.v.) injected in New Zealand White (NZW) rabbits with *E. coli* infection in the left thigh muscle. The imaging characteristics of both compounds were compared with those of the bivalent ^{111}In-labeled LTB4 antagonist.

Results: Both ^{99m}Tc-labeled LTB4 antagonists visualized the abscess from two hours after injection onwards. Abscess uptake at 8 h p.i. of both compounds was similar (0.22±0.08 %ID/g and 0.36±0.13 %ID/g for the bivalent and monovalent compound respectively). However, visualization of the abscess and the quality of the images after injection of MB88 were superior as compared to both bivalent LTB4 antagonists. The excellent delineation of the abscess by MB88 was mainly due to the more rapid clearance of this compound from non-target organs.

Conclusion: The ^{99m}Tc-labeled HYNIC conjugated LTB4 antagonists MB88 and MB81 visualized infectious foci in rabbits within a few hours after injection. Imaging characteristics of monovalent ^{99m}Tc-MB88 were superior to those of the bivalent LTB4 antagonists DPC11870 and MB81. Therefore, of the three LTB4 antagonists, the monovalent LTB4 antagonist MB88 is the most potent and promising agent to visualize infection and inflammation to evaluate in patients.

INTRODUCTION

Detection and localization of infectious and inflammatory lesions is important for appropriate treatment in patients. One of the methods for detection of infection and inflammation is scintigraphic imaging. For scintigraphic detection of inflammatory and infectious lesions in patients, ^{67}Ga-citrate and radiolabeled leukocytes are the most commonly applied radiopharmaceuticals[1]. However, there is a continuous search for new radiopharmaceuticals that allow rapid and accurate visualization of the lesions and lack the disadvantages of currently used compounds (laborious preparation, time consuming, contamination risks etc.)[2].

Chemotactic and chemokinetic peptides and their antagonists are attractive candidates for this application[3]. These compounds accumulate at the site of infection due to specific receptor interaction and clear rapidly from non-target tissues. Compounds like IL-2, IL-8 and PF4 accumulate at the site of infection due to specific interaction with receptors expressed on activated and infiltrated granulocytes[4,5,6]. The LTB4 receptor, expressed on polymorphonuclear granulocytes is involved in leukocyte function during the inflammatory response[7,8]. Several studies were performed with a radiolabeled LTB4 antagonist to visualize infection and inflammation by targeting of its specific receptors expressed on activated and infiltrated neutrophils[9,10]. The LTB4 antagonist, ^{111}In-DPC11870, rapidly visualized infectious and inflammatory lesions in several rabbit models of acute inflammation[11,12]. The compound cleared rapidly from the non-target tissues and physiologic uptake was only seen in spleen, bone marrow and kidneys. In an in vivo receptor blocking experiment we demonstrated that accumulation at the site of infection was receptor mediated[10].

Although the promising characteristics of ^{111}In-DPC11870 warranted clinical evaluation in patients, for this application a ^{99m}Tc-labeled tracer is preferred. The use of ^{99m}Tc could improve image resolution and would reduce the radiation dose to the patient. Therefore two analogs of DPC11870 were synthesized in which the DTPA chelator was replaced by the bifunctional chelator succinimidyl-hydrazinonicotinamide (S-HYNIC). One compound was structurally almost identical to DPC11870, only differing in metal ligand and consisted of two LTB4 receptor-binding sites, the other LTB4 antagonist was a monomeric derivative of DPC11870, consisting of one LTB4 binding site and again conjugated with HYNIC. Here both LTB4 antagonists were labeled with ^{99m}Tc and the imaging characteristics of both compounds were compared with those of ^{111}In-DPC11870.

MATERIALS AND METHODS

Radiolabeling

The chemical structure of the two HYNIC-conjugated LTB4 antagonists is presented in Fig.1. Synthesis of the HYNIC-conjugated LTB4 antagonist MB81 (bivalent, BMS57868-81) and MB88 (monovalent, BMS57868-88) is described in detail elsewhere[13]. MB81 and MB88 (25 µg) were labeled with 555 MBq Na-$^{99m}TcO_4$ (Tyco Healthcare Mallinkrodt, The Netherlands) in the presence of 15 mg tricine, 2 mg isonicotinic acid in 350 µL phosphate buffered saline (PBS), pH 7.0 and 25 µL $SnSO_4$ (1 mg/mL) in 0.1 N HCl. After incubation for 30 minutes at 100 °C quality control was performed using RP-HPLC (Agilent 1100, S.a./N.V) on a C18 column (Zorbax Rx-C18 4.6 mm x 250 mm, Agilent) at a flow rate of 1

mL/min with a gradient mobile phase starting from 100 % 10 mM ammonium acetate pH 7.2 to 100% acetonitrile in 20 minutes.

DPC11870 was labelled with $^{111}InCl_3$ (TycoHealthcare Mallinkrodt, The Netherlands) as described previously [10,12]. The 20 µg LTB4 antagonist DPC11870 was labeled with ^{111}In with 74 MBq DPC11870. Quality control of the DPC11870 compound was performed using the same HPLC protocols as described above.

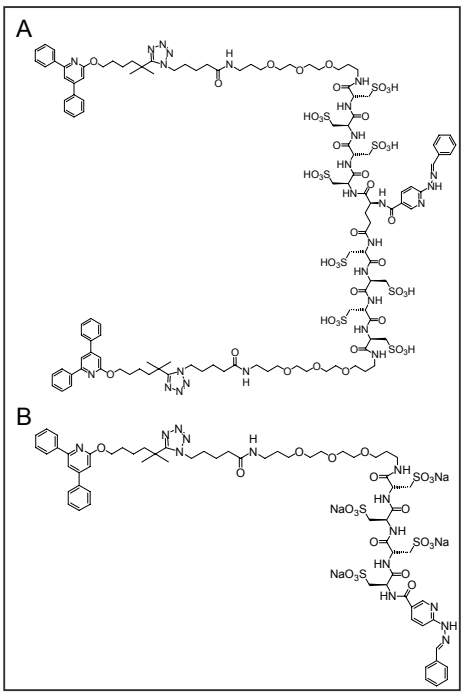

Figure 1.
Chemical structure of MB81 (A) and MB88 (B).

Infection Model

Fifteen female New Zealand White (NZW) rabbits weighing 2.3-2.8 kg were kept in cages (one rabbit per cage) and fed standard laboratory chow and water ad libitum. Rabbits were anaesthetized by subcutaneous injection of 0.7 mL of a mixture of 0.315 mg/mL fentanyl and 10 mg/mL fluanison (Hypnorm®, Janssen Pharmaceutica, Buckinghamshire, UK). Twenty minutes after administration of anesthesia, an *E. coli* infection was induced in the left thigh muscle by intramuscular (i.m.) injection of 4 x 10^9 colony-forming units (CFU) of *E. coli* bacteria.

All animal experiments were approved by the local animal welfare committee in accordance with the Dutch legislation and carried out in accordance with their guidelines.

Imaging and Biodistribution

Twenty-four hours after induction of the abscess, when swelling of the infected muscle was apparent, five rabbits were intravenously injected with 37 MBq ^{99m}Tc-MB81 (3.0 µg), five animals were injected with 37 MBq ^{99m}Tc-MB88 (3.0 µg) and five rabbits received 11 MBq ^{111}In-DPC11870 (3.0 µg) via the lateral ear vein. For scintigraphic imaging, the rabbits were immobilized in a mold and placed prone on a gamma camera (Orbiter, Siemens, Hoffman Estates, IL) using a low-energy parallel hole collimator in case of the ^{99m}Tc-labeled compounds, whereas a medium-energy collimator was used during acquisition of rabbits injected with ^{111}In-DPC11870. Images (300,000 cts/image) were obtained at several time points after injection starting immediately after injection until 8 h postinjection (p.i.). Images were stored digitally in a 256x256 matrix. All images were adjusted at the same background and intensity level, allowing a fair comparison among the various images. The scintigraphic results were analyzed by drawing regions of interest (ROI) over the heart, lungs, liver, spleen, kidneys, bone marrow, abscess and the contralateral muscle (background). Abscess-to-organ ratios were calculated. Blood samples were drawn at 1 minute and at 3, 5, 10, 30, 60, 120, 240 and 480 minutes p.i.. The activity in the samples was determined in a gamma counter (Wizard, Canberra Packard, Belgium) and expressed as a percentage of the injected dose assuming that the total blood weight accounted for 6% of total body weight[14]. The t½α and t½β were calculated assuming a two-phase linear model for the blood clearance. At 8 h p.i. all rabbits were euthanized. A blood sample was taken by cardiac puncture. Tissues were dissected and weighed. The activity in tissues was measured in a shielded well-type gamma counter together with the injection standards and was expressed as the percentage of the injected dose per gram (%ID/g).

Statistical Analysis

All mean values are presented as mean ± standard deviation. Statistical analysis was performed using one-way ANOVA. Results were corrected for multiple data sets with the Bonferroni Multiple Comparisons Test. The level of significance was set at 0.05.

RESULTS

Radiolabeling

Results of the HPLC radioactivity analysis indicated that both the bivalent MB81 compound and the monovalent MB88 could be labeled with ^{99m}Tc with a specific activity of 37 MBq/µg (110 MBq/nmol MB81, 60 MBq/nmol MB88). The labeling efficiency exceeded

95%. RP-HPLC analysis showed that the labeling efficiency of DPC11870 was above 95% with a specific activity of 3.7 MBq/µg (12 MBq/nmol).

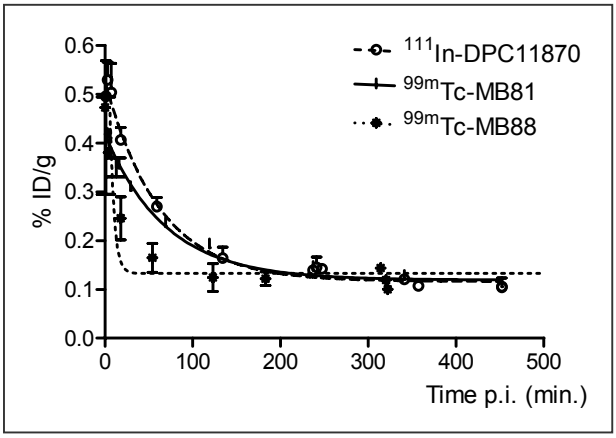

Figure 2.
Blood clearance of ^{111}In-DPC11870, ^{99m}Tc-MB81 and ^{99m}Tc-MB88 in NZW rabbits. The average amount of radioactivity of three rabbits is expressed as %ID/g present in the blood. The curves represent the best non-linear exponential decay curve calculated by the software program (Graphpad Prism).

Imaging and Biodistribution

Analysis of the blood samples indicated that ^{99m}Tc-MB88 cleared rapidly from the circulation (Fig 2). Calculation of t½α, revealed a distribution half-life (t½α) of 7 minutes for ^{99m}Tc-MB88 and 20 minutes for the bivalent ^{99m}Tc-labeled antagonist MB81. The clearance half-life (t½β) also differed between the ^{99m}Tc-labeled LTB4 antagonists. The clearance half-life of monovalent MB81 was 16.5 hour, while the t½β of ^{99m}Tc-MB88 was much longer (t½β = 85.6 hours).

The scintigraphic images after the injection of bivalent ^{111}In-DPC11870, bivalent ^{99m}Tc-MB81 and monovalent ^{99m}Tc-MB88 are shown in Fig. 3. Immediately after injection the whole body distribution of all three radiolabeled LTB4 antagonists was similar. Accumulation of radioactivity was observed in lungs, liver, kidneys and bone marrow of all animals. At two hours after injection of the three LTB4 antagonists the abscesses were already visualized in all animals. However, the images of the monovalent LTB4 antagonist at this time point were qualitatively superior to the images acquired with both bivalent antagonists. The 2 hour images and images at later time points indicated that monovalent MB88 cleared more rapidly from the circulation and non-target tissues as compared to the bivalent LTB4 antagonists MB81 and DPC11870. Additionally, MB88 showed hardly any retention in the kidneys. Due to the low radioactivity concentration in the non-target tissues the visualization of the abscess in the animals injected with ^{99m}Tc-MB88 was better as compared to the images acquired after injection of both ^{111}In-DPC11870 and ^{99m}Tc-

MB81 at equal time points. Abscess-to-organ ratios calculated from the ROI analysis of the images acquired at 8 h p.i. are shown in Fig. 4. When the HYNIC-conjugated antagonists were compared, only a few differences between the monovalent and bivalent compounds were observed. The abscess-to-kidney ratio for monovalent ^{99m}Tc-MB88 was significantly higher as compared to that of the bivalent ^{99m}Tc-MB81 ($p<0.0001$). Furthermore, as all ratios of the monovalent LTB4 antagonist exceeded one, with MB88, the radioactivity concentration in the abscess was the highest of all organs and tissues. When ratios of MB88 were compared with ^{111}In-DPC11870, it was noticed that only the abscess-to-kidney ratio differed significantly ($p<0.01$). The abscess-to-organ ratios of both bivalent radiolabeled compounds (respectively, ^{99m}Tc-MB81 and ^{111}In-DPC11870) were similar.

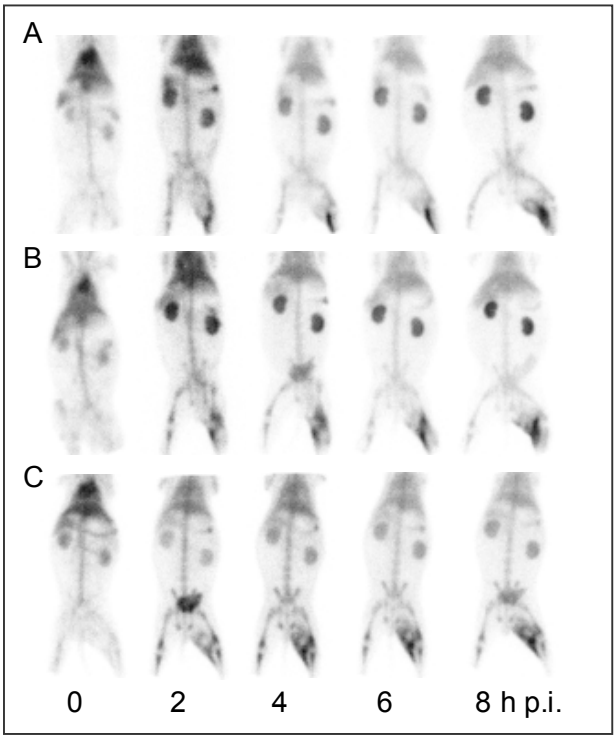

Figure 3.

Anterior images of rabbits induced with an intramuscular infection. Images were acquired immediately, 2, 4, 6 and 8 h p.i of 11 MBq ^{111}In-DPC11870 (A), 37 MBq ^{99m}Tc-MB81 (B) and 37 MBq ^{99m}Tc-MB88 (C).

The biodistribution data derived from ex vivo counting of dissected tissues as summarized in Fig. 5, were in agreement with the scintigraphic images. Blood levels of both ^{99m}Tc-labeled compounds were low (0.10±0.01% ID/g and 0.09±0.01% ID/g for the bivalent and the monovalent ^{99m}Tc-labeled compounds at 8 h p.i., respectively). Furthermore, the abscess uptake did not differ significantly between the two HYNIC-conjugated

antagonists. However, there were significant differences in radioactivity concentration between the compounds in liver and in the kidneys. The kidney uptake of ^{99m}Tc-MB88 was significantly lower as compared to the bivalent ^{99m}Tc-MB81 (0.58±0.06 %ID/g) ($p<0.001$). Also the radioactivity concentration in the liver was higher after injection of ^{99m}Tc-MB81. When the results of the HYNIC-conjugated antagonists were compared to those of the initially synthesized reference compound (^{111}In-DPC11870), more differences were found.

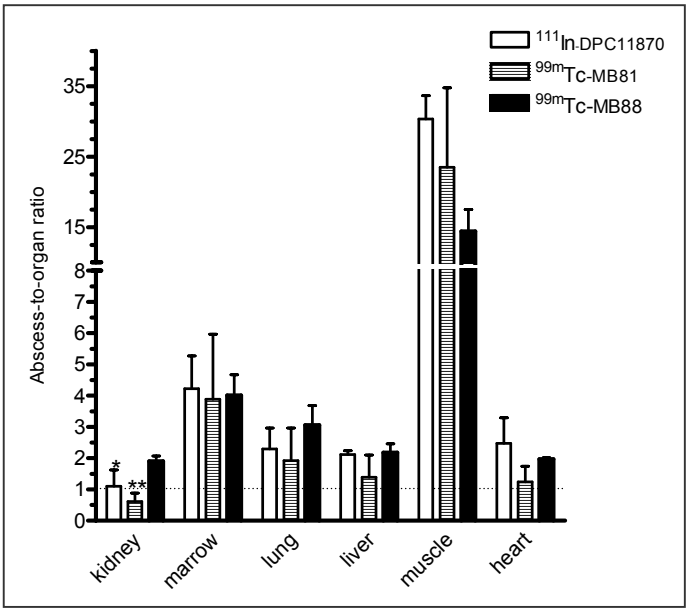

Figure 4.
*Abscess-to-organ ratios calculated from the ROI data, presented for several organs and tissues after injection of respectively ^{111}In-DPC11870, ^{99m}Tc-MB81 and ^{99m}Tc-MB88. ROI data obtained from the images at 8 h postinjection were used for the calculation. * = P <0.05, ** = P <0.01.*

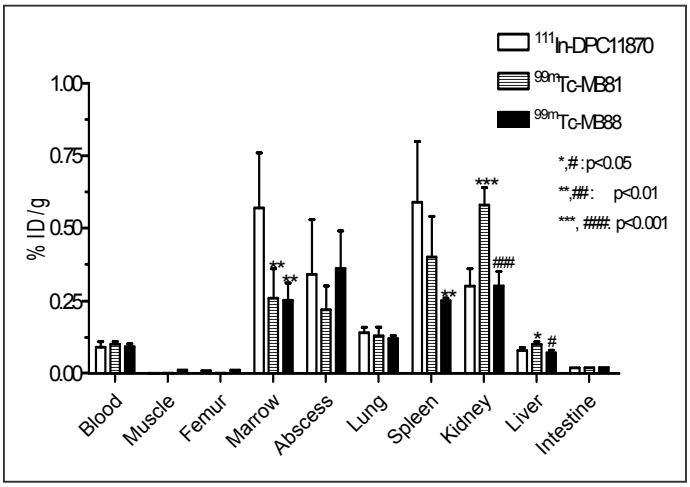

Figure 5.
*Biodistribution data obtained 8 h postinjection of ^{111}In-DPC11870, ^{99m}Tc-MB81 and ^{99m}Tc-MB88. Each bar represents the mean values ± SD. Values were analyzed using ANOVA; * and $^{\#}$= P <0.05, ** and $^{\#\#}$= P <0.01, *** and $^{\#\#\#}$=P<0.001. P-values refer to differences in radioactivity concentration between rabbits injected with ^{111}In-DPC11870 and ^{99m}Tc-MB81 or ^{99m}Tc-MB88 (*) or between rabbits injected with ^{99m}Tc-MB81 and ^{99m}Tc-MB88 ($^{\#}$).*

Firstly, ^{111}In-DPC11870 showed very high radioactivity concentration in the bone marrow (0.57±0.19 %ID/g) as compared to both ^{99m}Tc-labeled compounds (0.26±0.1% ID/g and 0.25±0.06 for respectively MB81 and MB88). Secondly, the kidney uptake of ^{111}In-DPC11870 was low and significantly different from the radioactivity concentration of bivalent ^{99m}Tc-MB81 ($p<0.001$). However, the kidney uptake of ^{111}In-DPC11870 was comparable with that of monovalent ^{99m}Tc-MB88. Thirdly, significant differences were found between the radioactivity concentration of the three compounds in liver and spleen. In both organs the concentration of ^{99m}Tc-MB88 was lowest (0.07±0.01 %ID/g and 0.25±0.01 %ID/g for respectively liver and spleen). The spleen and the bone marrow were the two organs that contained the highest radioactivity concentration of ^{111}In-DPC11870. For the bivalent ^{99m}Tc-MB81 the highest concentration of was found in the kidneys, while after injection of monovalent ^{99m}Tc-MB88 the highest radioactivity concentration was present in the abscess. As a result, the ^{99m}Tc-MB88 revealed the best visualization and the highest concentration of radioactivity in the abscess.

DISCUSSION

In previous studies we demonstrated that the bivalent ^{111}In-labeled LTB4 antagonist DPC11870 adequately visualized infectious and inflammatory foci in distinct rabbit models[10,11,12]. Although previous results warranted clinical studies, we synthesized two HYNIC-conjugated analogs of this compound to allow radiolabeling with ^{99m}Tc. In this study the imaging characteristics of ^{111}In-DPC11870 were compared with those of the ^{99m}Tc-labeled bivalent analog MB81 and the monovalent ^{99m}Tc-labeled derivative MB88.
The results of the imaging and biodistribution experiments indicated that besides the ^{111}In-DPC11870 also both ^{99m}Tc-labeled antagonists visualized infectious foci within a few hours after injection. Furthermore, both MB81 and MB88 compounds showed physiologic uptake in bone marrow, spleen and in the kidneys. The radioactivity concentration of the infected tissue measured at 8 h p.i. was similar for both ^{99m}Tc-labeled compounds. Radioactivity concentration in the kidney of monovalent ^{99m}Tc-MB88 was much lower as compared to the concentration in the kidneys of bivalent ^{99m}Tc-MB81. Comparison of the ^{99m}Tc-labeled bivalent and monovalent LTB4 antagonist revealed that images acquired after injection of the monovalent ^{99m}Tc-MB88 were superior in abscess visualization due to very fast clearance of ^{99m}Tc-MB88 from non-target tissues and good accumulation of radioactivity in the abscess. Additionally, the delineation of the abscess by ^{99m}Tc-MB88 occurred earlier after injection as compared to the bivalent analog. When the characteristics of the best performing ^{99m}Tc-labeled antagonist, MB88, were compared with those of ^{111}In-DPC11870, again the images

acquired after injection of the ^{99m}Tc-compound were superior. In this case, despite similar abscess and kidney uptake, better images were obtained due to lower radioactivity concentrations in the bone marrow of animals injected with monovalent ^{99m}Tc-MB88.

In a previous study we cautiously analyzed the pharmacodynamics of the ^{111}In-labeled LTB4 antagonist DPC11870[15]. From the results found in this study we concluded that accumulation at the site of infection was based on initial targeting of receptor-positive cells in the bone marrow, followed by migration of radioactivity from the bone marrow to the site of infection. In addition, we determined that ^{111}In-DPC11870 showed physiologic uptake in spleen, liver and bone marrow, similar to radiolabeled leukocytes[16,17]. The radioactivity concentration in the bone marrow after injection of both newly synthesized HYNIC-conjugated LTB4 antagonists was lower as compared to that of ^{111}In-DPC11870. The lower bone marrow concentration was an important factor determining the quality of abscess visualization after injection of the ^{99m}Tc-labeled compounds. The rapid blood clearance of the monomeric LTB4 antagonist may explain the low bone marrow uptake. However, since blood clearance of both bivalent compounds (^{99m}Tc- and ^{111}In-labeled) was similar this could not explain the lower bone marrow uptake of the bivalent ^{99m}Tc-MB81. Another explanation for the lower bone marrow uptake of both HYNIC compounds might be the introduction of the HYNIC chelator, which could affect the kinetics of the compound. The low radioactivity concentration in the spleen for both HYNIC compounds supports this explanation.

Present results indicated that the chelator (HYNIC or diethylenetriaminepentaacetic acid (DTPA)) obviously affected the in vivo behaviour and biodistribution of the radiolabeled LTB4 antagonist. Several studies have focused on the in vivo effect of a chelator[18,19]. These studies demonstrated that a chelator may affect the in vivo characteristics of a compound. In a comparative study where the biodistribution of ^{99m}Tc-labeled and ^{111}In-labeled octreotide was evaluated, they also found that kidney retention of the ^{99m}Tc-labeled compound was less as compared to the ^{111}In-DTPA-octreotide[20]. MB81 showed less favourable characteristics as compared to MB88 due to higher kidney retention and the slower t½α of the compound. Since the distribution half-life of ^{111}In-DPC11870 (t½α=30 minutes) is comparable with that of MB81, the longer t½α of MB81 probably is caused by its bivalency. The higher radioactivity concentration of ^{99m}Tc-MB81 in the kidney is difficult to explain. The kidney retention of both ^{111}In-DPC11870 (bivalent, DTPA) and ^{99m}Tc-MB88 (monovalent, HYNIC) were lower as that of ^{99m}Tc-MB81 and therefore it is not clear whether the kidney retention is caused by the bivalency and/or the HYNIC-conjugation of the LTB4 antagonist. The high quality images obtained with ^{99m}Tc-MB88 were the result of the use of the high-resolution radiolabel ^{99m}Tc, the rapid clearance of

MB88 from non-target tissues and the preserved accumulation of this LTB4 antagonist to the site of infection.

The ideal imaging agent for detection of infectious and inflammatory foci should satisfy several requirements. First of all, the agent has to accumulate in the foci specifically and rapidly and should clear from the non-target tissues quickly in order to visualize the lesion in a limited time after injection. Secondly, the labeling procedure ought to be relatively easy and simple and labeling with ^{99m}Tc is preferred over other radionuclides. Finally, the ideal imaging agent should not provoke side effects when administered to patients[21]. The results found in present study indicated that ^{99m}Tc-MB88 suffices the requirements for a potential infection-imaging agent. When these results are compared with other currently studied compounds, ^{99m}Tc-MB88 remains a very promising candidate. Other agents currently under investigation are other radiolabeled cytokines and chemotactic peptides (IL-2, IL-8 and PF4)[4,22,23]. These compounds, however, exhibit biologic activity, and have the disadvantage that they may provoke side effects after administration in patients. Furthermore, the production of these recombinant peptides is complicated and expensive. Another group of compounds are the antimicrobal agents (Infecton® and human neutrophil peptides)[24,25]. These compounds have the advantage over ^{99m}Tc-MB88 that they may target specifically to bacteria. Therefore, these agents can potentially differentiate between infectious lesions and inflammatory foci. Infecton® has been evaluated in several clinical studies and yields a high overall sensitivity and specificity (respectively 85.4% and 81.7%)[24]. Another advantage of Infecton® over MB88 is the lack of bone marrow uptake which makes Infecton® possibly suited for detection of infection after orthopedic intervention (e.g. osteomyelitis).

In summary, clinical evaluation with ^{99m}Tc-MB88 is warranted to assess the value of ^{99m}Tc-MB88 as an infection-imaging agent in patients. Clinical studies are warranted to allow a fair comparison with the other currently studied agents.

CONCLUSION

In the present study we compared the imaging characteristics of three radiolabeled LTB4 antagonists to visualize infection and inflammation. The LTB4 antagonist ^{99m}Tc-MB88 revealed images that visualized the infectious foci with superior quality as compared to the other two compounds. Therefore, we consider the ^{99m}Tc labeled monovalent LTB4 antagonist MB88 as a potent and promising agent to visualize infection and inflammation in patients.

REFERENCES

1. Knight LC. Non-oncologic applications of radiolabeled peptides in nuclear medicine. Q J Nucl Med. 2003;47:279-291.
2. Weiner RE, Thakur ML. Radiolabeled peptides in diagnosis and therapy. Semin Nucl Med. 2001;31:296-311.
3. Signore A, Chianelli M, Bei R, Oyen WJ, Modesti A. Targeting cytokine/chemokine receptors: a challenge for molecular nuclear medicine. Eur J Nucl Med Mol Imaging. 2003;30:149-56.
4. Bleeker-Rovers CP, Boerman OC, Rennen HJ, Corstens FH, Oyen WJ. Radiolabeled compounds in diagnosis of infectious and inflammatory disease. Curr Pharm Des. 2004;10:2935-2950.
5. van Eerd JE, Boerman OC, Corstens FH, Oyen WJ. Radiolabeled chemotactic cytokines: new agents for scintigraphic imaging of infection and inflammation. Q J Nucl Med. 2003;47:246-255.
6. Signore A, Annovazzi A, Barone R, et al. ^{99m}Tc-interleukin-2 scintigraphy as a potential tool for evaluating tumor-infiltrating lymphocytes in melanoma lesions: a validation study. J Nucl Med. 2004;45:1647-52.
7. Pettersson A, Richter J, Owman C. Flow cytometric mapping of the leukotriene B4 receptor, BLT1, in human bone marrow and peripheral blood using specific monoclonal antibodies. Int Immunopharmacol. 2003;3:1467-1475.
8. Yokomizo T, Izumi T, Chang K, Takuwa Y, Shimizu T. A G-protein-coupled receptor for leukotriene B4 that mediates chemotaxis. Nature. 1997;387:620-624.
9. Brouwers AH, Laverman P, Boerman OC, et al. A 99mTc-labeled leukotriene B4 receptor antagonist for scintigraphic detection of infection in rabbits. Nucl Med Commun. 2000;21:1043-1050.
10. van Eerd JE, Oyen WJ, Harris TD, et al. A bivalent leukotriene B(4) antagonist for scintigraphic imaging of infectious foci. J Nucl Med. 2003;44:1087-1091.
11. van Eerd JE, Laverman P, Oyen WJ, et al. Imaging of experimental colitis with a radiolabeled leukotriene B4 antagonist. J Nucl Med. 2004;45:89-93.
12. van Eerd JE, Rennen HJ, Oyen WJ, et al. Scintigraphic detection of pulmonary aspergillosis in rabbits with a radiolabeled leukotriene B4 antagonist. J Nucl Med. 2004;45:1747-1753.
13. Broekema M, van Eerd JE, Oyen WJ, et al. Synthesis of Leukotriene B4 antagonists labeled with In-111 or Tc-99m to image infectious and inflammatory foci. Submitted to the Journal of medicinal chemistry.
14. Blood volume and water balance. In: Jain NC, ed. Shalm's Veterinary Hematology. Vol 91. Philadelphia, PA: Lea and Febiger; 1986:87–102.
15. van Eerd JE, Oyen WJ, Harris TD, et al.. Scintigraphic imaging of infectious foci with an ^{111}In-LTB4 antagonist is based on in-vivo labeling of granulocytes. J Nucl Med. 2004. In Press.
16. Hughes DK. Nuclear medicine and infection detection: the relative effectiveness of imaging with ^{111}In-oxine-, ^{99m}Tc-HMPAO-, and ^{99m}Tc-stannous fluoride colloid-labeled leukocytes and with ^{67}Ga-citrate. J Nucl Med Technol. 2003;31:196-201.
17. Love C, Palestro CJ. Radionuclide imaging of infection. J Nucl Med Technol. 2004;32:47-57.
18. Ono M, Arano Y, Mukai T, Uehara T, Fujioka Y, Ogawa K, Namba S, Nakayama M, Saga T, Konishi J, Horiuchi K, Yokoyama A, Saji H. Plasma protein binding of (99m)Tc-labeled hydrazino nicotinamide derivatized polypeptides and peptides. Nucl Med Biol. 2001;28:155-164.
19. Qu T, Wang Y, Zhu Z, Rusckowski M, Hnatowich DJ. Different chelators and different peptides together influence the in vitro and mouse in vivo properties of ^{99m}Tc. Nucl Med Commun. 2001;22:203-215.

20. Decristoforo C, Melendez-Alafort L, Sosabowski JK, Mather SJ. ^{99m}Tc-HYNIC-[Tyr3]-octreotide for imaging somatostatin-receptor-positive tumors: preclinical evaluation and comparison with ^{111}In-octreotide. J Nucl Med. 2000;41:1114-1119.

21. Corstens FH, van der Meer JW. Chemotactic peptides: new locomotion for imaging of infection? J Nucl Med. 1991;32:491-494.

22. Rennen HJ, Boerman OC, Oyen WJ, Corstens FH. Kinetics of ^{99m}Tc-labeled interleukin-8 in experimental inflammation and infection. J Nucl Med. 2003;44:1502-1509.

23. Signore A, Procaccini E, Annovazzi A, Chianelli M, van der Laken C, Mire-Sluis A.The developing role of cytokines for imaging inflammation and infection.Cytokine. 2000;12:1445-54.

24. Britton KE, Wareham DW, Das SS, Solanki KK, Amaral H, Bhatnagar A, Katamihardja AH, Malamitsi J, Moustafa HM, Soroa VE, Sundram FX, Padhy AK. Imaging bacterial infection with 99mTc-ciprofloxacin (Infecton). J Clin Pathol. 2002;55:817-23.

25. Welling MM, Nibbering PH, Paulusma-Annema A, Hiemstra PS, Pauwels EK, Calame W. Imaging of bacterial infections with 99mTc-labeled human neutrophil peptide-1.J Nucl Med. 1999;40:2073-80.

Chapter 8

General discussion

Imaging of infection and inflammation

Diagnosis of infection and inflammation is eminent for management of patients suspected for infectious and inflammatory disorders. Visualization of the localization and the extent of an inflammatory process will allow guided verification procedures and initiation of appropriate treatment in most cases. For the detection of infectious and non-infectious processes, radiological techniques (e.g. CT and MRI) and scintigraphic techniques are available. In most institutions, scintigraphic imaging to detect inflammatory and infectious foci is performed with radiolabeled leukocytes or gallium-67 citrate. However, due to several insuperable disadvantages of these agents, there is a great interest in the development of a new radiopharmaceutical for this application.
In this thesis, the potential of three radiolabeled LTB4 receptor antagonists to image infectious and inflammatory foci were described. LTB4 is a chemotactic mediator that targets specific receptors expressed on leukocyte sub-populations. Radiolabeled LTB4 analogs can potentially be used, like other chemotactic compounds, to visualize infection and inflammation since they comprise several characteristics essential for an infection-imaging agent.
The requirements for the ideal radiotracer are:

- Efficient and specific accumulation in inflammatory foci
- Visualization of inflammatory lesion rapidly after injection
- Good retention in the inflammatory lesion
- Rapid clearance from the background
- No toxicity
- Good availability, low costs
- Easy and non-hazardous preparation
- Low radiation exposure
- Possibility to differentiate between infection and sterile inflammation

Efficient and specific accumulation in inflammatory foci
Distinct imaging experiments described in this thesis demonstrated that all three LTB4 antagonists, accumulated rapidly and efficiently at the site of infection. Furthermore, the receptor saturation experiment, demonstrated that the interaction of the LTB4 antagonist in the infectious foci was receptor mediated. Therefore, the LTB4 antagonists investigated in this thesis meet the requirements of efficient and specific accumulation.

Visualization rapidly after injection

New agents suitable to visualize infectious and inflammatory disorders should allow rapid and timely diagnosis. Early detection is preferred but not always necessary as in the case of osteomyelitis and infected bone/joint prothesis. In case of severe and acute illness a one-day imaging protocol is intended. The radiolabeled LTB4 antagonists were able to delineate infectious and inflammatory foci already a few hours after the injection. Depending on the organ of interest, visualization of the inflammation was achieved between 1 and 6 hours after the injection. Due to relatively slow clearance of ^{111}In-DPC11870 from the normal lung tissue, visualization of the pulmonary lesions tooke place at later time points as compared to delineation of acute colitis and intramuscular *E. coli* abscess. With ^{111}In-DPC11870 images can be obtained easily up to at least 48 hours after injection. With the ^{99m}Tc-labeled compounds imaging is limited within 24 hours.

With monovalent ^{99m}Tc-MB88, detection of the intramuscular abscess occurred more rapidly after injection as compared to the bivalent agents ^{99m}Tc-MB81 and ^{111}In-DPC11870, due to efficient clearance from non-target tissues, low physiologic uptake in bone marrow and spleen and lack of retention of radioactivity in the kidneys. Although the monovalent compound has not been evaluated in a model of pulmonary infection, it is expected that -due to the overall faster clearance- visualization of pulmonary infection with ^{99m}Tc-MB88 occurs at earlier time points as compared to ^{111}In-DPC11870.

With each of the three LTB4 antagonists rapid and timely diagnosis in patients is expected.

Retention of the radiolabel in the inflammatory foci

Chemotactic compounds are retained at the site of inflammation due to specific interaction with their receptors expressed on leukocytes, infiltrated at the site of the lesion. The LTB4 antagonists accumulated and were retained in the inflammatory foci due to their interaction with the receptor expressed by neutrophilic granulocytes. Imaging and biodistribution studies, performed up to 24 h after injection, demonstrated that radioactivity present in the inflammatory lesion was retained almost completely. Within 24 hours, a decrease in the radioactivity concentration in the inflammatory site could not be observed.

Rapid clearance from non-target tissues

Radiolabeled small molecular weight compounds exhibit a rapid blood clearance and a short biological half-life. The molecular weight of the LTB4 antagonists was 3127, 2975 and 1631 for the bivalent DPC11870, MB81 and monovalent MB88, respectively. The images and analysis of blood samples demonstrated that all compounds exhibited a short

distribution half-life and were cleared rapidly from the background. Due to a more efficient clearance of ^{99m}Tc-MB88 and the lack of retention of this compound in non-target organs, the visualization of infectious lesions with this compound was superior to the images obtained after injection of ^{111}In-DPC11870 and ^{99m}Tc-MB88.
Physiologic uptake of the three LTB4 antagonists was seen in bone marrow, spleen and kidneys, although the radioactivity concentration in these organs differed for each compound. The highest uptake in the bone marrow was found after injection with ^{111}In-DPC11870, while low, uptake was found after injection of both ^{99m}Tc-HYNIC-conjugated LTB4 antagonists. The presence of radiolabeled LTB4 antagonists in the kidney is a result of normal renal clearance of small agents. Since ^{99m}Tc-MB88 showed less retention in the kidneys as compared to both bivalent analogs, ^{99m}Tc-MB88 has the most favorable biodistribution of the three LTB4 antagonists for application as imaging agent.

Absence of biological effects
In general, radiolabeled chemotactic peptides are an interesting class of compounds to visualize infectious and inflammatory foci because they meet several requirements that are essential for an ideal imaging agent. One of the disadvantages of many of these compounds however, is their potency, which causes a biologic response after interaction with the receptor. Side-effects, that may occur after administration of these compounds, are leukopenia, leukocytosis, fever and hypotention and due to the biologic activities, clinical applicability of these compounds is limited. Often, receptor antagonists, that lack biological activity, exhibit low receptor affinity and consequently reduced imaging potential. The LTB4 antagonists investigated in this thesis, showed efficient and good accumulation at the infectious foci reflecting their high receptor affinity. White blood cell counts were not affected bij ^{111}In-DPC11870, not even after administration of 2 mg DPC11870.

Good availability, low costs, easy and non-hazard preparation
The use of radiolabeled autologous leukocytes is considered the “gold standard” nuclear medicine technique to detect infection and inflammation. The radiolabeled leukocytes accumulate specifically in inflammatory foci and demonstrate a high diagnostic accuracy to visualize inflammatory disorders. Unfortunately, the preparation of radiolabeled leukocytes is time consuming, requires specialized equipment and is associated with hazardous risks. The radiolabeling of the ^{111}In-DPC11870 and the ^{99m}Tc-labeled LTB4 antagonists, is easy, fast and without the handling of potentially contaminated material. The ^{111}In-DPC11870 labeling is performed at room temperature, while ^{99m}Tc-labeling is performed at 100°C. All antagonists can be prepared and stored in kit formulation, where

a one step labeling procedure is sufficient. Due to chemical synthesis, these compounds can be prepared in large quantities and are readily available. As compared to other chemotactic analogs (e.g. recombinant cytokines), synthesis is relatively inexpensive.

Low radiation exposure

The LTB4 antagonists investigated in this study were labeled with ^{111}In or ^{99m}Tc. For scintigraphic imaging the use of ^{99m}Tc is preferred over ^{111}In because of the more favorable γ-energy, physical half-life, availability of ^{99m}Tc and dosimetry. On the other hand, these radionuclides require a chelator for radiolabeling which might affect the pharmacokinetics of the compound. Especially, low molecular weight compounds, like the LTB4 antagonists used in this study, might therefore demonstrate different in vivo behavior after conjugation with different chelators. The monovalent HYNIC-conjugated analog ^{99m}Tc-MB88 demonstrated the most favorable characteristics, with similar accumulation of radioactivity in the infectious lesion and low physiologic uptake and retention in non-target tissues. For imaging of infection with radiolabeled LTB4 antagonists the use of HYNIC-conjugated ^{99m}Tc-MB88 is preferred over DTPA-conjugated ^{111}In-DPC11870, due to the most optimal characteristics and the most favorable radionuclide.

Differentiation between infection and sterile inflammation

Detection of infection and inflammation with radiolabeled leukocytes or radiolabeled compounds that target to leukocytes, is based on the induced immune response of the host that recruits leukocytes towards the site of infection. With these agents there is no targeting of the agent that causes the infectious process. Therefore, with these radiopharmaceuticals it is not possible to differentiate between infection and sterile inflammation. The radiolabeled LTB4 antagonists investigated in this thesis accumulates at the site of inflammation due to specific interaction with receptors expressed by leukocyte populations. The presence of radioactivity is an indication for leukocyte infiltration but not for infection. When discrimination between infection and inflammation is essential, the LTB4 antagonists cannot be used. In this case radiolabeled compounds that specifically target micro-organisms are required. Compounds that specifically interact with micro-organisms have been studied for the scintigraphic detection of infection (radiolabeled ciprofloxacin derivatives, radiolabeled antifungal drugs) but are not yet available for use in clinical practice.

^{99m}Tc-MB88 versus other leukocyte receptor targeting agents used for scintigraphic imaging

The studies described in this thesis demonstrate that the LTB4 antagonist ^{99m}Tc-MB88 has ideal characteristics for imaging of infection and inflammation. Additionally, the considerations mentioned above, indicate that ^{99m}Tc-MB88 meets several requirements of the ideal radiopharmaceutical. However, the radiolabeled LTB4 antagonist is only one potential imaging agent that is currently under investigation. Also other cytokines and chemotactic molecules are intensively studied for this application. The use of radiolabeled cytokines to visualize infection and inflammation is often limited due to biological activity of these molecules (C5a, fMLF and IL-1). Studies with the ^{111}In-labeled LTB4 antagonist did not show any changes in white blood cell counts in rabbits after injection of doses up to 2 mg. Other cytokine receptor antagonists, that lack biological activity like IL-1ra, often display reduced affinity for their receptor and therefore demonstrate insufficient accumulation in the inflammatory lesion. There are also radiolabeled cytokines that do not induce biologic effects but display too low receptor affinity for high accumulation at the site of infection (C5adR, NAP-2). Only a few high affinity peptides can be labeled with ^{99m}Tc in high specific activities to prevent biologic activity. The cytokines IL-2 and IL-8 are two peptides that have been successfully studied for the detection of infection and inflammation. Radiolabeled IL-2 targets IL-2 receptors mainly expressed on T-lymphocytes, whereas IL-8 targets CXCR1 and CXCR2 receptors expressed on neutrophils. Biologic activity induced by IL-8 can be circumvented because this compound can be labeled with very high specific activity. Both IL-2 and IL-8 have proven their imaging abilities in preclinical animal models. IL-2 has also demonstrated its applicability in clinical trials to visualize T-cell infiltrates in patients with chronic inflammatory and autoimmune disorders.

Taken together, when ^{99m}Tc-MB88 is compared to other leukocyte receptor targeting agents, currently under investigation for this purpose, ^{99m}Tc-MB88 is a very promising candidate. Therefore the results found with ^{99m}Tc-MB88 warrant further evaluation in patients.

Chapter 9

Summary

Samenvatting

SUMMARY

The aim of the studies described in this thesis, was to investigate the potential of radiolabeled Leukotriene B4 antagonists for the scintigraphic detection of infectious and inflammatory lesions.

Scintigraphic imaging of infectious and inflammatory lesions using radiolabeled leukocytes, generally allows adequate and rapid delineation of infectious and inflammatory foci. Visualization of the localization and extent of an inflammatory process enable guided verification procedures, therapeutic decisions and initiation of appropriate treatment in most cases. In most institutions, scintigraphic imaging of inflammatory and infectious foci is performed with radiolabeled leukocytes as standard imaging agent. However, due to several inevitable disadvantages of this agent, there is a great interest in the development of a new radiopharmaceutical for this application. A new radiopharmaceutical should accumulate efficiently and rapidly in the infected/inflamed tissue. Furthermore, it should clear rapidly from the blood and other non-target tissues.
A promising class of compounds are chemotactic and chemokinetic mediators and their analogs. The use of radiolabeled chemotactic compounds (fMLF, cytokines, chemokines) is based on the high affinity interaction of these compounds, for their receptors expressed on specific leukocyte sub-populations. In addition, due to their low molecular weight, they can penetrate rapidly into the inflamed tissue and clear rapidly from the non-target tissue and from the circulation. In addition, the antagonists of these chemotactic mediators may provide good alternative agents, especially when biological effects of the agonistic peptides limit clinical application. Since the knowledge of the human inflammatory response has expanded and the number of identified chemokines and chemokine receptors has increased, it is now possible to investigate in detail those chemokines that potentially can be applied as radiopharmaceutical for visualization of inflammatory and infectious processes.

Chapter 1 describes the specific characteristics of the chemotactic and chemokinetic compounds that are currently under investigation as potential radiopharmaceuticals to visualize infectious and inflammatory foci. The characteristics of a series of cytokines (IL-1, IL-2), chemokines (IL-8, PF-4, MCP-1, NAP-2), complement factors (C5a, C5adR), chemotactic peptides (fMLF) and other chemotactic factors (LTB4) are described. The potentials of these compounds to serve as an imaging agent are discussed.

In **Chapter 2** a fundamental study is described to determine the potential of the bivalent ^{111}In-labeled leukotriene B4 (LTB4) antagonist, DPC11870, to visualize infectious foci scintigraphically. The LTB4 antagonist DPC11870 was labeled with ^{111}In and i.v. injected in NZW rabbits with intramuscular *E. coli* infection in the left thigh muscle.
The in vivo characteristics were determined by serial scintigraphic imaging and by ex vivo counting of dissected tissues. The receptor-mediated in vivo localization of the compound was investigated in rabbits that received an excess of non-radioactive agent, prior to the administration of the ^{111}In-labeled LTB4 antagonist. The results of the in vivo receptor blocking experiment indicated specific receptor-ligand interaction of the radiolabeled compound.
The scintigraphic images showed that ^{111}In-DPC11870 clearly visualized infectious foci within a few hours after injection. Furthermore, the data from the biodistribution analysis indicated that the compound accumulated in the infectious tissue and was cleared rapidly from the circulation, resulting in high abscess-to-background ratios.

Once it was observed that ^{111}In-DPC11870 accumulated in infected muscle tissue and could visualize infectious lesions, in **Chapter 3** and **Chapter 4** the applicability of this compound was determined in a rabbit model of acute colitis and a model of pulmonary infection, respectively. The imaging characteristics of ^{111}In-DPC11870 were compared with those of ^{18}FDG, ^{99m}Tc-labeled leukocytes and ^{67}Ga-citrate, the radiopharmaceuticals generally used for detection of respectively abdominal and pulmonary infection. In rabbits with chemically-induced colitis, the inflammatory lesions were clearly delineated from one hour after injection. Compared with ^{99m}Tc-granulocytes and ^{18}F-FDG, the radiolabeled LTB4 antagonist revealed the highest uptake in the infectious lesions as well as the highest target-to-non-target tissue ratio.
Additionally, ^{111}In-DPC11870 also distinctly visualized pulmonary aspergillosis infection in the rabbits. Due to relatively slow clearance from the non-target tissues as compared to ^{67}Ga-citrate, the visualization of the pulmonary abscess by ^{111}In-DPC11870 occurred at later time points. Good visualization of pulmonary lesions with ^{111}In-DPC11870 was observed from 6 hours after injection onwards. Due to ongoing clearance of radioactivity from the circulation and ongoing accumulation at the pulmonary infection, infected-to-normal lung ratios found with ^{111}In-DPC11870 increased with time and resulted in higher ratios for ^{111}In-DPC11870 as compared to ^{67}Ga-citrate at 24 h postinjection.

In **Chapter 5** studies on the pharmacodynamics of ^{111}In-DPC11870 are described. In addition, several experiments to determine the mechanism of accumulation of the radiolabeled LTB4 antagonist in the abscess are described. In previous animal studies it was found that accumulation of ^{111}In-DPC11870 in the abscess continued while radioactivity had cleared from the circulation almost completely. The pharmacodynamics of ^{111}In-DPC11870 were studied by serial imaging and by ex vivo counting of dissected tissues. The mechanism of accumulation of the ^{111}In-labeled LTB4 antagonist in the abscess was investigated in rabbits with intramuscular infection that was induced 16 h *after* i.v. administration of ^{111}In-DPC11870. In addition, heterologous leukocytes and bone marrow cells of a donor rabbit were labeled with ^{111}In-DPC11870 in vitro and in vivo distribution of these in vitro radiolabeled cells was compared with the biodistribution of ^{111}In-DPC11870.

Quantitative analysis of the images confirmed accumulation of ^{111}In-DPC11870 in the abscess at time points when the compound had cleared almost completely from the circulation. From the pharmacokinetic analysis a hypothesis was derived: ^{111}In-DPC11870 associates with receptor positive (bone marrow) cells and due to subsequent migration of cell-associated activity, radioactivity accumulates in the abscess. Results of the study showed that at the time of induction of the abscess, 16 hours after injection of ^{111}In-DPC11870, the tracer had cleared from the circulation completely. Surprisingly however, despite the low radioactivity concentrations in the blood, ^{111}In-DPC11870 accumulated in the rising abscess. Additional studies with peripheral blood leukocytes and bone marrow cells labeled ex-vivo with ^{111}In-DPC11870 confirmed the ability of these cells to migrate to the abscess. Overall, the results of these studies demonstrated that ^{111}In-DPC11870 accumulated in infectious foci due to initial targeting of receptor-positive bone marrow cells and subsequent migration of radioactivity from the bone marrow to the infected muscle tissue.

Since ^{99m}Tc is a radionuclide with better imaging characteristics as compared to ^{111}In (physical half-life, gamma-energy, availability), we developed two LTB4 antagonists that were structurally related to DPC11870. In **Chapter 6** the chemical synthesis of the bivalent DTPA conjugated LTB4 antagonist DPC11870, the bivalent HYNIC-conjugated analog MB81 and the monovalent HYNIC-conjugated LTB4 antagonist MB88 is described. In addition, we investigated the labeling efficiency and in vivo characteristics of ^{99m}Tc-MB81 in a rabbit model of intramuscular *E. coli* infection after radiolabeling with three different coligand systems (tricine, TPPTS or isonicotinic acid).

HPLC analysis showed that MB81 could be labeled with ^{99m}Tc rapidly and efficiently with each of the three coligand systems. Scintigraphic images demonstrated that all three analogs delineated intramuscular abscesses in rabbits. Furthermore, the results of the imaging and biodistribution experiments showed that the in vivo behavior of the ^{99m}Tc-labeled LTB4 antagonist MB81 was affected by the coligand used for labeling. The best imaging characteristics are obtained when the HYNIC-conjugated LTB4 antagonist was labeled with ^{99m}Tc using isonicotinic acid as coligand.

In **Chapter 7** the imaging characteristics and pharmacokinetics of both HYNIC-conjugated LTB4 antagonists, MB81 and MB88 were evaluated in rabbits with intramuscular *E. coli* infection. In addition, the results found with both HYNIC-compounds were compared with the characteristics of ^{111}In-DPC11870 which was used as a reference compound in this study. Images demonstrated that both ^{99m}Tc-labeled LTB4 antagonists visualized the abscess from two hours after injection onwards.
Furthermore, abscess uptake at 8 h p.i. of both compounds was similar. However, the monovalent antagonist, ^{99m}Tc-MB88 showed superior imaging characteristics as compared to both bivalent LTB4 antagonists (^{99m}Tc-MB81 and ^{111}In-DPC11870) mainly due to lower retention of radioactivity in the kidneys and the bone marrow. After injection of monovalent ^{99m}Tc-MB88, the abscess was the tissue with the highest radioactivity concentration at 8 h p.i.. From the results of this study, we concluded that the ^{99m}Tc labeled monovalent LTB4 antagonist MB88 is a potent and promising agent to visualize infection and inflammation in patients.

Conclusion

The three radiolabeled LTB4 antagonists investigated in this thesis appeared to have excellent imaging characteristics for detection of infectious and inflammatory lesions. In a comparative study however, the monovalent LTB4 antagonist MB81 revealed superior imaging characteristics as compared to both bivalent compounds. Since preparation of the compound is convenient and safe, the use of this agent may be preferred over radiolabeled white blood cells, the current gold standard technique. The results obtained in various studies warrant evaluation of ^{99m}Tc-MB81 in patients, to determine the value of this agent in clinical situations.

SAMENVATTING

In dit proefschrift worden studies beschreven waarin onderzocht wordt of radioactief gelabelde Leukotriene B4 (LTB4) antagonisten de potentie hebben om ontstekingen en infectiehaarden op een scintigrafische manier te detecteren.

Detectie en lokalisatie van acute en chronische ontstekings- en infectiehaarden is belangrijk voor het tijdig en adequaat instellen van de juiste behandeling. Voor het lokaliseren van een infectie- of ontstekingshaard zijn verschillende onderzoekstechnieken beschikbaar. Behalve radiologische technieken zoals röntgenfoto's, echografie, CT-tomografie en MRI-scan, kan met behulp van scintigrafische technieken, waarbij gebruik gemaakt wordt van van radioactieve stoffen, diagnostisch onderzoek uitgevoerd worden. Bij scintigrafische detectie van infectie- en ontstekingshaarden wordt in de meeste instituten gebruik gemaakt van radioactief gelabelde leukocyten, de gouden referentie standaard. Echter, de bereiding van radioactief gelabelde leukocyten brengt een aantal belangrijke nadelen met zich mee. Daarom is binnen de nucleaire geneeskunde veel belangstelling voor de ontwikkeling van een nieuw radiofarmacon voor deze toepassing. Het nieuw te ontwikkelen radiofarmacon dient aan een aantal eisen te voldoen. Het ideale radiofarmacon wordt snel en efficiënt in het ontstoken weefsel opgenomen. Daarnaast moet het radiofarmacon snel uit de normale weefsels klaren. Vanzelfsprekend moet de bereiding van het radiofarmacon eenvoudig en snel kunnen gebeuren en gaat de voorkeur uit naar een preparaat dat met ^{99m}Tc gelabeld kan worden vanwege de gunstige radioactieve eigenschappen hiervan (γ-energie, stralenbelasting, halfwaardetijd).
Chemotactische peptiden en cytokinen zouden mogelijk voor deze toepassing gebruikt kunnen worden. De toepassing van radioactief gelabelde chemokines (fMLF, cytokinen) voor visualisatie van ontstekingen, is gebaseerd op de hoge affiniteit van deze moleculen voor hun specifieke receptor aanwezig op het celoppervlak van bepaalde leukocyten-populaties. Daarnaast, kunnen deze peptiden, ten gevolge van hun lage moleculaire gewicht, efficiënt penetreren in het ontstoken weefsel en worden deze stoffen snel geklaard uit normale weefsels en organen. Bovendien, biedt het gebruik van radioactief gelabelde antagonisten een alternatief indien toepassing van het chemotactisch peptide zelf een belemmering is vanwege zijn biologische activiteit.
Doordat de kennis betreffende het immunologisch systeem de laatste jaren enorm is uitgebreid en een aantal goed gekarakteriseerde chemotactische peptiden beschikbaar is gekomen, is het mogelijk specifiek die chemokines te onderzoeken, waarvan de verwachting bestaat dat deze geschikt zijn voor het visualiseren van ontstekingshaarden.

In **hoofdstuk 1** worden de specifieke kenmerken beschreven van een aantal biologische eiwitten en de chemisch structureel afgeleiden hiervan. Deze worden momenteel bestudeerd worden als potentieel radiofarmacon voor de detectie van ontstekings- en infectiehaarden.
De kenmerken van een aantal cytokinen (IL-1, IL-2), chemokines (IL-8, PF-4, MCP-1, NAP-2), complement factoren (C5a, C5adR), chemotactische peptiden (fMLF) en andere chemotactische factoren (LTB4) worden beschreven. Daarnaast worden de belangrijkste bevindingen uit recente studies met deze radioactief gelabelde moleculen samengevat. De potentie van de verschillende stoffen voor de toepassing als radiofarmacon voor het detecteren van ontstekingshaarden wordt bediscussieerd.

Hoofdstuk 2 beschrijft een fundamentele studie waarin wordt onderzocht of de bivalente met ^{111}In-gelabelde LTB4 antagonist, DPC11870, in staat is om infectiehaarden te visualiseren. Hiertoe werd de LTB4 antagonist DPC11870 na labeling met ^{111}In, intraveneus ingespoten in konijnen met een intramusculair *E. coli* abces in de linker dijbeenspier. Na injectie werden op verschillende tijdstippen opnamen gemaakt met de gamma-camera. Daarnaast werd bij een aantal konijnen de LTB4 receptor geblokkeerd met behulp van een injectie van 2 mg niet radioactief DPC11870. Hierdoor kon onderzocht worden of de lokalisatie van ^{111}In-DPC11870 in het abces het gevolg was van specifieke interactie met de receptor.
De intramusculaire infectiehaarden werden gevisualiseerd vanaf een paar uur na de injectie van ^{111}In-DPC11870. Uit de biodistributie analyse bleek dat het ^{111}In-DPC11870 efficiënt accumuleerde in het geinfecteerde weefsel en tegelijkertijd snel klaarde uit de circulatie en andere receptor-negatieve weefsels, waardoor hoge abces/spier verhoudingen gevonden werden. Het receptor-saturatie experiment toonde aan dat opname van de LTB4 antagonist op de plaats van de ontsteking receptor gemedieerd is.

Nu vastgesteld was dat ^{111}In-DPC11870 accumuleerde in geïnfecteerd spierweefsel, werd, zoals beschreven in **hoofdstuk 3** en **hoofdstuk 4**, de toepassing van ^{111}In-DPC11870 onderzocht in een konijnen model van acute colitis en een model van pulmonaire aspergillosis, eveneens in konijnen. Het in-vivo gedrag van ^{111}In-DPC11870 in deze modellen, werd vergeleken met ^{18}FDG, ^{99m}Tc-gelabelde leukocyten en ^{67}Ga-citraat, de radiofarmaca welke standaard gebruikt worden voor het aantonen van dit soort ontstekingen in patiënten.
In de konijnen met chemisch geïnduceerde colitis was opname van ^{111}In-DPC11870 in het ontstoken colon reeds zichtbaar vanaf 1 uur na de injectie.

Ten opzichte van ^{18}FDG en ^{99m}Tc-gelabelde leukocyten werd met de radioactief gelabelde LTB4 antagonist behalve de hoogste opname in ontstoken weefsel ook de hoogste target-to-non-target ratio gevonden.
^{111}In-DPC11870 was ook in staat de pulmonaire longinfecties in de konijnen zichtbaar te maken. Echter, in vergelijking met ^{67}Ga-citraat was de pulmonaire infectie met behulp van ^{111}In-DPC11870 pas zichtbaar op latere tijdstippen. Dit werd veroorzaakt door een langzamere klaring van ^{111}In-DPC11870 uit de longen. Duidelijke afbeelding van de pulmonaire infectie, met behulp van ^{111}In-DPC11870, ontstond vanaf 6 uur na de injectie. Ten gevolg van voortdurende klaring van de tracer uit het bloed en het niet-ontstoken longweefsel waren de target-to-non-target ratio's op het tijdstip van biodistributie (24 uur p.i.) hoger met ^{111}In-DPC11870 dan met ^{67}Ga-citraat.

In **hoofdstuk 5** is een uitgebreide studie naar de farmacodynamiek van ^{111}In-DPC11870 beschreven. Daarnaast zijn een aantal experimenten beschreven waarin het mechanisme van ^{111}In-DPC11870 accumulatie in het abces nader werd onderzocht.
In eerdere studies met ^{111}In-DPC11870 werd gezien dat - op tijdstippen waarop de tracer bijna volledig uit de circulatie was geklaard - er nog steeds accumulatie van radioactiviteit in het abces plaatsvond. De farmacodynamiek van ^{111}In-DPC11870 werd bestudeerd aan de hand van seriële opnames en het meten van radioactiviteit in gedissecteerde weefsels en organen. Het mechanisme van accumulatie van ^{111}In-DPC11870 in het abces werd bestudeerd door het induceren van een intramusculair *E. coli* abces, 16 uur *na* injectie van ^{111}In-DPC11870. Daarnaast werden heterologe witte bloedcellen en beenmergcellen afkomstig van een donor konijn, gelabeld met ^{111}In-DPC11870. De biodistributie van deze in-vitro gelabelde cellen werden geëvalueerd naast de biodistributie van ongebonden ^{111}In-DPC11870 in konijnen met een intramusculaire *E. coli* infectie.
Kwantitatieve analyse van de gamma-camera opnamen, bevestigde de eerdere bevindingen van accumulatie van radioactiviteit op tijdstippen waarop ^{111}In-DPC11870 concentraties in het bloed laag waren. Vanuit de resultaten van de farmacokinetiek experimenten werd een hypothese opgesteld: ^{111}In-DPC11870 detecteert infectie- en ontstekingshaarden ten gevolge van associatie met receptor-positieve cellen in het beenmerg en daarop volgende migratie van radioactiviteit vanuit het beenmerg naar de ontsteking. In konijnen waarbij de ontsteking werd geïnduceerd 16 uur na de injectie van ^{111}In-DPC11870, was op het moment van de inductie van de ontsteking een zeer lage concentratie van het radiolabel aanwezig in de circulatie. Ondanks deze lage concentratie werd normale accumulatie van radioactiviteit in het ontwikkelende abces waargenomen.

Dit duidde erop dat accumulatie van radioactiviteit in het abces, niet direct afkomstig kon zijn uit de circulatie. Het verschil in klaring van radioactiviteit uit het beenmerg van gezonde en geïnfecteerde konijnen impliceerde dat ^{111}In-DPC11870 mogelijk vanuit het beenmerg naar het abces zou kunnen migreren. De in-vitro met ^{111}In-DPC11870 gelabelde cellen toonde bovendien aan dat deze cellen in staat waren naar het abces te migreren.
Samenvattend, toonden de resultaten uit deze studie aan dat ^{111}In-DPC11870 in ontstekingshaarden lokaliseert ten gevolge van initiële binding aan receptor-positieve beenmergcellen en daaropvolgende migratie van radioactiviteit vanuit het beenmerg naar het abces.

Voor scintigrafische detectie wordt bij voorkeur gebruik gemaakt van een met ^{99m}Tc-gelabelde tracer. Dit omdat ^{99m}Tc een radionuclide is met een gunstigere half-waarde tijd en foton-energie. Bovendien is ^{99m}Tc een generator product en daardoor eenvoudig beschikbaar. Daarom zijn naast de DTPA-geconjugeerde LTB4 antagonist DPC11870, twee structureel verwante met HYNIC geconjugeerde LTB4 antagonisten, MB81 en MB88, gesynthetiseerd. In **hoofdstuk 6** is de chemische synthese beschreven van de bivalente met DTPA geconjugeerde LTB4 antagonist DPC11870 en de met HYNIC geconjugeerde bivalente antagonist MB81 en monovalente analoog MB88. In dit hoofdstuk zijn de resultaten beschreven van de initiële labelings-experimenten van MB81 met ^{99m}Tc, gebruik makend van de verschillende coligand systemen (tricine, TPPTS en isonicotinezuur).
Met behulp van HPLC analyse werd aangetoond dat MB81 efficiënt gelabeld kon worden met ^{99m}Tc ongeacht de gebruikte coligand. Uit de gamma-camera opnames en biodistributie analyse bleek dat het coligand, gebruikt tijdens de ^{99m}Tc labeling, van invloed was op de farmacokinetiek van MB81. De meest optimale farmacokinetische eigenschappen werden gevonden wanneer MB81 gelabeld was met ^{99m}Tc en isonicotinezuur werd gebruikt als coligand. De scintigrafische opnamen toonden verder aan dat de drie LTB4 antagonisten geschikt zijn voor de scintigrafische detectie van ontstekingshaarden.

Nadat was aangetoond dat de HYNIC-geconjugeerde LTB4 antagonisten, MB81 en MB88, gelabeld konden worden met ^{99m}Tc, bij voorkeur met behulp van isonicotinezuur, werden in **hoofdstuk 7** de farmacokinetische en imaging eigenschappen van beide stoffen beschreven. ^{99m}Tc-MB81 en ^{99m}Tc-MB88 werden geëvalueerd in konijnen met een acute infectie in de dijbeenspier. ^{111}In-DPC11870 werd meegenomen als referentie.

De scintigrafische opnamen toonden aan dat het abces werd gevisualiseerd door beide ^{99m}Tc-gelabelde preparaten vanaf twee uur na de injectie. Na dissectie en meting van de radioactiviteit in de weefsels bleek dat de concentratie radioactiviteit van beide preparaten in het geïnfecteerde spierweefsel gelijk was. Echter, met ^{99m}Tc-MB88 werd een duidelijkere afbeelding van het abces waargenomen dan met ^{99m}Tc-MB81. Dit werd veroorzaakt door het feit dat de concentratie ^{99m}Tc-MB88 in de nieren veel lager was dan concentratie ^{99m}Tc-MB81.
De concentraties ^{99m}Tc-MB81 en ^{99m}Tc-MB88 aanwezig in het abces, waren vergelijkbaar met die van ^{111}In-DPC11870. Opnieuw was echter de afbeelding van het abces na injectie van ^{99m}Tc-MB81 beter dan na injectie van ^{111}In-DPC11870. Nu kon superieure abces visualisatie door ^{99m}Tc-MB88 verklaard worden uit het feit dat de concentratie ^{99m}Tc-MB88 in het beenmerg veel lager was dan die van ^{111}In-DPC11870. Uit biodistributie data bleek dat na injectie van ^{99m}Tc-MB88 de hoogste concentratie radioactiviteit aanwezig was in het abces.
Op basis van de resultaten van deze studie werd geconcludeerd dat de monovalente ^{99m}Tc-gelabelde LTB4 antagonist MB88 de meest potente en veelbelovende tracer is voor het detecteren en visualiseren van infecties en ontstekingen.

CONCLUSIE

In dit proefschrift zijn meerdere studies beschreven waarbij drie verschillende radioactief gelabelde LTB4 antagonisten zijn onderzocht voor de geschiktheid om infecties en ontstekingen te detecteren. De resultaten toonden aan dat elke van deze LTB4 antagonisten geschikt is voor de scintigrafische detectie van ontstekingen en infectiehaarden. Uit een vergelijkende evaluatie is echter gebleken dat de monovalente HYNIC-geconjugeerde LTB4 antagonist, MB88, superieure farmacokinetische eigenschappen bezit, ten opzichte van MB81 en DPC11870. Aangezien de bereiding van deze stof eenvoudig, snel en veilig is, zou het gebruik van ^{99m}Tc-MB88 mogelijk geprefereerd worden boven het gebruik van radioactief gelabelde leukocyten, momenteel de gouden standaard voor deze toepassing in de kliniek. Met de in dit proefschrift beschreven resultaten zijn voldoende argumenten naar voren gekomen die een klinische evaluatie van ^{99m}Tc-MB88 in patiënten rechtvaardigen.

LIST OF PUBLICATIONS

1. Troost EG, Bussink J, Kaanders JH, **van Eerd J**, Peters JP, Rijken PF, Boerman OC, van der Kogel AJ. Comparison of different methods of CAIX quantification in relation to hypoxia in three human head and neck tumor lines. *Radiother Oncol.* 2005 Jul.

2. Kok PJ, **Eerd JE**, Boerman OC, Corstens FH, Oyen WJ. Biodistribution and Imaging of FDG in Rats with LS174T Carcinoma Xenografts and Focal Escherichia coli Infection. *Cancer Biother Radiopharm*. 2005;20:310-315.

3. **van Eerd JE**, Broekema M, Laverman P, Harris TD, Edwards DS, Oyen WG, Corstens FH, Boerman OC. Imaging of Infection and inflammation with an improved ^{99m}Tc-labeled LTB4 antagonist. *J Nucl Med. 2005; In Press*

4. Broekema M, **van Eerd JEM**, Oyen WJG, Corstens FHM, Liskamp RMJ, Boerman OC, Harris TD. Synthesis of Leukotriene B4 antagonists labeled with In-111 or Tc-99m to image infectious and inflammatory foci. *J Med Chem. 2005; In Press*

5. **van Eerd JE**, Oyen WJ, Harris TD, Rennen HJ, Edwards DS, Corstens FH, Boerman OC. Scintigraphic Imaging of Infectious Foci with an ^{111}In-LTB4 Antagonist is Based on In-vivo Labeling of Granulocytes. *J Nucl Med*. 2005;46:786-793.

6. van Schaijk FG, Broekema M, Oosterwijk E, **van Eerd JE**, McBride WJ, Goldenberg DM, Cortsens FH, Boerman OC. Residualizing iodine markedly improved tumor targeting using bispecific antibody-based pretargeting. *J Nucl Med*. 2005;46:1016-1022.

7. Rennen HJ, Bleeker-Rovers CP, **van Eerd JE**, Frielink C, Oyen WJ, Corstens FH, Boerman OC. ^{99m}Tc-labeled interleukin-8 for scintigraphic detection of pulmonary infections. *Chest*. 2004;126:1954-1961.

8. **van Eerd JE**, Rennen HJ, Oyen WJ, Harris TD, Edwards DS, Corstens FH, Boerman OC. Scintigraphic detection of pulmonary aspergillosis in rabbits with a radiolabeled leukotriene B4 antagonist. *J Nucl Med.* 2004;45:1747-53.

9. Brouwers A, Verel I, **Van Eerd J**, Visser G, Steffens M, Oosterwijk E, Corstens F, Oyen W, Van Dongen G, Boerman O. PET radioimmunoscintigraphy of renal cell cancer using ^{89}Zr-labeled cG250 monoclonal antibody in nude rats. *Cancer Biother Radiopharm*. 2004;19:155-63.

10. **van Eerd JE**, Boerman OC, Corstens FH, Oyen WJ. Radiolabeled chemotactic cytokines: new agents for scintigraphic imaging of infection and inflammation. *Q J Nucl Med*. 2003;47:246-55. Review.

11. Brouwers AH, **van Eerd JE**, Frielink C, Oosterwijk E, Oyen WJ, Corstens FH, Boerman OC. Optimization of radioimmunotherapy of renal cell carcinoma: labeling of monoclonal antibody cG250 with ^{131}I, ^{90}Y, ^{177}Lu, or ^{186}Re. *J Nucl Med*. 2004;45:327-337.

12. **van Eerd JE**, Laverman P, Oyen WJ, Harris TD, Edwards DS, Ellars CE, Corstens FH, Boerman OC. Imaging of experimental colitis with a radiolabeled leukotriene B4 antagonist. *J Nucl Med*. 2004;45:89-93.

13. de Geus-Oei LF, **van Eerd-Vismale J**, Molthoff C, Corstens F, Oyen W, Boerman O. Tracers to monitor the response to chemotherapy: in vitro screening of four radiopharmaceuticals. *Cancer Biother Radiopharm*. 2004;19:457-465.

14. Verel I, Visser GW, Boellaard R, Boerman OC, **van Eerd J**, Snow GB, Lammertsma AA, van Dongen GA. Quantitative ^{89}Zr immuno-PET for in vivo scouting of ^{90}Y-labeled monoclonal antibodies in xenograft-bearing nude mice. *J Nucl Med*. 2003;44:1663-1670.

15. Verel I, Visser GW, Boerman OC, **van Eerd JE**, Finn R, Boellaard R, Vosjan MJ, Stigter-van Walsum M, Snow GB, van Dongen GA. Long-lived positron emitters zirconium-89 and iodine-124 for scouting of therapeutic radioimmunoconjugates with PET. *Cancer Biother Radiopharm*. 2003;18:655-661.

16. **van Eerd JE**, Oyen WJ, Harris TD, Rennen HJ, Edwards DS, Liu S, Ellars CE, Corstens FH, Boerman OC. A bivalent leukotriene B(4) antagonist for scintigraphic imaging of infectious foci. *J Nucl Med.* 2003;44:1087-1091.

17. Rennen HJ, **van Eerd JE**, Oyen WJ, Corstens FH, Edwards DS, Boerman OC. Effects of coligand variation on the in vivo characteristics of Tc-99m-labeled interleukin-8 in detection of infection. *Bioconjug Chem*. 2002;13:370-377.

18. Boerman OC, **van Eerd J**, Oyen WJ, Corstens FH. A 3-step pretargeting strategy to image infection. *J Nucl Med*. 2001;42:1405-11.

DANKWOORD

Graag zou ik de mensen die aan de totstandkoming van dit proefschrift hebben bijgedragen bedanken:

Allereerst natuurlijk de personen die mij de mogelijkheid voor dit promotieonderzoek hebben geboden, de promotores Prof. Dr. F.H.M. Corstens en Prof. Dr. W.J.G.Oyen en co-promotor Dr. O.C.Boerman. Frans, Wim en Otto, zonder jullie steun en vertrouwen was deze promotie nooit tot stand gekomen. Beste Frans, vanaf de eerste dag dat ik op de afdeling nucleaire geneeskunde kwam werken heb je me aangespoord om verder te komen in het onderzoek en me alle vrijheid gegeven om me verder te ontwikkelen. Met name jij hebt me de mogelijkheid gegeven om mijn studie te volgen en het promotieonderzoek uit te voeren. Wim, jou heldere visie, analytische denkwijze en de combinatie van wetenschappelijke en medische kennis zijn essentieel geweest voor de totstandkoming van dit proefschrift. Meerdere malen, vooral op het gebied van de infectie modellen, heb ik je adviezen ter harte genomen. Otto, dankzij jouw positieve houding en enthousiaste karakter is het bespreken van resultaten en het bedenken van nieuwe experimenten altijd een uitdaging. Mede door je stimulerende geestdrift kon dit proefschrift vlot en efficiënt voltooid worden.

Natuurlijk wil ik ook mijn collega's bedanken die mij geholpen hebben tijdens de werkzaamheden op het laboratorium en in het dierenlaboratorium. Cathelijne, Annemieke en Ingrid, dank je wel voor jullie hulp en leuke samenwerking. Peter, Huub, Frank en Manuel, dank je wel voor jullie goede adviezen en hulp bij het opzetten van experimenten en de leuke gesprekken die we hadden. Ook Emile hartelijk dank voor je steun en suggesties tijdens menig labeling experiment. Natuurlijk wil ik jullie ook bedanken voor de goede werksfeer en de gezelligheid in het aquarium. Ook Adrienne, inmiddels vanuit het aquarium naar Groningen vertrokken, ik wil je bedanken voor de leuke tijd samen. Daarnaast zou dit proefschrift niet gereed gekomen zijn zonder de hulp van alle andere collega's van de afdeling nucleaire geneeskunde. Vele van de afdeling hebben geholpen tijdens de camera experimenten, en met zijn allen kon het werk altijd op een plezierige manier gedaan worden. Dank je wel iedereen voor de collegialiteit en de prettige werksfeer.

Essentieel voor dit promotieonderzoek was de bekwaamheid van de mensen van het Centraal Dierenlaboratorium. Ik wil bij deze dan ook met name Gerrie Grutters, Hennie

Eijkholt en Bianca Lemmers bedanken voor hun hulp en inzet bij de uitvoering van het dier experimenteel werk. Door jullie expertise konden de experimenten op de meest diervriendelijke wijze verlopen.

Whithout the help of Matthias and the cooperativeness of Bristol-Myers Squibb (BMS) Medical Imaging, the LTB4 antagonists would not be available. Therefore I would like to thank Matthias and BMS, especially Thomas Harris, for their contribution to this project.

Behalve de mensen uit de werkkring wil ik ook mijn familie en vrienden bedanken. Mam en pap, Jo, Toon, Jolanda en Geert-Jan, overige familie, vrienden, vriendinnen en iedereen die interesse heeft getoond tijdens mijn studie en tijdens de werkzaamheden voor mijn promotieonderzoek, bedankt voor jullie belangstelling en steun. Dorée, Rombout, Harrie en Francis, bedankt voor de gezellige tijd en onze goede vriendschap, jullie zorgden voor de nodige ontspanning tussen het studeren en werken door.

Mijn allerliefste Jan, zonder jouw onvoorwaardelijke steun was het nooit gelukt om tegelijkertijd mijn werk, mijn studie en mijn promotie onderzoek te volbrengen. Doordat je er altijd voor me bent en je mij je volledige vertrouwen en steun geeft, ben ik zo ver gekomen. Dank je wel hiervoor, en dank je wel voor al het andere.

CURRICULUM VITAE

Julliëtte Vismale, geboren op 1 mei 1968 te Sint-Oedenrode, begon in 1985 met de Hogere Laboratorium Opleiding aan de Hogeschool van Eindhoven. Deze studie, waarbij als afstudeerrichting Algemene Microbiologie was gekozen, werd in 1989 afgerond met een diploma. In de periode van 1990 tot en met 1999 was Julliëtte werkzaam bij de Gezondheidsdienst voor Dieren, eerst als research analist op de afdeling Onderzoek en Ontwikkeling, vervolgens als 1^{e} analist en gedurende de laatste vijf jaar als hoofdanalist van de afdeling Immunologie en Virologie waar zij leiding gaf aan de mensen werkzaam binnen deze afdeling. In 1999 werd zij aangesteld als research analist bij de afdeling Nucleaire Geneeskunde van het Universitair Medisch Centrum St.Radboud te Nijmegen (Prof. Dr. F.H.M. Corstens). In september 2002 werd begonnen met de Master opleiding Biomolecular Sciences aan de universiteit van Utrecht. Deze opleiding werd in juni 2004 Cum Laude afgerond, na onder andere een onderzoeksstage bij de afdeling Moleculaire Biologie van het Nijmegen Center for Molecular Sciences (Prof.Dr. H.G. Stunnenberg). De eveneens in het kader van deze opleiding uitgevoerde onderzoeksstage bij de afdeling Nucleaire Geneeskunde was mede aanleiding voor de werkzaamheden die geleid hebben tot dit proefschrift.